SEPTEMBER 1960 VOLUME 2 (1960) No. 3

JOURNAL OF NUCLEAR MATERIALS

JOURNAL DES MATERIAUX NUCLEAIRES

A JOURNAL ON METALLURGY, CERAMICS AND SOLID STATE PHYSICS IN THE NUCLEAR ENERGY INDUSTRY

CONTENTS

NORTH-HOLLAND PUBLISHING COMPANY – AMSTERDAM

Papers or letters should be sent to one of the Editors,

R. W. CAHN (Dept. of Metallurgy, University of Birmingham, Birmingham 15, England).
J. P. HOWE (Atomics International, P.O. Box 309, Canoga Park, California, U.S.A.).
P. LACOMBE (Centre de Recherches Métallurgiques de l'Ecole des Mines, Blvd. St. Michel 60, Paris VI, France)

either directly or through a member of the Editorial Advisory Board.

Papers or letters should be written in English, French or German; papers should have a summary in the appropriate language. Translations of the summary into the two other languages will be added by the Editors.

Instructions to contributors will be found in Vol. 1, No. 1 (pp. 111–112).

Books for review should be sent to one of the Editors.

The Journal of Nuclear Materials will initially be published quarterly.

The subscription price of a volume of 360 pages is $ 18.00, 130 s., Gld. 68.50 per volume, post-free.

Subscriptions should be sent to the publishers, North-Holland Publishing Company, P.O. Box 103, Amsterdam or to any subscription-agent.

Les articles ou les lettres devront être envoyés à un des Rédacteurs-en-chef,

R. W. CAHN (Dept. of Metallurgy, University of Birmingham, Birmingham 15, England).
J. P. HOWE (Atomics International, P.O. Box 309, Canoga Park, California, U.S.A.).
P. LACOMBE (Centre de Recherches Métallurgiques de l'Ecole des Mines, 60 Bd. St. Michel, Paris VI, France)

ou directement ou par un membre du Conseil des Rédacteurs.

Les articles ou les lettres devront être rédigés en anglais, français ou allemand, les articles avec un résumé dans la langue correspondante. Les traductions du résumé dans les deux autres langues seront ajoutées par les éditeurs.

Les instructions aux auteurs se trouvent dans le Vol. 1, No. 2 (pp. 211–212).

Les Livres (exemplaires de presse) devront être envoyés à un des Rédacteurs-en-chef.

Le Journal des Matériaux Nucléaires paraîtra initialement tous les trois mois.

Prix de souscription par volume d'environ 360 pages: $ 18.00, 130 s., Gld. 68.50, franco.

Les abonnements devront être envoyés aux éditeurs, North-Holland Publishing Company, P.O. Box 103, Amsterdam, ou à votre librairie.

JOURNAL OF NUCLEAR MATERIALS 2, No. 3 (1960) 197-208, NORTH-HOLLAND PUBLISHING CO., AMSTERDAM

CONSTITUTION OF LOW CARBON U-C ALLOYS

BERNHARD BLUMENTHAL

Argonne National Laboratory, Lemont, Ill., USA †

Received 7 April 1960

The uranium-carbon phase diagram at low carbon concentration was determined by saturation experiments, thermal analyses and metallography. The system has an eutectic point of 0.98 at % carbon at 1116.6° C and two eutectoid reactions:

$$U_{(\gamma)} \rightleftharpoons U_{(\beta)} + UC \text{ and } U_{(\beta)} \rightleftharpoons U_{(\alpha)} + UC,$$

at 771.8° C, and 665.9° C, respectively, 3.0° and 1.8° C below the transformation temperatures of the pure metal. The gamma solubility decreases from 0.30 ± 0.075 at % at the eutectic temperature to 0.09 ± 0.04 at % at the eutectoid temperature. The solubility of carbon in beta uranium is probably less than 10 ppm by weight, in alpha uranium less than 3 ppm.

Le diagramme de phase du système uranium-carbone à faible teneur en carbone a été déterminé par des expériences de saturation, d'analyse thermique et de métallographie. On trouve un eutectique pour 0,98 at % C à 1116,6° C et deux réactions eutectoïdes: $U_{(\gamma)} \rightleftharpoons U_{(\beta)} + UC$ et $U_{(\beta)} \rightleftharpoons U_{(\alpha)} + UC$ à 771,8° C et 665,9° C respectivement, à 3,0° C et 1,8° C en-dessous des températures de transformation du métal pur. La solubilité en γ diminue de 0,30 ± 0,075 at % à la température de l'eutectique à 0,09 ± 0,04 at % à la température de l'eutectoïde. La solubilité du carbone dans l'uranium β est probablement inférieure à 10 ppm en poids, dans l'uranium α inférieure à 3 ppm.

Das Zustandsdiagramm U–C wurde im Bereich niedriger Kohlenstoffgehalte durch Sättigungsversuche, thermische Analysen und metallographische Untersuchungen bestimmt. Das System weist einen eutektischen Punkt bei 0,98 At % C und 1116,6° C, sowie zwei eutektoide Umwandlungen folgender Art auf:

$$U_{(\gamma)} \rightleftharpoons U_{(\beta)} + UC \text{ bei } 771{,}8° \text{ C und}$$
$$U_{(\beta)} \rightleftharpoons U_{(\alpha)} + UC \text{ bei } 665{,}9° \text{ C.}$$

Diese Umwandlungstemperaturen liegen 3,0 und 1,8° C unter den Umwandlungspunkten des Reinmetalls. Die Löslichkeit im γ-Uran sinkt von 0,30 ± 0,075 At % bei der Temperatur des Eutektikums auf 0,09 ± 0,04 At % bei der Temperatur des Eutektoids ab. Die Löslichkeit von Kohlenstoff ist wahrscheinlich kleiner als 10 Gew ppm in β-Uran, kleiner als 3 Gew ppm in α-Uran.

1. Introduction

Carbon is the most important contaminant in uranium. Reactor-grade uranium may contain up to 500 ppm (1 at %) †† carbon, or more, whereas oxygen and nitrogen rarely attain concentrations as high as 35 to 50 ppm, respectively, and individual metallic contaminants seldom reach a concentration of 100 ppm [1]. The system in general was most recently reviewed by Hansen and Anderko [2], Rough and Bauer [3] ††† and earlier by Katz and Rabinowitch [4]. Hansen's interpretation is accepted.

The liquidus curve for alloys containing up to 50 at % carbon was determined by Snow [5], Carter [6] and Mallet, Gerds and Nelson [7]. The curve does not extend below 3 to 2 at %. Thermal analyses by Carter [6] of alloys containing 0.6 to 23 at % (0.03 to 1.5 wt %) gave thermal arrests ranging from 1120° to 1134° C at high cooling rates of 50° to 70° C/min. A first indication that the system was an eutectic one was given by measurements of the freezing point of uranium by Dahl and Cleaves [8], who found a relationship between a decreasing carbon

† Presently on leave of absence from ANL and Consultant to the Centre d'Etude de l'Energie Nucléaire (C.E.N.), Mol, Belgium.

†† All data in ppm refer to parts per million by weight. Wt % and at % are convenient abbreviations for weight and atomic percent.

††† The quoted gamma-solubility data of [3] are no longer valid and are superseded by the present publication

content and an increasing freezing point. Zone-melting experiments by Dunworth [9]) also pointed towards an eutectic system.

The solid-state transformation data by Carter [6]) (cooling curves only) varied from 759° to 775° C for the $\gamma \rightarrow \beta$ transition and from 635° to 650° C for the $\beta \rightarrow \alpha$ transition; he concluded that the carbon content does not affect the transformation temperatures. Metallographic observations on high-purity uranium by Blumenthal [10]) on the response of heterogeneous uranium to solution heat treatment in the gamma phase and to reprecipitation of the second phase at a high temperature in the range of stability of alpha uranium, indicated a significant solubility of carbon in gamma uranium. Workers at Battelle Memorial Institute [11]) concluded, from heat-treating experiments on biscuit metal with 100 ppm carbon, that the solubility of carbon in alpha uranium is substantially below 0.01 wt % and in beta uranium is of the order of 0.02 to 0.03 wt %.

Though scant, the information reviewed above was invaluable in planning the present investigation, as it helped to anticipate some of the factors that would require experimental control. Thus, it was expected that the transformation temperatures of uranium-carbon alloys would not differ very much from those of the pure metal and the present investigation was closely linked with a precision determination of the transformation points of high-purity uranium [12]). Possible changes of composition during thermal analysis had to be considered, and the large hysteresis between heating and cooling required an evaluation of this factor. The investigation became possible after the development of high-purity uranium [13,14,10]), of urania refractories, and of precision analytical methods for the determination of low concentrations of carbon, nitrogen, and oxygen in uranium.

The present work deals with:

1. a determination of that part of the liquidus curve for alloys with up to 2 at % carbon, in which the liquid is in equilibrium with uranium carbide;
2. a determination of the temperature of the three-phase reaction between liquid uranium, uranium carbide and gamma uranium;
3. a determination of the effect of carbon on the solid-state transformation temperatures; and
4. a determination of the solid solubility of carbon in gamma uranium.

This information is sufficient to determine the basic features of the uranium-carbon system at low concentrations of carbon. No attempt was made to determine the liquidus curve between liquid and gamma uranium. The thermal effects are so small that only extremely precise measurements of temperature on superpure material of very uniform composition may be expected to give reasonable results. Neither was an attempt made to determine the very low solubility limits of carbon in alpha and beta uranium as the best available analytical methods would not have sufficed.

2. The liquidus curve

2.1. Method

The conventional method of thermal analysis for determining liquidus temperatures is usually not feasible in cases where the concentration of the alloying element and the accompanying thermal effects are small. The methods which seemed most promising were liquation and saturation experiments. The equilibrium concentration is approached at constant temperatures; in the case of liquation, from a higher concentration, and in the case of saturation, from a lower concentration. Both approaches should have given the same results; however, this did not happen. Since liquation is a process in which a light, insoluble phase floats upward and is collected at the top of the melt, the carbon concentration was determined by analyzing the liquated ingot at different levels. These experiments were carried out in urania-crucibles similar to those used in the earlier work on the refining of uranium [15]). In the saturation experiments high-purity uranium was held in high-purity graphite crucibles for

various lengths of time. After cropping the top and bottom ends from each ingot and removing the skin of high carbon concentration, circumferential layers were analysed. To freeze-in the high-temperature equilibrium, a provision for rapid solidification was made.

When a large gap was found between the results of liquation and saturation, a third approach was tried. The carbon concentration in a saturation experiment is influenced by several rates: the rate of carbide formation at the interface between crucible and melt, the rate of carbide diffusion into the interior, and the rate of carbide liquation. Diffusion occurs in two directions: from the crucible wall radially into the melt, and from the crucible bottom upward. A simplification was attempted by letting the elementary processes proceed in one direction only. The graphite crucible was replaced by an inert urania crucible, and a carbon source, in the form of a graphite disk, was placed on top of the melt. In this manner liquation was minimized and saturation proceeded by diffusion unidirectionally downward. Near the top of the melt a layer of uranium carbide, in whose neighbourhood the melt was saturated with carbon, was formed. Carbon analyses were made at various distances from the UC-metal interface. A constant number would have shown that the entire melt had been saturated with carbon. When a concentration gradient was found, the number obtained from the immediate neighborhood of the interface was indicative of the equilibrium concentration.

2.2. Experimental Details

The previously described [10]) high-vacuum resistance furnace was used for the liquation and saturation experiments. The temperature was controlled by a Pt/Pt-10 % Rh thermocouple touching the outside of the furnace tube. The temperature drop between this point and the center of the melt was about 12° C. The reported temperatures are correct to within a few degrees. To freeze-in the high temperature equilibrium, the cage carrying the melt was quickly lowered into the cold end of the furnace tube upon completion of the experiment. It is probable that solidification took place within a few seconds.

For the liquation experiments, supersaturated alloys were prepared by melting high-purity uranium crystal compacts in high-purity graphite crucibles in the resistance furnace and holding for one hour at 1400° C. The saturated melts were quickly solidified. Later supersaturated alloys were made by an induction melting process. Analyses of high-purity uranium are not reported here since its composition and interaction with various crucible materials were described before [10]). Two grades of high-purity graphite were used. One grade contained (in ppm): 5 Al, 0.2 B, 10 Ca, 1 Cu, 15–30 Fe, 0.5 Mg, 2 Si; the other one: 1 Ag, 5 Ca, 1 Cu, 20 Fe, 5 Mg, 1 Pb, 15 Si. The ingots, of 860 to 900 g, were scalped to remove the graphite-impregnated surface and rolled at 600° C to a 1.6 cm ($\frac{5}{8}$ in.) diameter rod.

The sample size in the liquation studies was about 300 g. In most cases analytical samples were taken from the bottom center, the center and a region above the center (called top center) of each liquated ingot. The high carbon contents of some of the top samples indicated that it was not always possible to obtain a true representative sample. High carbon analyses that were out of line were rejected. No other changes in composition in these and the following experiments were observed.

For the saturation experiments, high-purity uranium was kept molten in a high purity graphite crucible and solidified just as done for the liquation melts. After removing the ingot top, analytical samples were prepared on a lathe by means of a series of circumferential cuts. The first two cuts were 0.16 cm ($\frac{1}{16}$ in.) deep, the other 0.32 cm ($\frac{1}{8}$ in.) deep. Each ingot had a skin of high carbon concentration. The carbon content rapidly decreased towards the interior; the second eighth of one inch appeared to be in equilibrium with the remainder of the melt. The last eighth of an inch, representing

core material of 0.6 cm ($\frac{1}{4}$ in.) diameter, deviated from the mean concentration in several experiments, probably because non-directional solidification caused the formation of shrinkage cavities in the center of the ingots. Therefore, the first and last cuts were disregarded in computing the mean saturation concentration.

In the unidirectional diffusion experiments, solidification was again accomplished by the technique of rapid lowering. The exact location of the UC/metal interface was determined metallographically. Although UC formed a distinct layer, no precise line of separation existed between the two phases, making it difficult to take representative samples from the immediate vicinity of the top layer. Analytical samples were prepared from a sequence of horizontal layers of 0.50 cm (0.20 in.) thickness.

2.3. Liquidus Data

Liquations were made for 5, 12, 24 and 48 hours at 1200° C and for 5 and 12 hours at 1300° C. Since the data were scattered widely, many analyses were made. The distribution curves (fig. 1) showed a maximum of carbon in

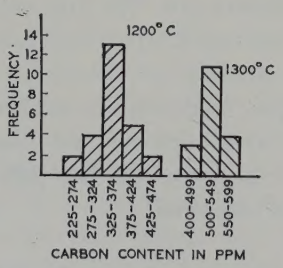

Fig. 1. Distribution of carbon content in liquated high-purity uranium-carbon alloys.

the range of 325 to 374 ppm at 1200° C, the mid-mean being 358 ppm. The mid-mean of the more uniform data of the 1300° C liquations was 529 ppm. Liquation was complete after five hours. The oxygen content of all melts was low, in most cases between 8 and 15 ppm. The data for 1200° C agree with those for reactor-grade uranium reported earlier [15]). A combined plot is shown at the left-hand side of fig. 2.

Saturation experiments were made at 1200°,

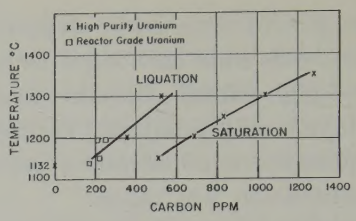

Fig. 2. Liquidus curves of uranium-carbon alloys from liquation and saturation experiments.

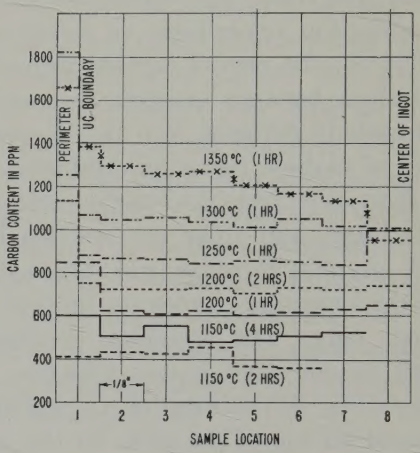

Fig. 3. Distribution of carbon content of uranium-carbon alloys in saturation experiments.

1250°, 1300° and 1350° C. Fig. 3 shows a plot of carbon content versus sample location for various saturation periods. At 1200° C equilibrium was reached after two hours, since the results of the two and four-hour melts agree. At 1150° C four hours were necessary to attain equilibrium. At 1250° C and above, one hour sufficed. The right-hand side of fig. 2 shows a plot of temperature versus concentration determined from saturation experiments. The liquidus curve obtained from the saturation experiments was found to be at a considerably higher concentration of carbon than the one obtained from the liquation experiments.

The results of the unidirectional saturation experiments at 1200° C are plotted in fig. 4. The curves indicate a high carbon concentration near the metal/carbide interface at equilibrium and favor the results of the saturation over the liquation experiments. They also show that the liquation rate is greater than the saturation rate and that the liquation rate is

the dominant kinetic factor in all saturation experiments.

The question remains as to why liquation produced alloys of low carbon content. At the eutectic temperature gravity segregation of the UC phase may occur. This process has been described for other alloy systems, such as U-Al, by Allen and Isserow [16]). If the rate of dissolution of the UC phase in molten uranium is very slow, gravity segregation may also take place at a higher temperature, leaving behind a liquid of concentration less than that corresponding to equilibrium.

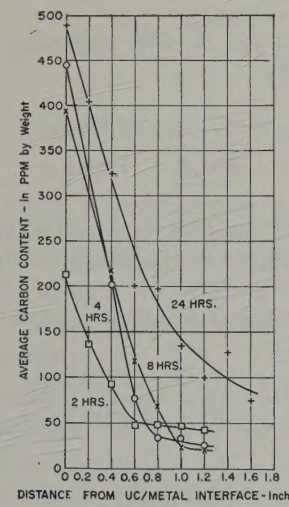

Fig. 4. Diffusion of carbon into molten uranium at 1200° C.

3. The Eutectic Temperature

3.1. Method

Thermal analysis was used to determine the temperature of the three-phase reaction between the uranium-carbon alloy liquid, solid uranium carbide and gamma uranium. The method and apparatus were the same as those used by the author for the determination of the $\gamma \rightleftharpoons$ L transformation temperature of the pure metal [12]).

3.2. Data

The first experiment (B-723) was made with an alloy which had a carbon content of 1850 ppm. In the course of six cycles, made at a rate of 0.74° C/min, in a urania crucible, the carbon content decreased to 450 ppm in a sample taken near the bottom of the ingot, and to 165 ppm in a sample taken near the top. The first two cycles gave very clear arrest temperatures of 1116.4° C on melting and of 1116.9° C on freezing. In subsequent cycles the arrests began to show a slight slope. The precision of the data decreased from 1116.6 $\pm$ 0.2° C to 1116.5 $\pm$ 1.1° C (standard deviation).

In another experiment, (B-743), high-purity metal of initially 10 ppm carbon content was cycled 14 times in two days in a high-purity graphite crucible at the same rate. Its carbon content was increased to 515 ppm. The early arrest temperatures were near 1130° C. A deterioration of the quality of the arrest was apparent when compared with the arrests of high-purity uranium in a urania crucible; the arrest assumed a distinct slope. Beginning with the ninth cycle a recalescence occurred on freezing at the end of the arrest and a small horizontal section appeared at a temperature of 1115.9° C, while the beginning of the arrest was still near 1120° C.

In an experiment, (B-747), in a graphite crucible starting with an alloy containing 724 ppm carbon and ending with 642 ppm †, the arrest had a slight slope throughout the seven cycles. The mean temperatures for the beginning and end of melting and freezing were 1120.7° C and 1122.8° C for melting and 1122.7° C and 1120.6° C for freezing, with deviations of a few tenths of a degree in each group.

It is believed that the closeness of liquidus and solidus temperatures was mainly responsible for the difficulty of obtaining clean arrest temperatures in the concentration range of the alloys B-743 and B-747. Low rates of heat transfer through the urania protection tube to the thermocouple increased the difficulty. It is felt that experiment B-723 should be given the greatest weight, because liquidus and solidus temperatures were far enough apart at the

† The decrease in carbon content shows again that liquation of UC proceeds faster than diffusion of UC into the melt.

initial high concentration of carbon so that they did not influence each other. The temperature of 1116.6 $\pm$ 0.3° C was adopted and it was concluded that the three-phase reaction between the liquid, UC and gamma uranium is an eutectic one.

4. The Alpha-Beta Transformation

4.1. Method

The extrapolation method that was used to determine the transformation temperatures of high-purity uranium was applied to uranium-carbon alloys, containing 1875 ppm and 1725 ppm of carbon. The bare specimen was suspended in the thermal-analysis apparatus, as described in ref. [12]).

4.2. Data

A considerable difference between the transformation temperatures for heating and cooling persisted, and this difference decreased with decreasing rates of heating and cooling (table 1). As in the case of high-purity uranium, a straight-line relationship was assumed between arrest temperature and the decadic logarithm of the rate of heating or cooling.

Equations of the types

$$T_H = a_1 + b_1 \log r$$

and

$$T_C = a_2 - b_2 \log r$$

were calculated by the method of least squares, where T_H and T_C are the transformation temperatures in °C on heating and cooling, respectively, r the rate of heating or cooling in °C/min, and a_1, a_2, b_1 and b_2 are constants. The two lines intersect at the equilibrium transformation temperature:

$$T = T_H = T_C.$$

For alloy B-727 B, the following equations were obtained:

$$T_H = 671.9 + 2.82 \log r$$
$$T_C = 661.3 - 1.46 \log r.$$

The two lines intersect at the equilibrium temperature of 664.9° C. Equilibrium would be attainable at a rate of 0.0033° C/min. The equations for alloy B-727 T were:

$$T_H = 676.6 + 6.29 \log r$$
$$T_C = 662.2 - 3.09 \log r.$$

Table 1
Alpha-beta eutectoid transformation temperatures of high-purity uranium-carbon alloys at various rates

Rate of heating or cooling (°C/min)	Mean eutectoid temperature							
	B–727 B				B–727 T			
	Heating		Cooling		Heating		Cooling	
	°C	N*	°C	N*	°C	N*	°C	N*
4.0	673.0	17	660.2	17	680.5	3	661.2	3
					680.6	4	660.3	4
2.0	673.1	8	660.7	8	678.4	2	660.7	2
1.0	672.7	5	661.5	5	675.7	4	662.0	4
0.5	671.0	6	662.1	6	674.5	2	661.6	1
0.33	669.9	4	662.2	4	673.5	3	663.8	2
					674.2	1	665.1	2
0.17	669.8	1	661.9	1	—	—	—	—

* N is the number of measurements in mean.

The point of intersection is $T = 666.9°$ C at $r = 0.029°$ C/min. The data are plotted in fig. 5. The mean $\alpha \rightleftharpoons \beta$ equilibrium temperature is 665.9 $\pm$ 1° C. Since the $\alpha \rightleftharpoons \beta$ temperature of high-purity uranium is 667.7 $\pm$ 1.3° C, the transformation temperature is 1.8° C lower in uranium-carbon alloys than in high-purity uranium. The reaction in uranium-carbon alloys is of the eutectoid type:

$$U_{(\beta)} \rightleftharpoons U_{(\alpha)} + UC.$$

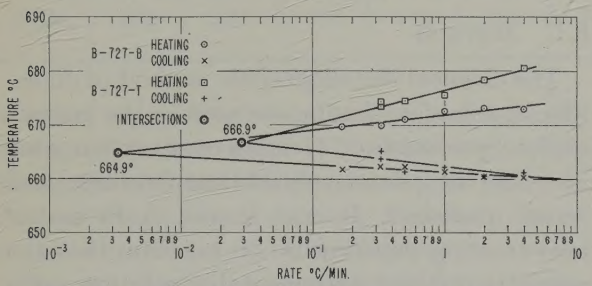

Fig. 5. Effect of heating and cooling rate on the $\alpha \rightleftharpoons \beta$ transformation temperature of high-purity uranium-carbon alloys.

5. The Beta-Gamma Transformation

5.1. Method

Satisfactory arrests were obtained on cooling in applications of the same method to the $\beta \rightleftharpoons \gamma$ transformation of a uranium-carbon alloy of high carbon content. Since undercooling of several degrees was observed, the constant temperature obtained after recalescence was regarded as the correct temperature of transformation. Difficulties arose in measuring the arrest temperatures on heating, since the transformation occurred over a temperature range. At the slower rates of heating, the midpoint of the arrest temperature range was easily read from the curves, since there was a sufficiently long horizontal section. At higher rates the midpoint was determined by geometric means. The beginning of the arrest was distinct at all rates. Data for both the midpoint and the beginning of transformation were obtained and evaluated.

5.2. Data

The mean corrected data for the $\beta \rightleftharpoons \gamma$ transformation of an alloy with 1725 ppm carbon (B-727 T) are listed in table 2; they yield, by the method of least squares, the functions

$$T_H \text{ (initial)} = 772.6 + 0.51 \log r$$
$$T_H \text{ (midpoint)} = 776.2 + 2.41 \log r$$
$$T_C = 767.2 - 2.81 \log r.$$

Table 2

Beta-gamma eutectoid transformation temperatures of a high-purity uranium-carbon alloy at various rates (B–727 T)

Rate of heating or cooling (°C/min)	Mean eutectoid temperature				
	Heating			Cooling	
	Initial point (°C)	Midpoint (°C)	N*	°C	N*
2.22	773.6	777.4	5	766.1	5
0.74	772.2	775.9	6	768.3	6
0.37	771.2	773.8	3	767.7	3
0.19	772.8	775.4	4	769.5	3

* N is the number of measurements in mean.

The points of intersection of each pair of equations are

for T_H (initial) and T_C . . . . . 771.8° C at 0.025° C/min

for T_H (midpoint) and T_C . . . . . 772.1° C at 0.024° C/min

for T_H (initial) and T_H (midpoint) . . . . . 771.6° C at 0.012° C/min.

All three pairs of lines intersect near one point (see fig. 6). By extrapolation of the arrest temperatures to the point of intersection, the differences between the beginning of transformation and the midpoint disappear, as they should if the observed data represent an

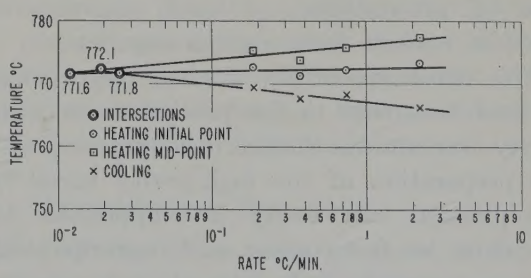

Fig. 6. Effect of heating and cooling rate on the $\beta \rightleftharpoons \gamma$ transformation temperature of high-purity uranium-carbon alloy (B-727 T).

invariant equilibrium in a binary system. It follows that 771.8° C is the equilibrium temperature.

The experiments were repeated with an alloy containing only 325 ppm of carbon (B-733). Although an alloy with such a carbon content should have given a clear indication of the eutectoid temperature, no equivalent arrest was found upon thermal analysis. Unexpectedly the experimental data agreed rather closely with those obtained for the $\beta \rightleftharpoons \gamma$ transformation of high-purity uranium (table 3). The relationship between thermal arrest and heating rate is given by the function

$$T_H = 777.6 + 2.02 \log r.$$

For cooling the mean value is

$$T_C = 775.6 \pm 1.1° \text{ C}.$$

TABLE 3

Beta-gamma transformation temperatures in a high-purity uranium-carbon alloy with 325 ppm carbon (B–733)

Rate of heating or cooling (°C/min)	Mean transformation temperature			
	Heating		Cooling	
	°C	N*	°C	N*
2.47	778.7	3	775.5	3
0.83	777.1	6	774.0	6
0.41	776.5	3	775.2	2
0.21	776.1	4	776.1	2
0.10	775.9	4	777.0	3

* N is the number of measurements in mean.

The abnormal behavior is due to the very low rate of precipitation of small amounts of uranium carbide from gamma uranium.

This effect was observed when the response to heat treatment of the precipitate in high-purity uranium was studied in conjunction with the preparation of the high-purity metal [10]). Precipitation can easily be suppressed by quenching or fast cooling, and reprecipitation from a supersaturated alpha solution requires a long time. Thus, it is concluded that the true transformation temperature was measured in the earlier experiment (B-727 T). The $\beta \rightleftharpoons \gamma$ transformation of uranium-carbon alloys is of the eutectoid type:

$$U_{(\gamma)} \rightleftharpoons U_{(\beta)} + UC.$$

It occurs at 771.8° $\pm$ 0.3° C which is 3.0° C below the transformation point of 774.8° $\pm$1.6° C for the pure metal.

6. Solubility of Carbon in Gamma Uranium

6.1. Method

The classical metallographic method of determining solubility limits was used in the present study. Specimens of variable composition were annealed at predetermined temperatures and water quenched. It was known from earlier heat-treating experiments on uranium that the solute is retained in metastable solution upon quenching, even though two solid-state transformations are transgressed. Neither the $\gamma \rightarrow \beta$ nor the $\beta \rightarrow \alpha$ transformation can be suppressed by quenching of pure uranium or uranium-carbon alloys, (cf. ref.[10]), ANL-5019, figs. 36 to 42). Slowly cooled cast alloys of sufficient carbon content show the eutectoid precipitate described in ref.[10]), aside from angular inclusions of UC. Gamma-annealed and water-quenched material shows no eutectoid precipitate and the angular inclusions are rounded off. Water quenching causes the metal to be severely strained, which manifests itself by the appearance of irregular grain boundaries, subgraining and twin formation. Solute carbon may be reprecipitated from its metastable solid solution by long-time anneals at a temperature in which the alpha phase is stable. This precipitate will appear in the form of fine dots throughout the recrystallized alpha grain or along its grain boundaries (ref.[10]), ANL-5019, figs. 43 to 46). Carbon reprecipitated at a temperature at which the gamma phase is stable from a solution prepared at a higher temperature in the region of stability of the gamma phase, is hardly distinguishable, since the concentration differences, and consequently the volume of such a precipitate, are small. Thus, the only reliable

TABLE 4

Carbon content of high-purity uranium-carbon alloys before and after heat treatment in a purified argon atmosphere

Ingot number	Carbon content in ppm											
	Original material before heat treatment			After heat treatment								
	Top	Center	Bottom	72 h at 760° C	24 h at 775° C	24 h at 800° C	17 h at 850° C	5 h at 900° C	4 h at 950° C	2 h at 1000° C	1 h at 1050° C	1 h at 1100° C
B 639	52	—	47	—	—	35,25	13,16	—	9,29	25,26	—	29,33
B 493	200	222	180	148	157	201	120	191	115	—	80	158

criterion of heterogeneity is the presence of light gray inclusions of UC, which are easily distinguished from dark gray inclusions of UO_2. The metallographic specimens, therefore, were prepared to retain the UC inclusions.

The specimens were prepared from high-purity uranium and an uranium-carbon master alloy. The ingots were homogenized at a high temperature in the region of stability of the gamma phase, then cut up and analyzed. Originally it was felt that such an alloy would retain its concentration of carbon throughout subsequent anneals. In the initial experiments the specimens were wrapped in tantalum foils, sealed in evacuated Vycor tubes, and annealed in a conventional vertical tube furnace. The Vycor envelope was a source of contamination and of interference with an effective quench. Therefore, the bare specimens were annealed in an atmosphere of highly purified argon and water quenched.

These series of heat treatments and metallographic examinations gave a solubility curve of unusual shape which led to a check of both the temperature and the concentration parameters. The temperature parameter was checked by annealing individual specimens, first above and then below the solubility limits, and examining them metallographically for the presence of precipitated particles. These experiments were unsuccessful.

The concentration parameter was checked by re-analyzing a portion of a heat-treated specimen from the immediate vicinity of the point of observation. The pie-shaped ingot sections were halved parallel to the pie-shaped surface. The inside surface of one half was examined metallographically, the other half was analysed. In 55 out of 67 cases the carbon content was substantially lower than in the original ingot material. In seven cases the samples contained more carbon and in five cases the carbon content had remained unchanged. Six of the cases in which a higher carbon content was reported pertained to an anneal at 1100° C in which contamination could have occurred. Some characteristic data are listed in table 4. The loss of carbon averaged between 30 and 50 %, with individual cases going beyond these points.

Decarburization of uranium in the solid state has not been observed before. The literature contains no indication that annealing of uranium in an atmosphere of purified argon would decrease the carbon content of the metal. In the present and subsequent work so many decarburization experiments have been carried out that there is no doubt about the reality of the effect. It was obvious that the solubility curve which was plotted against the carbon content of the original ingot material was false and that only the carbon contents after heat treatment should be used to plot the solubility curve.

6.2. Experimental Details

Most of the alloys were prepared from a uranium-carbon master alloy of known composition. High-purity uranium ingot material was melted together with a quantity of the

master alloy in a urania crucible, held for one hour at 1400° C and solidified by quickly lowering the crucible into the cold zone of the resistance furnace. The rapidly solidified ingots contained sink holes which, however, did not interfere with their usefulness. The ingots were sectioned into pie-shaped pieces each weighing 6 to 8 g.

The annealing furnace was a vertical, wire-wound resistance element which had separately controlled heating elements at each end to obtain a 15 cm (6 in.) long zone of constant temperature. A McDanel porcelain tube, 5 cm (2 in.) O.D., 3.8 cm ($1\frac{1}{2}$ in.) I.D. and 120 cm (48 in.) in length, was inserted into the furnace. An atmosphere of highly purified argon gas at a slightly positive pressure flowed through the furnace in an upward direction. A water-cooled head supported the specimen and the thermocouple suspension. A disc, made of uranium for the anneals at low temperature and of molybdenum or alundum for those at high temperatures, held six specimens in the center of the furnace. The hot junction of the thermocouple was located just above this disc. The initial temperature measurements were correct within $\pm$ 5° C, later, more precise measurements, within $\pm$ 2° C, were made. To quench the specimen, the bottom flange was opened, the tungsten suspension wire cut electrically, and the disc supporting the specimens dropped into water.

6.3. Data

A partial constitutional diagram is shown in fig. 7. The diagram shows a region of overlap. Below the concentrations indicated by Curve A no heterogeneous alloys occurred; above the concentrations indicated by Curve B no homogeneous alloys occurred. The concentration range between the Curves A and B contained alloys which were either homogeneous or heterogeneous. The true solubility limit should lie between A and B and may be as low as 0.05 at % (25 ppm) or as high as 0.13 at % (65 ppm) at the eutectoid temperature, and as low as 0.22 at % (110 ppm) or as high as 0.37 at % (185 ppm) at the eutectic temperature. The spread of 0.08 and 0.15 at %, 40 and 75 ppm, respectively, indicates the limits of error. The mean between the two limits was used in the final diagram.

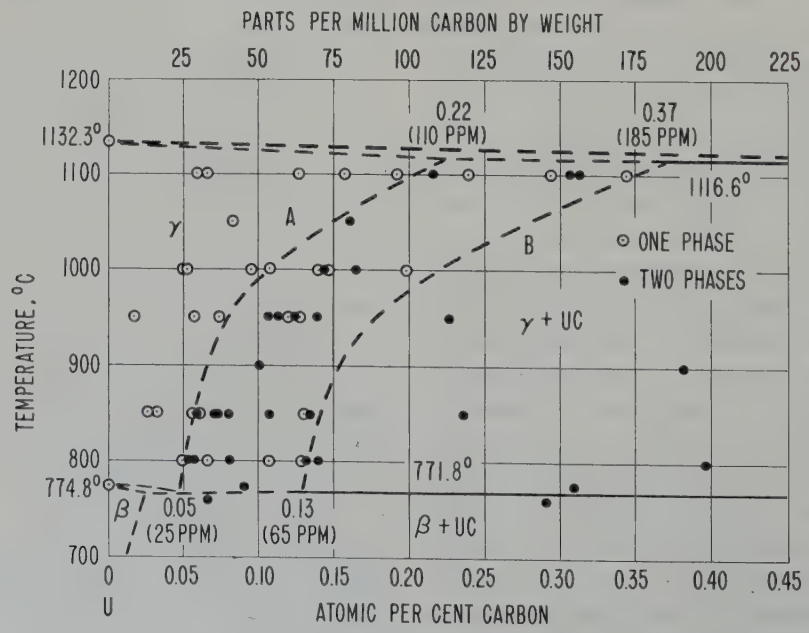

Fig. 7. Solubility of carbon in gamma uranium based on analyses after heat treatment. All alloys below curve A are homogeneous; all alloys above curve B are heterogeneous.

7. The Uranium-Carbon phase Diagram

The uranium-carbon phase diagram at low concentrations of carbon is shown in fig. 8. The system has an eutectic of 0.98 at % carbon at a temperature of 111.6° C. The gamma solubility decreases from about 0.30 at % carbon at the eutectic temperature to about 0.09 at % at the $U_{(\gamma)} \rightleftharpoons U_{(\beta)} + UC$ eutectoid temperature of 771.8° C. The solubility line is dot-dashed to indicate that it is the mean of two boundary curves, A and B of fig. 7. It is correct within $\pm$ 0.075 at % at the eutectic temperature and within $\pm$ 0.04 at % at the eutectoid temperature. Also, the reaction $U_{(\beta)} \rightleftharpoons U_{(\alpha)} + UC$ is of the eutectoid type. The temperatures of the invariant equilibria are 3° C below the temperature of the $\beta \rightleftharpoons \gamma$ transformation and 1.8° C below the temperature of the $\alpha \rightleftharpoons \beta$ transformation of the pure metal. Consequently, the solid solubilities of carbon in beta and alpha uranium must be very small. It is estimated that the solubility of carbon in the beta phase is less than 10 ppm, and in the alpha phase less than 3 ppm.

Acknowledgement

This work was done under the direction of Drs. F. G. Foote and H. H. Chiswik. The author acknowledges with pleasure many fruitful discussions with L. T. Lloyd. He thanks F. S. Tomkins, R. W. Bane, J. A. Goleb and B. D. Holt for the chemical analyses. W. J. Stuparitz assisted in setting up the experimental apparatus and making the measurements. The work was performed under the auspices of the U.S. Atomic Energy Commission.

References

1) B. Blumenthal, Argonne National Laboratory (USA) Report, ANL 5349 (1955)
2) M. Hansen and K. Anderko, Constitution of Binary Alloys (McGraw–Hill, New York, 1958)

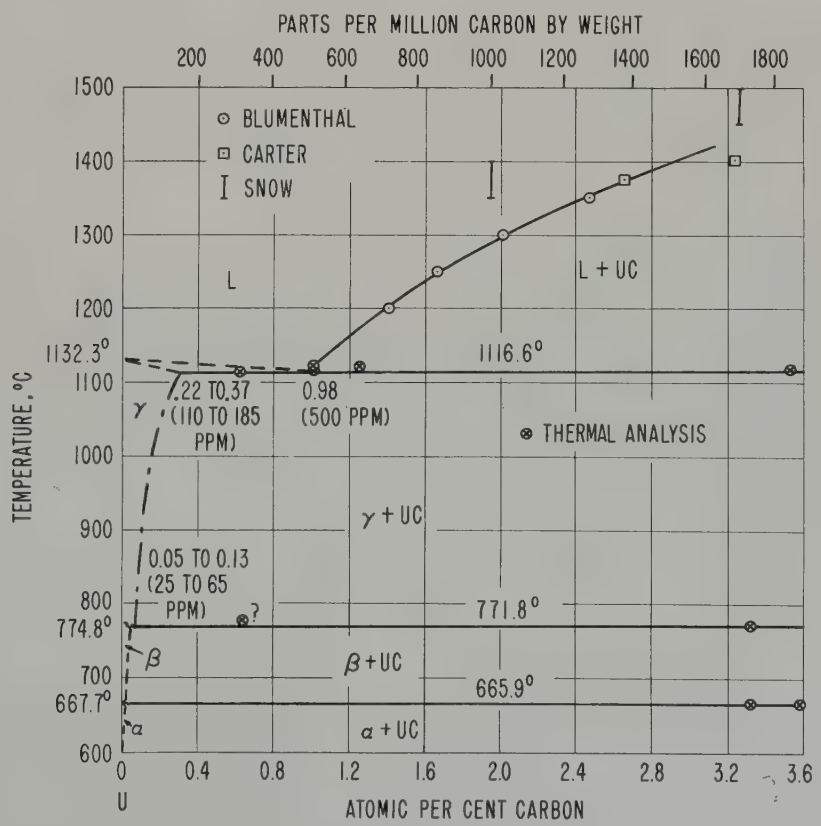

Fig. 8. Uranium-carbon phase diagram.

[3]) F. A. Rough and A. A. Bauer, Constitutional Diagrams of Uranium and Thorium Alloys (Addison Wesley Publ. Co., Reading, Mass., 1958)
[4]) J. J. Katz and E. Rabinowitch, The Chemistry of Uranium. Natl. Nucl. Energy Ser. Div. VIII, **5** (McGraw–Hill, New York, 1951)
[5]) A. I. Snow, Reports CT 954 (1943) and CT 1102 (1943) (USAEC. Technical Information Services Washington D.C.)
[6]) T. H. Carter, Report CT 609 (1943) (USAEC. Technical Information Services, Washington D.C.)
[7]) M. W. Mallet, A. F. Gerds and H. R. Nelson, J. Electrochem. Soc. **99** (1952) 197
[8]) A. J. Dahl and H. E. Cleaves, J. Res. Natl. Bur. Std. **43** (1949) 513
[9]) R. J. Dunworth, Unpublished data
[10]) B. Blumenthal, Argonne National Laboratory (USA) Report, ANL 5019 (1952). Also: Trans. AIME **203** (1955) 1199
[11]) Battelle Memorial Institute Reports CT 1697 and CT 1795 (1944) (USAEC. Technical Information Services, Washington DC)
[12]) B. Blumenthal, J. Nucl. Mat. **2** (1960) 23
[13]) C. Marzano and R. A. Noland, Argonne National Laboratory (USA) Report, ANL 5102 (1953)
[14]) B. Blumenthal and R. A. Noland, Progress in Nuclear Energy, Vol. 1, Series V (Pergamon Press, London, 1956) Ch. 1–6
[15]) B. Blumenthal, J. Nucl. Sci. Eng. **2** (1957) 407
[16]) B. C. Allen and S. Isserow, Acta Metallurgica **5** (1957) 465.

JOURNAL OF NUCLEAR MATERIALS 2, No. 3 (1960) 209–215, NORTH-HOLLAND PUBLISHING CO., AMSTERDAM

LATTICE SPACINGS IN THORIUM – YTTRIUM ALLOYS

D. S. EVANS and G. V. RAYNOR

Department of Physical Metallurgy, University of Birmingham, Birmingham 15, *UK*

Received 18 March 1960

Using all the precautions found to be necessary in previous work on the lattice spacings of very reactive alloy systems, the spacings for the face-centred cubic and close-packed hexagonal solid solutions based respectively on thorium and yttrium have been measured at a temperature of 25° C, following annealing at 750° C. The lattice spacings observed for yttrium were $a = 3.6441$, $c = 5.7358$ kX. Solution of thorium increases the c-spacing and decreases the a-spacing. By contrast the lattice spacing of thorium is only very slightly affected by the solution of yttrium. From the results of the lattice spacing measurements, and from those of a metallographic examination, the two-phase region between the cubic and hexagonal solid solutions extends from 49 to 69 at % yttrium. This is in conflict with the work of previous investigators (Eash and Carlson) and reasons for the discrepancy are discussed in terms of the effects of impurity on the relative stabilities of the two structures.

En utilisant toutes les précautions qui ont été trouvées nécessaires dans un travail précédent sur les paramètres de systèmes d'alliages très réactifs, les paramètres des solutions solides cubique à faces centrée et hexagonale compacte à base de thorium et d'yttrium ont été mesurées à 25° C après recuit à 750° C. Les paramètres mesurés pour l'yttrium étaient $a = 3{,}6441$ et $c = 5{,}7358$ kX. L'addition de thorium augmente le paramètre c et diminue a. Au contraire le paramètre du thorium n'est que très légèrement affecté par l'addition en solution solide de l'yttrium. Des résultats de ces mesures de paramètre et de ceux obtenues par examen métallographique, il en résulte qu'une région à deux phases existe entre les solutions solides cubiques et hexagonales extrêmes dans l'intervalle 49–69 atomes % d'yttrium. Ceci est en désaccord avec le travail de chercheurs antérieurs (Eash et Carlson) et les raisons de ce désaccord sont discutées en fonction des effets des impuretés sur les stabilités relatives des deux structures.

Unter Anwendung aller Vorsichtsmassnahmen, die sich bei früheren Arbeiten über die Gitterparameter von sehr reaktionsfreudigen Legierungssystemen als notwendig erwiesen haben, wurden die Gitterparameter von kubisch flächenzentrierten Mischkristallen auf der Thoriumseite und von hexagonal dichtest gepackten Mischkristallen auf der Yttriumseite gemessen. Die Mischkristallproben wurden bei 750° C geglüht und anschliessend bei 25° C untersucht. Für Yttrium wurden die Werte $a = 3{,}6441$ kX und $c = 5{,}7358$ kX ermittelt. Durch Lösen von Thorium werden die Abstände in c-Richtung vergrössert und in a-Richtung verkleinert. Demgegenüber wird der Gitterparameter von Thorium beim Zulegieren von Yttrium nur geringfügig beeinflusst. Nach den Ergebnissen der Gitterparametermessungen und nach einer metallographischen Untersuchung dehnt sich der Zweiphasenbereich zwischen den kubischen und hexagonalen Mischkristallen von 49 bis 65 At % Yttrium aus. Diese Angabe steht in Widerspruch zu früheren Befunden (Eash und Carlson). Die bestehenden Unterschiede werden als Folge von Verunreinigungen diskutiert, welche sich auf die Stabilität der beiden Strukturen auswirken.

1. Introduction

As part of a general programme on the alloying behaviour of thorium, lattice spacings in the thorium-yttrium system have been determined for comparison with the thorium-cerium [1]) and thorium-lanthanum [2]) systems previously investigated. In both these systems, at a temperature of 675° C, continuous series of solid solutions are found since the component metals have similar atomic diameters and the same (face-centred cubic) structure. Yttrium is similar to both cerium and lanthanum in atomic dia-

meter and in general chemical characteristics, but differs in that it exists in the close-packed hexagonal structure to a temperature near to its melting point. Therefore, while appreciable mutual solubility between thorium and yttrium would be expected, complete miscibility between the room temperature allotropes is impossible. This was recently confirmed by the work of Eash and Carlson [3]), who showed, while the present work was in progress, that the central two-phase region existed at compositions between approximately 39.5 and 52.8 at % yttrium. Preliminary results available at that time indicated appreciable differences both in the position of this two-phase region and also in the lattice spacings in the α-yttrium field; these have subsequently been confirmed.

2. Experimental Methods

The following materials were used:

(a) Van Arkel (iodide) thorium, for which a typical analysis showed 0.02 wt % carbon, less than 0.1 wt % metallic impurities, 0.01 wt % nitrogen and 0.01 wt % oxygen. This material was kindly supplied by AERE, Harwell.

(b) Yttrium, supplied by Messrs. Johnson Matthey and Co., Ltd., London, which was prepared by the reduction of spectroscopically standardised oxide. Except for 0.03 wt % iron, this material contained negligible amounts of metallic impurities.

Both materials were arc-melted before alloying to remove any volatile impurities.

Alloys were prepared in a non-consumable electrode arc-furnace previously evacuated to below 10^{-5} mm Hg through a diffusion/rotary pump combination. Specimens, weighing one to three grams, were melted in an atmosphere of approximately 15 cm argon which had been previously purified by melting a zirconium button and maintaining it molten for five minutes. Weight loss during melting was in general less than 0.5 wt %. Preliminary experiments indicated that this was almost entirely due to volatilisation of yttrium, which was therefore later allowed for in calculating the compositions. Check chemical analyses confirmed that these corrected compositions were satisfactory for use, and were within the maximum experimental error of $\pm$ 1 at % for alloys prepared by successive dilution. Alloys containing high proportions of yttrium were examined first, and then diluted with thorium; precautions were taken to guard against excessive increases in impurity levels and cumulative errors in composition.

Homogenisation was carried out for 14 days at 1000° C; the specimens were wrapped in degassed tantalum sheet and sealed two or three at a time in silica capsules degassed and evacuated to 2×10^{-6} mm Hg. As the lattice spacings of the alloys showed a slight variation with annealing temperature, which was probably due to the change in solubility of impurities, the alloys were given a final homogenisation treatment for several days at the temperature chosen for the strain relief of filings for X-ray examination, namely 750° C.

The techniques adopted for the preparation of annealed filings of the alloys for X-ray examination were the same as used for the thorium-lanthanum system [2]), which were developed following the study of the effects of annealing conditions on the lattice spacing of iodide thorium by Evans and Raynor [4]). This work showed that great care was necessary to avoid contact with the air at all stages in the preparation and annealing of filings previous to their examination by diffraction techniques. In addition contamination could also occur, in filings annealed in open trays, from the furnace atmosphere, possibly by silicon or carbon; this contamination could be completely prevented by enclosing the filings during the heat-treatment in tantalum containers. These were made by rolling up 0.08 mm thick sheet on a 3 mm diameter former, the ends being sealed by folding. Immediately before use the containers were degreased and outgassed at 950° C.

Filings were prepared and transferred to the tantalum container which was then sealed; all these operations were carried out under carbon tetrachloride. The boat and its contents were

quickly transferred to an outgassed annealing furnace tube capable of continuous evacuation, and the remaining carbon tetrachloride was evaporated through a separate vacuum pump, before the main pumps were connected. The heat-treatment, for two hours at 750° C, then followed, the rate of heating to the annealing temperature being controlled to prevent any rise in pressure above 5×10^{-5} mm Hg. Thereafter the vacuum in the system improved to 5×10^{-6} over 20 to 30 minutes, reaching 2×10^{-6} mm Hg after 60 minutes. At the end of such treatments, the filings were rapidly cooled by removing the furnace, and immediately made into Debye–Scherrer specimens by coating on to greased silica fibres. There was no evidence that any significant contamination of the filings took place during exposure to X-rays. In addition, diffraction patterns of the alloys were obtained from filings in the as-prepared and in a partially annealed condition. In certain cases slivers were cut from the massive homogenized alloys using the minimum of force; the diffraction patterns of these were also examined, but showed no differences from those of filings.

X-ray diffraction patterns were obtained at 25° C using a Philips Debye–Scherrer camera of diameter 11.483 cm, in which the specimens were exposed to copper K_α radiation ($\lambda_{\alpha_1} = 1.537\,395$ kX; $\lambda_{\alpha_2} = 1.541\,232$ kX). Satisfactory high angle diffractions were observed, and systematic errors were eliminated by the use of the Nelson–Riley [5]) extrapolation function. Correction was also made for refraction by the method of Wilson [6]). The reproducibility of lattice spacings for alloys in the α-thorium (face-centred cubic) field was within the limits $\pm$ 0.0002 kX. For alloys with a hexagonal structure, the reproducibility was less satisfactory ($\pm$ 0.001 kX). However, only a small proportion of this (0.0002 kX) was due to errors in measuring the diffraction pattern.

3. The Lattice Spacings of the Pure Metals

A summary of lattice spacings of face-centred cubic thorium reported by earlier workers has recently been made by Evans and Raynor [4]). The spacing of the iodide thorium used to prepare the present alloys was 5.0744 ± 0.0002 kX, for filings stress-relieved for two hours at 750° C, which is in good agreement with the value previously obtained by Evans and Raynor, and James and Straumanis [7]) (5.0741 $\pm$ 0.0002 kX) for similar material.

Table 1 summarizes the available data for the lattice spacings of close-packed hexagonal yttrium for comparison with the values obtained in the present work; where necessary spacings originally given in Å units have been converted to kX units by dividing by the factor 1.002 02. There is reasonable agreement between the results obtained in the present work and those of Spedding, Daane and Herrman [10]), but the agreement with the results of other workers is less satisfactory. In view of the chemical reactivity of yttrium, the latter values are possibly affected by appreciable contamination.

The diffraction patterns of yttrium, and also of all alloys with a hexagonal structure, con-

Table 1
The lattice spacings of α-yttrium

Preparation and purity	Lattice spacings (kX)			Year	Refer.
	a	c	c/a		
Reduction of 99.5 % pure oxide	3.663	5.814	1.588	1932	[8])
Reduction of chloride with alkali metal	3.629	5.750	1.585	1939	[9])
99.4 %	3.6400 $\pm$ 0.0007	5.7190 $\pm$ 0.0008	1.5712	1956	[10])
Reduction of fluoride with calcium	3.659 $\pm$ 0.001	5.785 $\pm$ 0.001	1.581	1959	[3])
99.9 %	3.6441 $\pm$ 0.0002	5.7358 $\pm$ 0.0004	1.5740 $\pm$ 0.0002	Present Work	

tained weak extra lines at low angles which indexed satisfactorily on the basis of a unit cell with the same a spacing as the main pattern, but having an axial ratio twice as large. The corresponding lines at higher angles which would be expected if the whole lattice were double spaced in the c direction, were not present in the diffraction pattern. It appears, therefore, that in yttrium and its alloys the lattice consists mainly of the ABAB . . . sequence of close-packed hexagonal planes but with some ABAC . . . faulting. The tendency of metals of the rare-earth type to have the latter form of packing is well illustrated by, for example, α-lanthanum and neodymium [10]).

4. Thorium – Yttrium Alloys. Experimental Results

Twenty four alloys covering the whole range of compositions, together with the pure metals, were prepared and examined using the techniques described above. Lattice spacing measurements obtained at 25° C from filings stress relieved for two hours at 750° C are tabulated in Appendix 1 and summarised for comparison with the results of Eash and Carlson [3]) in fig. 1.

The scatter in the lattice spacings of alloys lying in the α-thorium field is approximately $\pm$ 0.0002 kX; since the effect of small errors in composition is negligible, it is clear that errors arising from contamination of the alloys, and in the measurement of the diffraction patterns are within these limits. In the hexagonal α-yttrium field, the reproducibility of lattice spacings from alloy to alloy is generally satisfactory; excepting three results at a composition of approximately 89 at % yttrium, the scatter is within $\pm$ 0.001 kX. Only a small proportion of this (0.0002 kX) can be attributed to errors in measuring the diffraction patterns. As repeated heat-treatments, in some cases prolonged to 13 hours, have a negligible effect on lattice spacings, the scatter is unlikely to be due to contamination in the preparation of the annealed filings. In addition further alloys prepared from those showing a large scatter have spacings close to those expected by comparison

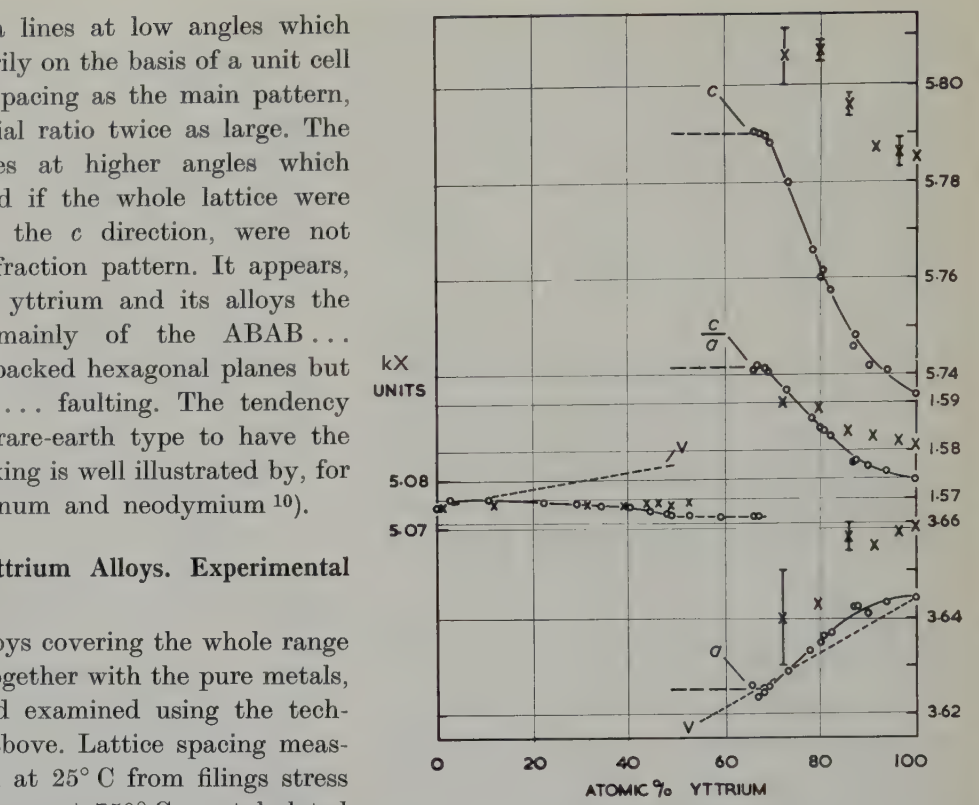

Fig. 1. Lattice spacings of the thorium-yttrium alloys.
○ present work. × according to Eash and Carlson [3]).

with other alloys. The reason possibly lies in the influence of stacking faults, and these are also considered to be partly the reason for the much greater scatter in the spacings of alloys lying in the central two-phase region. The use of copper radiation, while providing an abundance of high angle diffraction lines for both α-thorium and α-yttrium alloys, also causes difficulties in the distinction of the overlapping patterns in this region, and results in further uncertainty in the lattice spacing values. A similar scatter in the lattice spacings of the α-thorium phase in this region was also observed by Eash and Carlson [3]).

The diffraction patterns of filings containing a high proportion (approximately 75 at % or more) of yttrium, when examined in the as-prepared or partially annealed condition, showed a blurred but complete hexagonal pattern. However, alloys close to the α-yttrium phase boundary, when examined in the same con-

dition, showed a weak and incomplete hexagonal pattern at lower diffraction angles only, together with a reasonably well defined face-centred cubic pattern. This indicates the relative ease with which yttrium alloys in this range of compositions may suffer a considerable amount of stacking faulting on severe cold working, and that the difference in stability between the hexagonal and face-centred cubic structures in this region is marginal. The presence of less severe stacking faults in other hexagonal yttrium-rich alloys may also account for the scatter in the lattice spacings referred to above, although in view of the relative independence of the spacing on the duration of heat-treatment of the filings, this effect generally must be small.

The addition of yttrium reduces the lattice spacing of thorium slightly, except for an initial slight increase. The latter is considered to be due to contamination of the alloys by nitrogen, of which the yttrium appears to contain an appreciable amount. Alloys containing more than a few at % yttrium are probably saturated with this gas, although there was insufficient present as nitride for its pattern to be visible on the diffraction patterns of the alloys. The lattice spacings of the thorium-rich alloys extrapolate back to a value of approximately 5.078 kX, which corresponds, within the limits of extrapolation, to thorium completely saturated with nitrogen. Analogous behaviour is found in thorium-lanthanum alloys [2]).

Following from the large difference between the lattice spacings of yttrium in the present work, and that used by Eash and Carlson [3]), there is a corresponding difference in the lattice spacings of alloys lying in the α-yttrium field, although the forms of the lattice spacing/composition curves are similar. The yttrium used by the latter workers contained 0.05 wt % carbon and 0.01 wt % nitrogen, both of which would be expected to increase the lattice spacings of the metal. These impurities, together with accidental variations in the degree of contamination during the preparation of annealed filings, are possibly responsible for the generally large spacings and scatter in the results reported by these workers. The good agreement between the lattice spacings of alloys in the α-thorium field supports the interpretation given above that these alloys are saturated by small quantities of nitrogen; further contamination by this gas introduced either by alloying with yttrium containing a higher proportion of this gas, or during preparation of filings of the alloys, would then have no effect on the lattice spacings.

The lattice spacing results indicated that the central two-phase region lay between 49 and 69 at % yttrium, and these values were confirmed by metallographic examination of the alloys. This is in marked contrast with the results of Eash and Carlson, who obtained limits at approximately 39.5 and 52.8 at % yttrium, a difference of approximately 9.5 and 16.2 at % respectively.

5. Discussion

In general, "Vegard's Law" curves for metallic systems may be derived by calculating the equivalent spacings of the metals for the different structures. In the thorium-yttrium system, this procedure is difficult, since there are two close distances of approach of atoms in the yttrium structure. If, however, it is assumed that the lattice spacings of a hypothetical face-centred cubic form of yttrium would be approximately $\sqrt{2}$ times the mean closest distance of approach of atoms in the hexagonal structure, the value obtained is 5.092 kX, which is 0.34 % greater than the lattice spacing of thorium. Similarly, the "a" spacing of a hypothetical hexagonal form of thorium would be approximately 3.588 kX, as compared with the value of 3.6441 kX for the a spacing of yttrium. Alloys in the α-thorium field then show a negative deviation from the linear Vegard's Law curve calculated in this way, and shown as the dotted line marked "V" in fig. 1; the solution of thorium in yttrium results in a corresponding small initial positive deviation. These deviations are comparable in magnitude and sign with those observed for thorium-lanthanum alloys [2]). The positive deviation from approximately

75 at % to 100 at % yttrium may be attributed to the solution of 4-valent thorium in 3-valent yttrium; such positive deviations are common when the valency of the solute exceeds that of the solvent [11]). Conversely, the negative deviation in the thorium-rich alloys may be interpreted in terms of the solution of an element of lower valency than that of the solvent.

The main difference between the present results and those of Eash and Carlson lies in the position of the two-phase region between the cubic and hexagonal solid solutions. The small difference in stability between cubic and hexagonal structures in metals of the rare earth type is well known; for example, the dependence of the structures of cerium and lanthanum on purity and thermal history has been shown in the recent reviews and experiments of Weiner and Raynor [12]) and Ziegler, Young and Floyd [13]) respectively to be very complex. Although yttrium has not been investigated in such detail, evidence obtained in the present work that hexagonal alloys close to the α-yttrium phase boundary can be converted into the face-centred cubic form by heavy cold work also indicates that the difference in the stability of the two structures must be small. Since yttrium and thorium are very similar in atomic diameter and chemical characteristics, the free energy/composition curves for thorium-yttrium alloys would be expected to be very shallow, and the effect of contamination on these curves may be considered. Evidence has been presented which suggests that the thorium-rich solid solution is already saturated with nitrogen, so that further contamination would have no appreciable effect on the free energy/composition curve. There is, however, no evidence that the solid solution based on yttrium is saturated; the introduction of further impurity into this reactive solid solution may thus produce a stable ternary solid solution, for which the free energy is lower than for the binary alloys. The effect of this would be to lower the effective free energy/composition curve for the hexagonal alloys relative to that for the thorium-rich solid solution. Because both curves are expected to be shallow, the position of the two-phase region would be strongly dependent on the purity of the alloys; a small lowering of the curve for the hexagonal alloys would tend to shift both boundaries of the two-phase region towards the thorium-rich side of the equilibrium diagram, and it is suggested that the phase boundaries given by Eash and Carlson have been affected in this way by impurity, either in the yttrium used, or as a result of contamination. As discussed in an earlier section, the higher lattice spacings obtained by Eash and Carlson for alloys in the α-yttrium field may also be considered to be due to contamination; the

Appendix 1

Compositions and lattice spacings of thorium-yttrium alloys

Composition at %	Lattice spacings * (kX) at 25° C			Axial ratio
	f.c.c. a	Hex. a	Hex. c	
0	5.0744			
3.0	5.0762			
11.3	5.0761			
22.4	5.0756			
29.6	5.0753			
34.6	5.0748			
40.6	5.0745			
44.7	5.0735			
48.6	5.0732 ± 5			
49.2	5.0728 ± 5			
53.4	5.0729 ± 5	(3.60)		(1.59)
59.6	5.0723 ± 5	(3.60)		(1.59)
66.6	5.0725 ± 5	3.6260	5.7907	1.5970
67.4	5.0725 ± 5	3.6235	5.7904	1.5980
68.7		3.6247	5.7897	1.5973
69.6		3.6257	5.7884	1.5965
73.4		3.6288	5.7800	1.5928
78.6		3.6334	5.7658	1.5869
80.2		3.6349	5.7602	1.5847
80.9		3.6364	5.7619	1.5845
82.4		3.6369	5.7576	1.5831
87.1		3.6426	5.7458	1.5774
87.6		3.6424	5.7481	1.5781
90.2		3.6410	5.7419	1.5770
93.9		3.6433	5.7407	1.5757
100		3.6441	5.7358	1.5740

* Obtained for filings annealed for two hours at 750° C, and then rapidly cooled to room temperature.

interpretation of the position of the two-phase field given above tends to confirm this suggestion.

Acknowledgements

Grateful acknowledgement is made to the United Kingdom Atomic Energy Authority for the general support given to this work, and to the General Electric Company Limited, UK, for the award of a research scholarship to one of us (D.S.E.). We would like to thank Mr. T. B. Merryfield for his valuable help with the experimental work.

References

[1]) R. T. Weiner, W. E. Freeth and G. V. Raynor, J. Inst. Metals **86** (1957/58) 185

[2]) D. S. Evans, G. V. Raynor and R. T. Weiner, J. Nucl. Mat. **2** (1960) in the press

[3]) D. T. Eash and O. N. Carlson, Trans. Amer. Soc. Metals Preprint **52** (1959) 142

[4]) D. S. Evans and G. V. Raynor, J. Nucl. Mat. **1** (1959) 281

[5]) J. P. Nelson and D. P. Riley, Proc. Phys. Soc. **57** (1945) 160

[6]) A. J. C. Wilson, Proc. Cambridge Phil. Soc. **36** (1940) 485

[7]) W. J. James and M. E. Straumanis, Acta Cryst. **9** (1956) 376

[8]) L. L. Quill, Z. anorg. Chem. **208** (1932) 59

[9]) H. Bommer, Z. Electrochem. **45** (1939) 357

[10]) F. H. Spedding, A. H. Daane and K. W. Herrman, Acta Cryst. **9** (1956) 559

[11]) G. V. Raynor, Trans. Faraday Soc. **45** (1949) 698

[12]) R. T. Weiner and G. V. Raynor, J. Less Common Metals **1** (1959) 309

[13]) W. T. Ziegler, R. A. Young and A. L. Floyd, J. Amer. Chem. Soc. **75** (1953) 1215

JOURNAL OF NUCLEAR MATERIALS 2, No. 3 (1960) 216–224, NORTH-HOLLAND PUBLISHING CO., AMSTERDAM

EFFETS DE L'HYDROGENE SUR LES CARACTERISTIQUES DE RUPTURE PAR TRACTION D'ACIERS INOXYDABLES

R. BLANCHARD, J. PELISSIER et M. PLUCHERY

Centre d'Etudes Nucléaires de Grenoble, France

Reçu le 10 mars 1960

On étudie les effets de l'hydrogène sur des aciers inoxydables, qui sont des matériaux de gainage possibles pour des réacteurs utilisant l'hydrogène comme gaz de refroidissement. On montre que la charge apparente de rupture à la traction n'est plus que 80 % de sa valeur initiale lorsque la teneur en hydrogène atteint 50 cc TPN/100 g, et que la striction passe dans ces conditions de 80 % à 55 %. L'examen microfractographique qui a été effectué avec succès par une technique de double réplique malgré la petitesse des échantillons (ϕ 0,3 mm environ), révèle que tout en gardant un caractère ductile, l'aspect des surfaces de rupture évolue notablement avec la teneur en hydrogène.

This paper deals with the effects of hydrogen on stainless steel, which is a possible canning material in hydrogen-cooled reactors. Apparent ultimate tensile strength is only 80 % of the initial value for a hydrogen content of about 50 cc NTP/100 g and reduction in area decreases from 80 % to 55 %. A special two-stage replica technique has been developed which allows fracture surfaces of small tensile specimens (about 0.3 mm dia.) to be examined by electron microscopy. All the specimens showed evidence of ductile character throughout the range of hydrogen contents investigated, but the aspect of the fracture surface gradually changes with increasing hydrogen content.

Es wurde der Einfluss von Wasserstoff auf Edelstahl mit Hinsicht auf die eventuelle Verwendung als Hülsenmaterial in einem wasserstoffgekühlten Reaktor untersucht und diskutiert. Aus den vorliegenden Versuchen geht hervor, dass die Wasserstoffaufnahme eine merkliche Änderung der Zugeigenschaften bewirkt. Bei einer 50 cm³/100 g Wasserstoffaufnahme wird die Bruchlast auf 80 % ihres ursprünglichen Wertes und die Brucheinschnürung von 80 % auf 55 % herabgesetzt. Trotz den geringen Abmessungen der Zugstäbe ist es gelungen, Bruchflächen durch ein spezielles Abdruckverfahren elektronmikroskopisch zu beobachten. Obwohl sich die Bruchflächen keinen spröden Charakter zeigen, lässt sich jedoch eine kontinuierliche Änderung ihres Aussehens mit zunehmendem Wasserstoffgehalt einwandfrei feststellen.

1. Introduction

L'utilisation de l'hydrogène comme fluide d'échange dans les réacteurs nucléaires présenterait d'incontestables avantages. On montre par exemple [1]) que pour une géométrie du réacteur identique, une même température du cœur, la pression du gaz caloporteur et la puissance de soufflage étant inchangées, il serait possible de multiplier par un facteur de l'ordre de 3,5 la quantité de chaleur extraite en utilisant l'hydrogène au lieu du gaz carbonique comme fluide de refroidissement. Comme les frais fixes d'installation sont estimés être les mêmes dans les deux cas, on voit que l'on peut attendre de l'utilisation de l'hydrogène une diminution importante de l'investissement rapporté au kW installé.

Parmi les problèmes posés par l'utilisation de l'hydrogène, un des plus importants est celui de sa compatibilité avec les éléments constitutifs du réacteur (modérateur, matériaux de structure, de gaînage, etc.) et peu de choses sont encore connues à ce sujet.

Le travail que nous présentons ici fait partie d'une étude plus vaste consacré à ces problèmes. Il a pour objet de préciser l'action de l'hydrogène sur le comportement d'aciers inoxydables qui peuvent constituer en particulier un maté-

riau de gaînage intéressant pour un fonctionnement à température élevée. Des deux aspects de l'influence de l'hydrogène: décarburation, et "fragilisation" à la suite de l'absorption de quantités importantes d'hydrogène par le métal, nous nous limitons ici au second.

On sait que la solubilité de l'hydrogène dans les aciers inoxydables est notable: elle atteint par exemple, sous pression normale, des valeurs de 5 à 7 cc TPN/100 g entre 700 et 1000° C [2]). Ces quantités deviennent plus considérables sous les pressions de 10 à 20 atmosphères qui sont envisageables pour le fonctionnement de réacteurs refroidis à l'hydrogène. Par refroidissement brusque, l'hydrogène reste en sursaturation dans le métal et peut le "fragiliser". En ce qui concerne les aciers inoxydables qui sont réputés être les moins affectés, certains auteurs [3]) les considèrent comme insensibles, tandis que d'autres [4]) ont mis en évidence une diminution de la capacité de déformation du métal due à l'absorption d'hydrogène lorsque cette dernière est suffisamment importante.

Au cours du fonctionnement d'un réacteur nucléaire, ses éléments constitutifs, et en particulier les matériaux de gaînage peuvent être soumis à des échauffements et refroidissements rapides. Il importe donc de bien définir l'influence sur les caractéristiques mécaniques de l'hydrogène retenu dans le métal à la suite de ces cycles thermiques en étudiant une gamme de concentrations en hydrogène la plus large possible.

2. Méthodes Expérimentales

2.1. Acier étudié et types d'éprouvettes

L'acier étudié est du type Tophet 302, c'est-à-dire un acier 18/10 sans addition. Sa composition en dehors du chrome et du nickel qui existent en teneurs égales à la composition nominales, est la suivante: Mn 1,23 %, Si 1,1 %, Cu 0,08 %, C 0,12 %, en poids.

Les essais ont tous été effectués sur les fils de diamètre 0,4 mm. Nous avons choisi cette forme d'échantillon, malgré les délicates mises au point qu'elle a nécessitées en matière d'essais mécaniques (surtout mesure de striction) et d'examens au microscope électronique, parce qu'elle met en jeu de faibles quantités de matière, ce qui est intéressant pour les essais en pile ultérieurs, et aussi parce qu'elle a permis de résoudre de façon simple le problème du chauffage des échantillons, et par voie de conséquence celui du dosage de l'hydrogène mis en jeu. D'autre part ce faible diamètre favorise la diffusion et évite des différences de concentration du gaz dans le métal.

2.2. Mode de chargement

Pour introduire dans l'acier les quantités d'hydrogène nécessaires à l'étude des effets sur les propriétés mécaniques deux méthodes peuvent être utilisées: le chargement sous pression à chaud ou bien le chargement cathodique à froid. Nous avons préféré cette dernière méthode qui nous permet d'introduire jusqu'à 50 cc d'hydrogène par 100 g de métal à l'aide d'un matériel plus simple. Il évite d'autre part tout risque de décarburation du métal et permet l'étude de la "fragilisation" à l'état pur.

Le chargement cathodique est effectué de la façon suivante: le fil de 0,4 mm de diamètre et de 20 cm de long est placé à la cathode, l'anode est un fil de platine, l'électrolyte une solution d'acide sulfurique à 10 %. Nous nous sommes abstenus d'ajouter au bain des catalyseurs (soufre, arsenic, antimoine), de façon à éviter une action fragilisante parasite de ces éléments qui viennent se placer aux joints de grain [5]). Nous avons choisi une densité de courant de 100 mA/cm^2, après avoir fait une étude de la quantité d'hydrogène absorbée en fonction de la densité de courant. Cette valeur nous a conduits à des temps assez courts (80 heures) pour l'introduction de quantités d'hydrogène importantes (50 cc/100 g).

2.3. Dosages

L'hydrogène a été dosé par diffusion à l'état solide, c'est-à-dire chauffage du fil par effet Joule à une température de 950° C, séparation de l'hydrogène par une aiguille de palladium et mesure des variations de pression dans le

volume connu de la cellule d'analyse au moyen d'une jauge classique de MacLéod. L'utilisation des fils de 0,4 mm présente un grand avantage: seul le fil est chauffé par effet Joule, l'enceinte elle-même ne l'étant pas. Il n'y a ainsi pas de dégazage notable des parois au cours du dosage, ce qui nous permet d'avoir des essais "à blanc" négligeables.

2.4. Essais mécaniques

Les mesures de charge de rupture à la traction et de striction permettant d'étudier l'influence de l'hydrogène sur les propriétés mécaniques ont été effectuées avec une micromachine de traction Chevenard, la vitesse d'allongement étant 0,6 mm/minute.

Sur les échantillons rompus, la striction est mesurée de la façon suivante: sur un petit bâti en matière plastique placé sous une lunette binoculaire, nous procédons à une reconstitution de la microéprouvette, et l'immobilisons ensuite avec du mastic. L'éprouvette reconstituée est photographiée suivant deux plans à 90°. Les épreuves sont examinées à l'agrandisseur et nous permettent d'obtenir le diamètre avec une bonne précision: 0,5 % dans le cas le plus défavorable, ce qui donne une erreur maximum de 1 % sur la striction.

3. Observation de la Surface des Cassures au Microscope Electronique

Nous nous sommes inspirés de la méthode de double empreinte rhodoïd-carbone mise au point par Azam [6]). L'application s'est heurtée à de sérieuses difficultés par suite des dimensions extrêmement réduites des éprouvettes de traction (petitesse dont les raisons ont été exposées plus haut). Après fracture, le diamètre de la partie utile de l'éprouvette n'excède guère 0,3 mm et son relief très accidenté n'est guère favorable à l'exécution d'une réplique.

Après enrobage de l'éprouvette dans une matière plastique insoluble dans l'acétone (polyvinyle), et lavage de la surface de fracture on exécute une réplique au rhodoïd selon la méthode classique: on obtient alors l'empreinte de l'enrobage au milieu de laquelle on distingue l'empreinte de la cassure. La réplique de rhodoïd est recouverte d'un film de carbone d'une centaine d'Ångströms. Le film doit être d'autant plus épais que le relief est plus accidenté. La partie utile de la réplique correspondant à peu près à la surface d'une grille, est alors renforcée par une goutte de colle †.

Après séchage de la colle, le rhodoïd est dissous dans l'acétone et le film de carbone renforcé par la colle se détache; l'opération est assez longue et c'est d'elle que dépend la propreté de la préparation. Il faut deux heures pour dissoudre parfaitement le rhodoïd et il faut laver encore pendant 1 heure en renouvelant 2 ou 3 fois l'acétone. Pendant cette opération, l'échantillon doit être agité en permanence.

La colle est éliminée par dissolution dans l'eau à 80°. Le film, lavé à l'eau distillée, est recueilli sur une grille et ombré au chrome.

3.1. Observation du relief sur les micrographies

La combinaison du procédé classique d'ombrage au chrome et de la méthode stéréoscopique, telle qu'on peut la pratiquer sur l'Elmiskop I Siemens, permet l'appréciation visuelle du relief et sa mesure ††.

Les accidents de relief de grande amplitude sont évalués par stéréoscopie, à la suite de quoi on peut déterminer la direction d'ombrage, et enfin la nature des accidents secondaires.

Etant donnée l'irrégularité des accidents étudiés, il serait sans objet de vouloir déterminer leur amplitude avec précision. Les erreurs

† La colle doit être soluble dans l'eau et insoluble dans l'acétone: on peut employer par exemple la "Seccotine".

†† Le procédé stéréoscopique seul ne permet la vision exacte du relief que si l'objet présente des détails contrasté que l'on peut identifier sur les 2 images, ce qui n'est pas le cas pour un film de carbone sans ombrage. D'autre part, l'ombrage seul ne peut renseigner sans ambiguité sur le relief que si la direction de projection du métal est connue: on aurait également pu s'aider de particules de relief connu (sphères de latex ou même débris de film de carbone).

diverses [7]) qui affectent les différences de niveau de 10 % au maximum, peuvent donc être négligeables.

4. Résultats Expérimentaux

Les résultats concernant les caractéristiques mécaniques sont portés dans le tableau 1 et sur les graphiques (figs. 1 et 2) donnant la charge apparente de rupture (rapportée à la valeur initiale) et la striction en fonction de la quantité d'hydrogène absorbée.

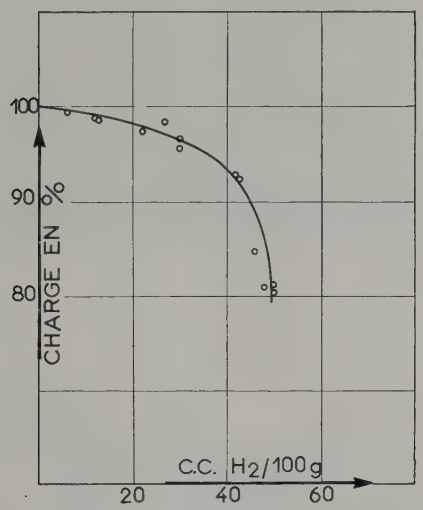

Fig. 1. Evolution de la charge de rupture en fonction de la teneur en hydrogène.

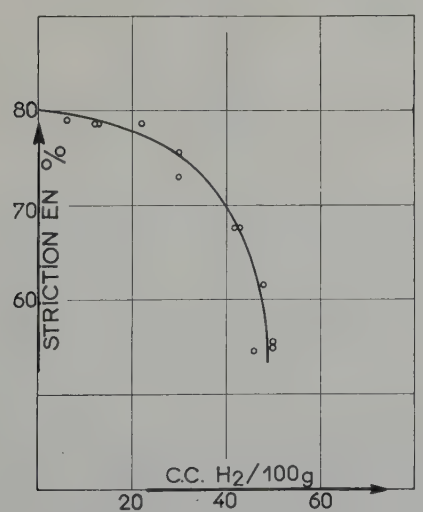

Fig. 2. Evolution de la striction en fonction de la teneur en hydrogène.

Tableau 1

cc H_2 par 100 g de métal	Charge apparente de rupture % de la charge initiale	Striction en %
0	100	80
6	99,5	79
12	98,7	78,5
13	98,5	78,5
22	97,4	78,5
27	98,3	74,5
30	96,7	75,5
30	95,6	73
42	92,8	67,6
43	92,4	67,6
46	84,8	54,6
48	80,9	61,6
50	81,1	55,7
50	80,4	55,7

La charge de rupture, jusqu'à une teneur en hydrogène d'une quarantaine de centimètres cubes par 100 g de métal, est peu affectée: elle présente une diminution de 6 % seulement par rapport à la valeur initiale. Au delà de 40 cc par 100 g, l'action de l'hydrogène devient importante, la charge de rupture est diminuée de 20 % pour 50 cc d'hydrogène.

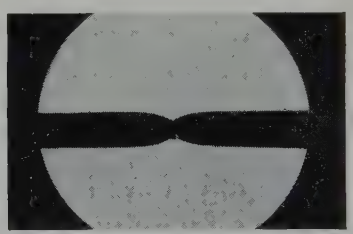

Fig. 3. Striction à la rupture. Teneur en hydrogène de l'échantillon: nulle.

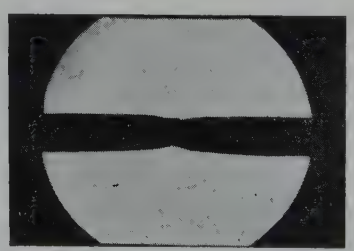

Fig. 4. Striction à la rupture. Teneur en hydrogène de l'échantillon: 50 cc TPN/100 g.

La striction, ainsi que l'ont montré Hobson et Hewitt [4]) est peu affectée jusqu'à 25 cc par 100 g; elle passe de 80 % à 76,5 %, mais pour les teneurs plus élevées que nous avons atteintes, l'effet sur la striction est plus important que sur la charge de rupture: on obtient des valeurs de 69 % pour 40 cc et de 55 % pour 50 cc. On peut voir sur les photos 3 et 4, deux types de fracture: sans hydrogène (fig. 3) et avec une teneur en hydrogène de 50 cc (fig. 4). Les différences de section à la cassure sont très nettes.

4.1. Résultats des observations microfractographiques

1) Toutes les microfractographies effectuées ont révélé un *faciès ductile à cupules juxtaposées* et aucune rupture fragile ou intergranulaire n'a pu être mise en évidence. Il faut donc admettre que même les éprouvettes considérées comme fragiles d'après les essais macroscopiques (allongement et striction faible) subissent à l'échelle microscopique une rupture de type ductile.

2) Les cupules sont plus ou moins allongées et leur aspect peut paraître *a priori* différer d'un échantillon à l'autre et d'une plage à l'autre d'un même échantillon; cependant l'allongement et l'orientation des cupules restent constants dans des domaines assez étendus. Si l'on admet avec Plateau *et al.*[8,9]), que les cupules s'amorcent par décohésion suivant un plan de glissement, cette diversité d'aspects traduirait simplement des variations dans l'orientation relative de la surface de fracture et de la direction de traction, et ne serait nullement caractéristique de modes de rupture différents: dans les zones où la contrainte principale est fortement inclinée sur la surface de fracture, la rupture par cisaillement donnerait des cupules très allongées (fig. 5), tandis que celles où la traction s'est exercée presque normalement présenterait des cupules grossière-

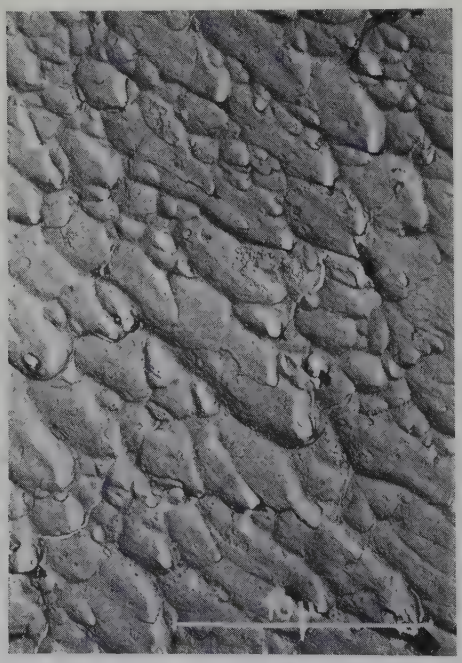

Fig. 5. Acier inoxydable chargé à 50 cc/100 g.

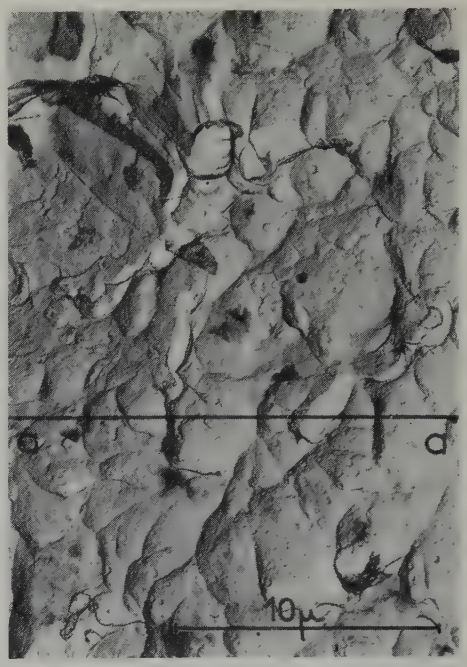

Fig. 6. Acier inoxydable chargé à 50 cc/100 g.

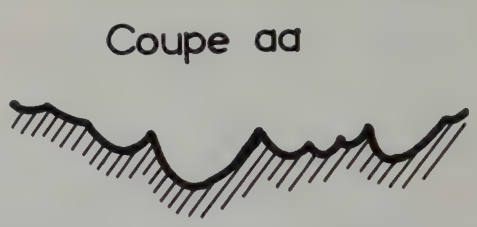

Fig. 6 bis. Coupe montrant le relief de l'échantillon fig. 6.

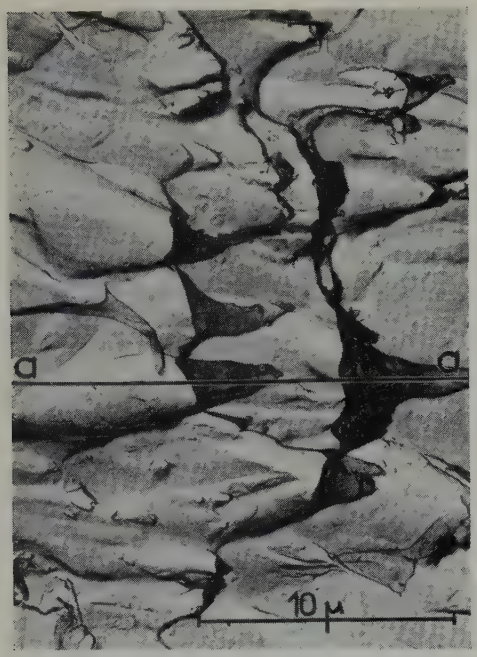

Fig. 7. Fer Armco.

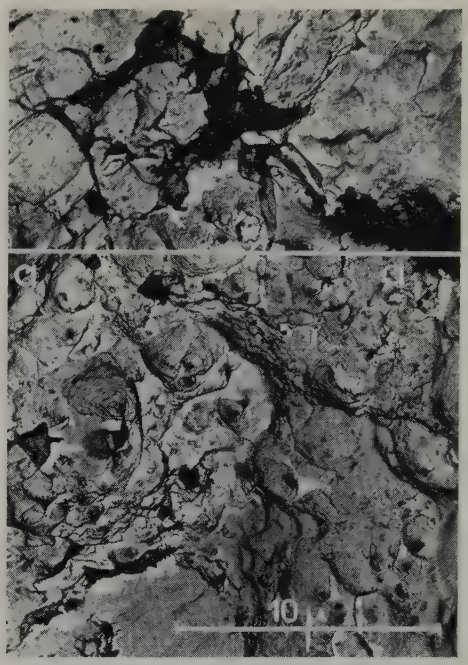

Fig. 8. Acier inoxydable non traité.

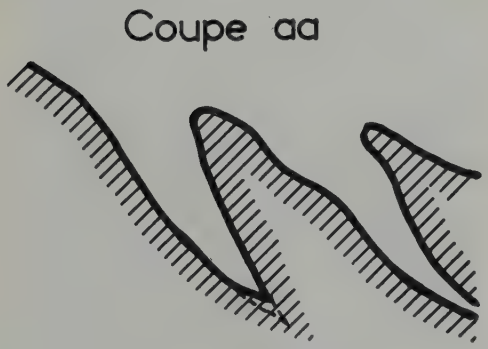

Fig. 7 bis. Coupe montrant le relief de l'échantillon fig. 7.

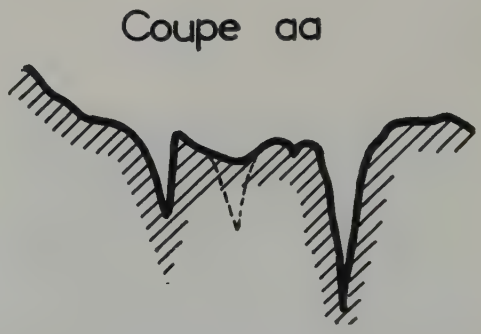

Fig. 8 bis. Coupe montrant le relief de l'échantillon fig. 8.

ment hémisphériques (figs. 6 et 6 bis). Cette interprétation est en accord avec les observations de Bernshtein *et al.*[10]).

3) La taille des cupules est indépendante du degré de fragilisation, mais selon toute vraisemblance liée à la grosseur du grain. Des micrographies optiques complétées par un examen aux rayons X ont révélé un grain de 1 à 5 μ, homogène dans un même échantillon, soit du même ordre que les cupules. Cependant, leur aspect change avec la fragilisation, évoluant entre deux extrèmes:

a) les éprouvettes non traitées présentent un faciès comparable à celui du fer ARMCO (figs. 7 et 7 bis), exemple type de matériau subissant la rupture ductile; la forme en cupules est conservée, mais leur profondeur qui peut atteindre cinq fois leur diamètre justifierait plutôt le terme de "cratère" (figs. 8, 8 bis et 9), sans toutefois qu'il s'agisse d'une rupture de type différent.

b) les échantillons saturés en hydrogène présentent le faciès à cupules indiqué plus haut.

Si l'on examine une série d'échantillons

Fig. 9. Acier inoxydable non traité.

Fig. 11. Acier inoxydable chargé à 8 cc/100 g.

Fig. 10. Acier inoxydable chargé à 8 cc/100 g.

Fig. 12. Acier inoxydable chargé à 40 cc/100 g.

classés par teneurs en hydrogène croissantes, on constate le passage progressif du faciès à cratères au faciès à cupules, par diminution du nombre des cratères, et non par une évolution du relief de chacun de ces accidents comme on aurait pu s'y attendre. La transformation des cratères en cupules s'effectue dès que le chargement en hydrogène est de l'ordre de 5 à 10 cc/100 g (fig. 10). On constate également que pour ce chargement les cratères et cupules coexistent (fig. 11). Au delà de 30 cc/100 g subsiste exclusivement le faciès à cupules qui reste inchangé jusqu'à la saturation en hydrogène, alors que la charge de rupture et la striction continuent à évoluer (figs. 5 et 12).

4) La surface des cupules est en général parsemée de protubérances arrondies, de 0,2 à 0,5 μ, en forme de "pustules" (figs. 6, 6 bis et 13). Leur nombre est, semble-t-il, d'autant plus important que la fragilisation est plus poussée. Il pourrait s'agir de bulles formées au sein du métal, ou plus vraisemblablement d'inclusions. Néanmoins, la répartition de ces accidents, sans relation avec celle des cupules, ne nous permet pas d'affirmer qu'ils soient à l'origine de la rupture, ni même que celle-ci se soit propagée préférentiellement par ces points.

Fig. 13. Acier inoxydable chargé à 65 cc/100 g. La teneur en hydrogène a été obtenue grâce à un artifice: l'éprouvette avait subi avant le traitement électrolytique un dégazage sous vide à 900°. Il s'agissait en fait de savoir si l'augmentation de la quantité d'hydrogène absorbé confirmait l'évolution constatée, en particulier si elle s'accompagnerait d'un accroissement du nombre des pustules. Mais les phénomènes supplémentaires qui ont pu se produire, tels que désoxydation, nous interdisent de relier l'aspect de ce cliché aux résultats précédents.

5. Conclusions

Notre étude montre que lorsque la teneur en hydrogène atteint une quarantaine de cc TPN par 100 g, les caractéristiques mécaniques des aciers inoxydables sont notablement affectées: leur réputation d'insensibilité n'est donc valable que pour des teneurs en hydrogène modérées.

En ce qui concerne l'utilisation éventuelle d'aciers inoxydables comme matériaux de structure ou de gaînage dans des réacteurs refroidis à l'hydrogène, il est clair que même en admettant † que la solubilité de ce gaz n'est pas affectée par son ionisation du fait des rayonnements, on atteindra facilement dans l'acier des teneurs en hydrogène voisines des valeurs critiques que nous avons précisées pour un fonctionnement à 600–800° C sous 15 à 25 atmosphères. Il faudrait donc pour éviter tout incident au cours de cycles thermiques subis par les structures ou les gaînes, imposer des régimes de décompression et de refroidissement permettant à l'hydrogène dissous de s'échapper par diffusion.

Nous avons d'autre part montré que si la "fragilisation" des aciers inoxydables se manifeste macroscopiquement par une diminution de la capacité de déformation du métal, les examens microfractographiques révèlent sans ambiguité le caractère ductile des fractures, qui est conservé dans l'évolution du faciès en fonction de la teneur en hydrogène.

† Des essais en pile sont actuellement en cours pour préciser ce point.

Références

[1]) D. Bradley, AERE (Harwell), Report HL 59/6890 (Sept. 1959)

[2]) R. Blanchard, C. R. Acad. Sci. Paris **248** (1959) 966

[3]) H. C. van Ness et B. F. Dodge, Chem. Eng. Prog. **51** (1955) 266

[4]) J. D. Hobson et J. Hewitt, J. Iron Steel Inst. **173** (1953) 131

[5]) S. Besnard, C. Messager et J. Talbot, C.R. Acad. Sci. Paris **248** (1959) 1516

[6]) Azam, Réunion Uranium, Compte Rendu CEA no 7 (21 juin 1956)

[7]) Garrod et Nankiwell, Brit. J. Applied Phys. **9** (1958) 214

[8]) J. Plateau, G. Henry et C. Crussard, Rev. Univ. Mines Mét. Méc. **12** (1956) 543

[9]) J. Plateau, G. Henry et C. Crussard, Rev. Mét. **54** (1957) 200

[10]) M. L. Bernshtein et I. Paisov, Zavods. Labor. **25** (1959) 186

JOURNAL OF NUCLEAR MATERIALS 2, No. 3 (1960) 225-233, NORTH-HOLLAND PUBLISHING CO., AMSTERDAM

THE HIGH TEMPERATURE OXIDATION OF BERYLLIUM

PART II

THE REACTION WITH CARBON DIOXIDE AND WITH CARBON MONOXIDE

S. J. GREGG, R. J. HUSSEY and W. B. JEPSON

Department of Chemistry, University of Exeter, UK

Received 6 April 1960

The chemistry of the reaction of French Flake beryllium with carbon dioxide and with carbon monoxide has been investigated at temperatures in the range 500°–750° C by means of a radioactive tracer technique. The results lead to the conclusion that the following reactions occur:

$$\begin{aligned} Be + CO_2 &= BeO + CO, \\ 2Be + CO_2 &= 2BeO + C \quad \text{and} \\ Be + CO &= BeO + C \end{aligned}$$

and it is argued that the beryllium carbide which is also present in the oxide layer, is formed by the reaction

$$2Be + C = Be_2C$$

and not directly according to

$$4Be + CO_2 = 2BeO + Be_2C$$

or

$$3Be + CO = BeO + Be_2C.$$

There was no evidence for the reaction of carbon dioxide with deposited carbon according to the equilibrium

$$C + CO_2 \rightleftharpoons 2CO,$$

nor for the reverse reaction, viz. the decomposition of carbon monoxide to deposit carbon and evolve carbon dioxide.

A less detailed investigation suggests that for oxidation in carbon monoxide-carbon dioxide mixtures, there exists a minimal concentration of carbon monoxide above which carbon monoxide also reacts with beryllium.

La chimie de la réaction du beryllium français en paillettes avec le gaz carbonique et avec l'oxyde de carbone a été étudiée aux températures comprises entre 500° et 750° C au moyen d'une technique de traceurs radioactifs. Les résultats conduisent à la conclusion que les réactions suivantes se produisent

$$\begin{aligned} Be + CO_2 &= BeO + CO \\ 2Be + CO_2 &= 2BeO + C \\ \text{et} \quad Be + CO &= BeO + C. \end{aligned}$$

On en conclut que le carbure de beryllium qui est présent aussi dans la couche d'oxyde est formé par la réaction

$$2Be + C = Be_2C$$

et non directement par la réaction

$$4Be + CO_2 = 2BeO + Be_2C$$

ou

$$3Be + CO = BeO + Be_2C.$$

Il n'y a aucune preuve expérimentale que le gaz carbonique réagisse avec le carbone déposé suivant l'équilibre

$$C + CO_2 \rightleftharpoons 2CO.$$

De même il n'y a pas de preuve que la réaction inverse se produise, à savoir la décomposition de l'oxyde de carbone avec dépôt de carbone et dégagement de gaz carbonique.

Une étude moins détaillée suggère que dans le cas de l'oxydation dans des mélanges de $CO + CO_2$, il existe une concentration minimale d'oxyde de carbone au-dessus de laquelle l'oxyde de carbone réagit aussi avec le béryllium.

Die chemischen Vorgänge bei der Reaktion von French Flake Beryllium mit Kohlendioxyd und Kohlenmonoxyd wurde bei 500°–750° C mit Hilfe radioaktiver Indizierung untersucht. Die Ergebnisse weisen darauf hin, dass folgende Reaktionen stattfinden:

$$\begin{aligned} Be + CO_2 &= BeO + CO \\ 2Be + CO_2 &= 2BeO + C \\ \text{und} \quad Be + CO &= BeO + C. \end{aligned}$$

Es wurde bewiesen, dass das in der Oxydschicht ebenfalls vorhandene Berylliumkarbid gebildet wird durch die Reaktion

$$2Be + C = Be_2C$$

und nicht durch

$$4Be + CO_2 = 2BeO + Be_2C$$

oder

$$3Be + CO = BeO + C.$$

Hinweise auf die Reaktion von Kohlendioxyd mit Kohlenstoff gemäss dem Gleichgewicht

$$C + CO_2 \rightleftharpoons 2CO$$

waren nicht vorhanden. Auch fehlten Anzeichen für die entgegengesetzte Reaktion, also die Zersetzung von Kohlendioxyd unter Abscheidung von Kohlenstoff und Entstehen von Kohlendioxyd.

Auf Grund einer weniger eingehenden Untersuchung darf angenommen werden, dass bei der Oxydation in einer Kohlenmonoxyd-Kohlendioxyd-Mischung eine minimale Konzentration an Kohlenmonoxyd existiert, oberhalb welcher Kohlenmonoxyd ebenfalls mit Beryllium reagiert.

1. Introduction

Published work on the oxidation of beryllium in carbon dioxide seems to be limited to that of Munro and Williams [1]) covering the temperature range 500° to 750° C; they followed the course of the oxidation by intermittent weighing, the sample being cooled to room temperature for each measurement. The chemistry of the reaction was not investigated. No studies of the oxidation of beryllium in either carbon monoxide alone or in carbon monoxide-carbon dioxide mixtures appear to have been reported.

For the oxidation of beryllium in carbon dioxide, one may write down the following reactions, all of which [by reference to the free energy data [2,3]) in table 1] are seen to be thermodynamically possible at the pressures (2–10 cm) and temperatures (500° to 750° C) of the present study:

$$Be + CO_2 = BeO + CO \quad (1)$$

$$2Be + CO_2 = 2BeO + C \quad (2)$$

$$4Be + CO_2 = 2BeO + Be_2C \quad (3)$$

$$Be + CO_2 = BeO + C + \tfrac{1}{2}O_2. \quad (4)$$

If reaction (2) occurs, there are two further possibilities: the deposited carbon may react to form the carbide

$$2Be + C = Be_2C \quad (5)$$

or it may react with carbon dioxide according to the equation

$$C + CO_2 \rightleftharpoons 2CO \quad (6)$$

for which at 600° C the equilibrium partial pressure of carbon monoxide is 0.23 atm at a total pressure of 1 atm. The formation of beryllium carbonate [4]) appears unlikely at the relatively high temperatures of the present study, since this compound is reported to be very unstable.

For oxidation in carbon monoxide, only two reactions need be considered

$$Be + CO = BeO + C \quad (7)$$

$$3Be + CO = BeO + Be_2C \quad (8)$$

since the standard free energy change of the reaction

$$2Be + CO = Be_2C + \tfrac{1}{2}O_2 \quad (9)$$

is positive; if reaction (7) occurs, the deposited carbon may react as in (5). Finally there is of course the possibility of the reverse of reaction (6) proceeding until equilibrium is reached, with resultant deposition of carbon on the sample surface.

It is therefore clear that there are two distinct problems to be considered: the purely chemical one of establishing which of the above reactions do in fact occur, and the kinetic one of measuring the rates of the processes. The present Part is devoted to the first of these and Part III will deal with the kinetics of the oxidation.

2. Experimental

The method used was in essence volumetric, but the pressure of both carbon monoxide and carbon dioxide was measured indirectly by means of a radioactive tracer technique based on C^{14}. The apparatus (fig. 1) consisted of a

TABLE 1
Expressions for the standard free energy changes of the oxidation reactions

$\Delta G_0(T) = a + bT \log T + cT + dT^2$ (cal/mole)					
Reaction	a	b	c	d	$\Delta G_0(873)$ (cal/mole)
(1)	— 75 950	—1.66	+ 7.3	—	— 73 800
(2)	—192 700	—3.32	+56.3	—	—152 000
(3)	—220 028	—3.32	+63.988	-1.331×10^{-3}	—174 000
(4)	— 49 250	—1.66	+28.25	—	— 28 900
(5)	— 27 328	0	+ 7.688	-1.331×10^{-3}	— 21 600
(6)	+ 40 800	0	—41.7	—	+ 4 400
(7)	—116 750	—1.66	+49	—	— 78 200
(8)	—144 078	—1.66	+56.688	-1.331×10^{-3}	— 99 900
(9)		0	+28.638	-1.331×10^{-3}	+ 23 400

silica reaction chamber A connected through graded quartz-pyrex seals to a loop incorporating a glass counting cell B (volume: 20 cc) which was sealed on to an end-window Geiger–Müller tube C (20th Century Electronics, England; modified EW3H counter with a mica

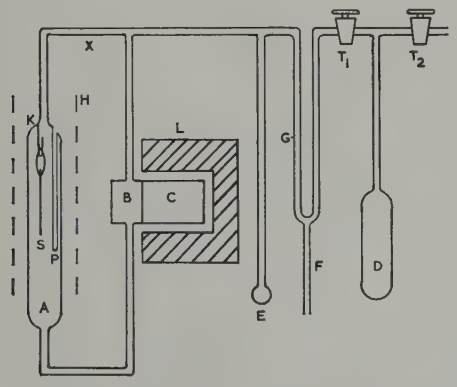

Fig. 1. The volumetric apparatus.

end window of thickness equivalent to 5 mg/cm^2), the counting cell being mounted inside the lead castle L. The total volume of the apparatus was about 140 cc. The furnace at H was controlled to $\pm$ 0.5° C, the temperature being measured on a calibrated chromel-alumel thermocouple housed in a pocket P adjacent to the sample S which was suspended from the hook K by a loop of stainless steel wire.

Before each run, the apparatus was first evacuated and then calibrated by filling the known volume between the taps T_1 and T_2, including the bulb D, with $C^{14}O_2$ at a known pressure measured on a mercury manometer (not shown); tap T_2 was then closed, tap T_1 opened and the gas distilled into bulb E which was immersed in liquid oxygen (saturated vapour pressure of carbon dioxide at $-183°$ C = 4×10^{-6} mm). Mercury was then raised into the cut-off F to the standard mark G and the condensate allowed to evaporate. From the measured count rate the total volume of the apparatus was calculated; the volume of that part of the apparatus which remained at room temperature during a run, which was variable, was obtained by subtracting the volume of the part of the apparatus enclosed by the furnace.

For runs in carbon dioxide, the sample was first outgassed at room temperature and then the furnace at H was switched on and outgassing continued as the temperature rose; after a period of 90 min, by which time the beryllium sample had been at reaction temperature for some 60 min, a known amount of carbon dioxide distilled into bulb E in the manner already described, and after raising the mercury into the cut-off F, the condensate was allowed to evaporate. The reaction was then followed by measuring the count rate at suitable intervals. For a run in carbon monoxide, the method was the same except that a known amount of gas was admitted to the apparatus by opening the tap T_1 and sharing the contents of bulb D.

Counts of 10 000 were taken for each experimental point to give a statistical accuracy of $\pm$ 1 % and the count rates were corrected for lost counts, etc., using standard methods; self-absorption in the gas was negligible. The sensitivity of the counting system was such that a pressure of carbon dioxide (specific activity 0.25 μc/cm^3 at N.T.P.) of 1 cm gave a count rate of 60 counts/sec.; with 1 cm of carbon dioxide the disappearance of 9 μg of "carbon" from the gas phase, i.e. the uptake of 9 μg by the specimen, could be detected; this is equivalent to a pressure change of 0.01 cm and corresponds to a sensitivity of 0.75 μg/cm^2 of surface.

The French Flake beryllium was from the same batch as that used for the oxidation studies in dry oxygen [for analysis, see Part I [5])] and had been fabricated in the same way. The surface preparation was also similar, the samples being chemically polished [6]) before use by immersion in a solution of phosphoric acid, sulphuric acid and chromic acid for 30 sec at 100° C.

The radioactive carbon dioxide was prepared[7]) by heating a mixture of lead chloride and barium carbonate to which had been added 0.5 mc of C^{14} in the form of barium carbonate; the gas evolved was dried by passing over anhydrous magnesium perchlorate and then distilling it six times through a column packed with phosphorus pentoxide. Traces of air were removed by pumping to a pressure of 10^{-6} mm with the carbon dioxide frozen in liquid oxygen. Radioactive carbon monoxide was prepared by diluting the highly active gas (obtained from The Radiochemical Centre, Amersham, England) with spectroscopically pure inactive carbon monoxide.

3. Oxidation in carbon dioxide

A preliminary study of the reaction of beryllium with carbon dioxide at a pressure of 1–2 cm was made at a number of temperatures in the range 500° to 700° C. It was soon realised that since reaction (1) certainly occurred, the carbon monoxide generated might build up to an appreciable concentration in the small volume of the apparatus and perhaps also react with the beryllium. A reaction of this kind did in fact occur, and this led to a second series of experiments in which the carbon monoxide generated was oxidised back to carbon dioxide over heated cupric oxide so that the oxidation in the pure gas could be studied (see Section 3.2 below).

3.1. Carbon monoxide concentration allowed to build up

At 500° C, in two runs each of 185 hours duration, there was no detectable change of count rate with time and a statistical analysis of the data showed that if there was any deposition of carbon † then the amount was less than 0.01 μg/cm^2. On immersing bulb E in a liquid oxygen bath at the end of the run and thus condensing the unreacted carbon dioxide, there was a residual pressure of radioactive gas which could only have been carbon monoxide (saturated vapour pressure at $-183°$ C = 152 cm). It may therefore be concluded that at 500° C only reaction (1) occurs.

Of the three runs (18B, 20B, 21B) at 550° C, one (18B) was similar to those at 500° C in that there was no deposition of carbon over a period of 120 h (count rate constant), but the course of the other two runs was strikingly different in that the count rate decreased with time. In run 20B, the count rate fell to the background value after 100 h (fig. 2), signifying that all the carbon had been transferred to the beryllium, and rather surprisingly there was a residual pressure of gas (0.2 cm, or 25 % of the initial pressure) which could not be condensed in liquid oxygen and will be referred to later. On pumping out the apparatus and admitting a further charge of carbon dioxide (at A in fig. 2), deposition of carbon occurred but at a smaller rate, and after a further 200 h (not shown in fig. 2) the additional uptake of carbon was 9 μg/cm^2. In run 21B (fig. 2) carbon was again

† The term "deposition of carbon" is meant to indicate either deposition of elementary carbon or the formation of beryllium carbide (see Section 3.3).

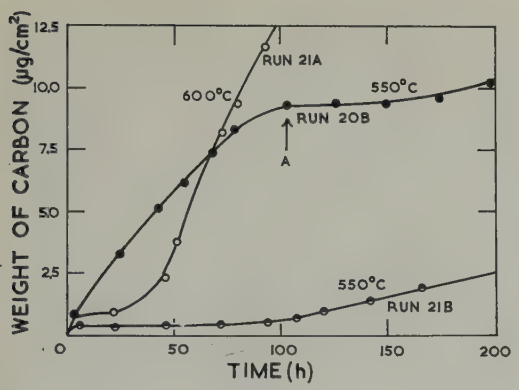

Fig. 2. Oxidation of beryllium in carbon dioxide at 550° C and 600° C; concentration of carbon monoxide increasing. In run 20B at 550° C, a further charge of carbon dioxide was admitted at the time represented by A.

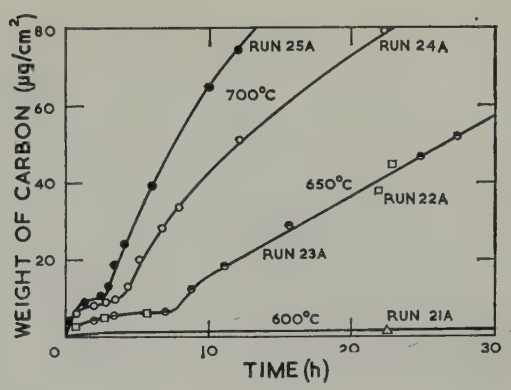

Fig. 3. Oxidation of beryllium in carbon dioxide at 600° C, 650° C and 700° C; concentration of carbon monoxide increasing.

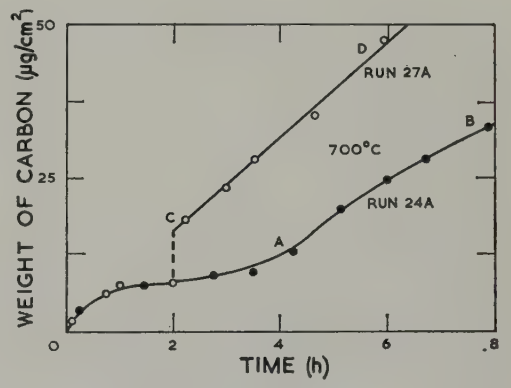

Fig. 4. Oxidation of beryllium at 700° C. Run 24A: oxidation in carbon dioxide, concentration of carbon monoxide increasing; run 27A: carbon dioxide condensed from the gas phase after 2 h (shown as a broken line) and the beryllium allowed to react with carbon monoxide alone.

deposited but at a smaller rate; and the presence of carbon monoxide, indicative of the occurrence of reaction (1), was revealed by freezing out the unreacted carbon dioxide.

At 600° C, two runs (20A and 21A) were carried out; in one of these (20A) there was no deposition of carbon over a period of 300 h, but in the other (21A, fig. 2) carbon was again deposited. After 120 h the run was interrupted and a further charge of carbon dioxide admitted; carbon deposition then ceased and there was no further uptake in the remaining 215 h period of the run. This run at 600° C and the runs at 650° C and 700° C (fig. 3) show the interesting feature that the initial decrease in rate is followed by a marked increase after a period of time which becomes shorter the higher the temperature. Reference to fig. 3 will show that the reproducibility at 650° C and 700° C is better than that at the lower temperatures. In a further run at 700° C (27A, fig. 4), the unreacted carbon dioxide was condensed out after 2 h and the beryllium allowed to react with the carbon monoxide which had been generated by reaction (1); as is seen the subsequent rate of carbon deposition along CD is not very different from that of an uninterrupted run (AB of run 24A), suggesting that the relatively rapid carbon deposition along the steeply rising branch AB is due to reaction of beryllium with carbon monoxide alone.

Since carbon was deposited in some of the experiments, there was the possibility that it might react with gaseous carbon dioxide [reaction (6)]; to test this point a run was carried out in which inactive carbon dioxide ($C^{12}O_2$) was admitted to a sample at 700° C on which radioactive carbon had been deposited. No activity appeared in the gas phase over the 40 h period of the experiment so that the exchange

$$C^{14} + C^{12}O_2 \rightleftharpoons C^{14}O + C^{12}O$$

evidently does not occur and reaction (6) can thus be disregarded; the pressure read on the mercury manometer did however fall, indicating

that carbon was still being deposited by one or more of reactions (2), (3), (4), (7) and (8). Of these, reaction (4) can probably be eliminated: when oxygen was admitted to a sample at 550° C carrying deposited radioactive carbon, activity was rapidly transferred to the gas phase and (by condensing out) was proved to be due to carbon dioxide ($C^{14}O_2$), though only 80 % of the carbon could be oxidised in this manner. It would seem likely therefore that the simultaneous formation of carbon and free oxygen as required by reaction (4) is very unlikely. Regarding the non-condensable gas formed in Run 20B, it would seem that this could not have been oxygen; it may have been some gas which was released from the metal subsequent to the initial outgassing. Unfortunately the result could not be repeated, so that it was not possible to obtain a sample of the gas for analysis.

3.2. Carbon monoxide re-oxidised to carbon dioxide

The experiments so far described show that reaction (1) occurs at all temperatures in the range 500° to 700° C whilst at 550° C and above, carbon deposition occurs either by reaction with carbon dioxide [(2) or (3)] or with carbon monoxide [(7) or (8)]. To distinguish between these possibilities, a further series of experiments were made in which the carbon monoxide was removed from the gas phase as fast as it was formed, by oxidation with cupric oxide: the apparatus was modified by introducing, between the reaction chamber and counting cell (at X in fig. 1), a bulb containing about 0.5 g of cupric oxide, maintained at 350° C. At this temperature carbon monoxide is readily oxidised, the ratio of the equilibrium partial pressure of carbon dioxide to that of carbon monoxide being at least 10^{11}:1. The cupric oxide was not incorporated in the reaction chamber itself because of the dissociation

$$2CuO \rightleftharpoons Cu_2O + \tfrac{1}{2}O_2$$

which at 650° C would have given a partial pressure of oxygen of 0.007 mm. A fresh sample of cupric oxide was used in each run and the efficiency of the method was tested by oxidising a beryllium sample at 700° C for 30 min and then sharing the gas with an evacuated bulb: subsequent analysis failed to detect any carbon monoxide.

Using this technique, runs were carried out at 650° C, 700° C and 750° C; as is seen from figs. 5 and 6, carbon deposition still occurred, but in contrast to the runs in the presence of carbon monoxide (figs. 2 to 4), it was now confined to the first few hours of each run; a statistical analysis of the data for run 22B at

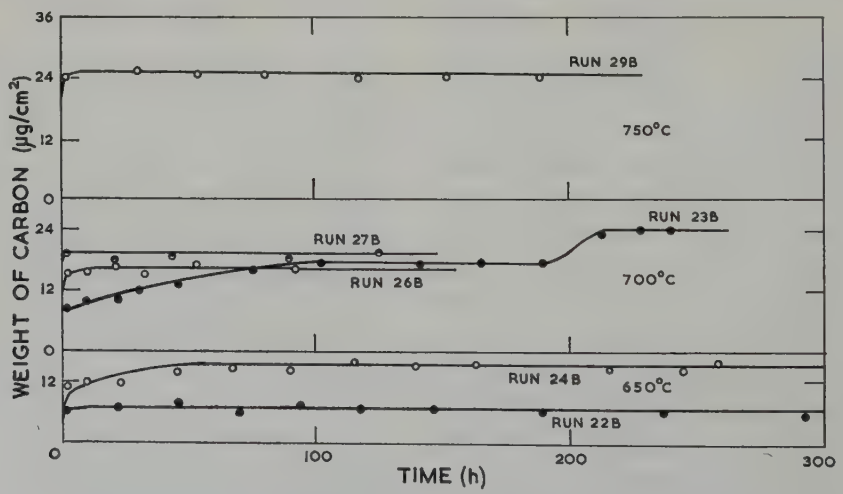

Fig. 5. Oxidation of beryllium in carbon dioxide at 650° C, 700° C and 750° C; carbon monoxide oxidised back to carbon dioxide.

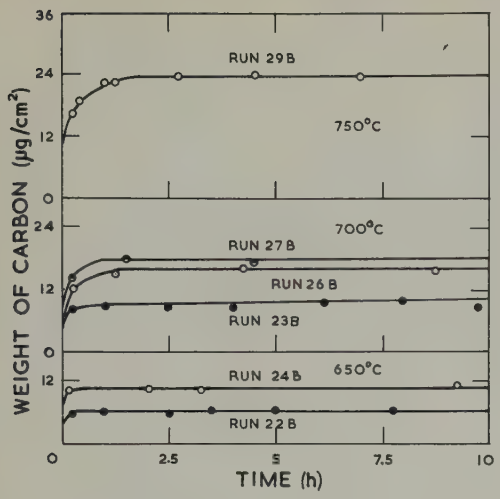

Fig. 6. Oxidation of beryllium in carbon dioxide at 650° C, 700° C and 750° C; carbon monoxide oxidised back to carbon dioxide. Showing the first 10 h of each run.

650° C showed that the rate of deposition over the interval 0.25 to 310 h was only 0.002 $\pm$ 0.0006 μg/cm^2·h and therefore negligible. In one run (23B) at 700° C, however, carbon deposition started again after 200 h with the deposition of a further 6.5 μg/cm^2, after which the rate fell again to zero.

In table 2 the weight w_c of carbon deposited (calculated from the loss of activity from the gas phase) is recorded for each run along with the corresponding weight w_o of oxygen taken up as beryllium oxide; w_o is obtained by subtracting w_c from the gain in weight of the sample as measured by direct weighing at the end of the experiment. As will be seen, both w_c and w_o increase fairly consistently as the temperature of the run increases, but the ratio w_c:w_o (apart from that for run 24B which seems anomalous) is approximately constant at 0.10 as compared with the value 0.375 (12:32) required by reaction (2) [or (3)]. It is clear therefore that reaction (1) predominates at all temperatures.

Table 2

Oxidation of beryllium in carbon dioxide; carbon monoxide oxidised back to carbon dioxide

Run No.	Length of run (h)	Temp. (°C)	w_c (μg/cm^2)[a]	w_o (μg/cm^2)	w_c/w_o
22B[b]	315	650	4.9	66.4	0.07
24B	260		15.7	74.3	0.21
23B	240		23.9	183.9	0.13
26B	90	700	16.3	165.2	0.10
27B	125		18.2	148.5	0.12
29B	190	750	22.5	241.0	0.09

[a] w_c is the weight of deposited carbon and w_o the weight of oxygen taken up as beryllium oxide.

[b] In all these runs, the initial pressure of carbon dioxide was 2 cm.

3.3. The form of the deposited carbon

The kinetic measurements do not distinguish between the deposition of elementary carbon [reaction (2)] and the formation of beryllium carbide [reactions (3) and (5)] so that a distinction can only be made by examination of the reaction product. Unfortunately, there was insufficient material for a chemical analysis and an indirect method had to be used. A sample which had been oxidised at 750° C, and for which the amount of deposited carbon was known, was treated with warm caustic soda solution (2N) in a simple volumetric apparatus and the methane formed on decomposition of the carbide was estimated from the "carbon" count in the gas phase. The result indicated that 40 % of the carbon was present as beryllium carbide.

4. Oxidation in Carbon Monoxide

The oxidation of beryllium in carbon monoxide at 10 cm pressure was studied at temperatures at 50° C intervals in the range 500° to 750° C. The chemistry of the reaction is simpler than that with carbon dioxide for no gaseous products are formed [reaction (9) is thermodynamically not possible] so that all the activity lost from the gas phase must appear on the specimen and the ratio of the weight of carbon deposited to the weight of oxygen taken up as beryllium oxide is fixed at 12:16.

An important problem is to decide what

proportion of carbon thus transferred to the solid is present as free carbon [reaction (7)] and what proportion is carbide [reaction (8), or reaction (7) followed by (5)]. Now during oxidation in carbon monoxide at 550° C and above, the reaction product spalls from the sample, and by combining the product from a number of runs, sufficient material (150 mg) was obtained to permit a quantitative analysis for beryllium [8]) †.

The beryllium content of the powder was thus found to be 31 wt %, and since the ratio of the weight of carbon to that of oxygen must be the same in the powder as in the carbon monoxide molecule, it follows that only 15 % of the deposited carbon is chemically combined with beryllium as beryllium carbide.

In addition to the chemical reaction of beryllium with carbon monoxide [(7) and (8)] there is of course also the possibility of decomposition of carbon monoxide on the specimen surface to deposit carbon and evolve carbon dioxide. This possibility was tested in a run at 700° C on the volumetric apparatus with bulb E immersed in a liquid oxygen bath; after the metal had been allowed to cool, the residual carbon monoxide was pumped off and the liquid oxygen bath removed, but no activity appeared in the gas phase demonstrating that no carbon dioxide had been formed by the reverse of the reaction (6).

5. Discussion and Conclusions

5.1. Oxidation in carbon dioxide

The present results show that when French Flake beryllium is heated in carbon dioxide at temperatures in the range 550° to 750° C, the following reactions occur:

$$\mathrm{Be} + \mathrm{CO_2} = \mathrm{BeO} + \mathrm{CO} \qquad (1)$$

$$2\mathrm{Be} + \mathrm{CO_2} = 2\mathrm{BeO} + \mathrm{C} \qquad (2)$$

whereas at 500° C, only reaction (1) has been detected. The presence of beryllium carbide in the oxide layer formed at temperatures of 550° C and above has been demonstrated but it is not possible to decide from the experimental results alone whether this is formed directly by the reaction

$$4\mathrm{Be} + \mathrm{CO_2} = 2\mathrm{BeO} + \mathrm{Be_2C} \qquad (3)$$

or indirectly by reaction of the metal with the carbon deposited in (2) according to

$$2\mathrm{Be} + \mathrm{C} = \mathrm{Be_2C}. \qquad (5)$$

Arguments will be adduced in Part III against reaction (3) [it would necessitate the simultaneous reaction of three Be^{++}-ions with one CO^{+}-ion, and this is considered unlikely], so that the indirect formation of carbide via the reactions (2) and (5) seems the more probable. That this view is a reasonable one is shown by the fact that the reaction between beryllium and graphite powders is known to start at a temperature of about 600° C [9]).

5.2. Oxidation in carbon monoxide

The product formed on oxidation of beryllium in carbon monoxide has been shown to consist of a mixture of the oxide, carbide and elementary carbon so that the reaction

$$\mathrm{Be} + \mathrm{CO} = \mathrm{BeO} + \mathrm{C} \qquad (7)$$

certainly occurs, while the beryllium carbide may be formed by one of two reactions

$$3\mathrm{Be} + \mathrm{CO} = \mathrm{BeO} + \mathrm{Be_2C} \qquad (8)$$

$$2\mathrm{Be} + \mathrm{C} = \mathrm{Be_2C}. \qquad (5)$$

For reasons which will be adduced in Part III, reaction (5) would seem the more probable.

5.3. Oxidation in carbon dioxide; carbon monoxide concentration allowed to increase

In those experiments where the carbon monoxide concentration was allowed to build

† The powder was dissolved in boiling 2*N* caustic soda solution and after neutralising to a slight excess of 2*N* sulphuric acid, the solution was boiled again and allowed to cool. The elementary carbon was filtered off, and the solution was buffered by addition of ammonium phosphate, nitrate and acetate; on adding urea, the beryllium was precipitated as beryllium ammonium phosphate which was then ignited to the pyrophosphate.

up, curves of the type of fig. 3 were obtained where the rate of carbon deposition, after falling to a very low value, abruptly increased; since however the abrupt increase was no longer obtained in those experiments where the carbon monoxide was removed by oxidation with cupric oxide, it is reasonable to attribute its presence to reaction with carbon monoxide, which is faster than that with carbon dioxide (see fig. 4). That the effect only appears after an interval of time indicates that a minimal concentration of carbon monoxide must be reached before it can react in this manner. Now in the interrupted run (27A, fig. 4) at 700° C it was possible, by comparing the count rates before and after the unreacted carbon dioxide was condensed from the gas phase, to calculate that the composition of the gas mixture after 2 hours' oxidation was 16 mm of carbon monoxide and 1.7 mm of carbon dioxide. Since the increase in the rate of carbon deposition in an uninterrupted run at 700° C occurred at a time greater than 2 h, it follows that the minimal proportion of carbon monoxide at the pressure used was at least 90 %. The concept of a minimal concentration is supported by those experiments where carbon deposition either ceased (21A) or was retarded (20B) on admitting a further charge of carbon dioxide: this would lower the proportion of carbon monoxide below the minimal value.

Acknowledgements

It is a pleasure to thank Dr J. E. Antill for his interest in this work and for the benefit of several helpful discussions and Mr E. Bishop for advice on the analysis of the reaction product. We are also grateful to the U.K. Atomic Energy Authority for financial support and to 20th Century Electronics Ltd. for developing the modified EW3H Geiger–Müller tubes.

References

1) W. Munro and J. Williams, Harwell (UK), Report AERE M/M 108 (1956)
2) O. Kubaschewski and E. LL. Evans, Metallurgical Thermochemistry (Pergamon Press, London, 1956)
3) B. D. Pollock, J. Phys. Chem. **63** (1959) 587
4) H. Remy, Treatise on Inorganic Chemistry, Vol. I, Elsevier Publishing Company, (London, 1956) p. 274
5) D. W. Aylmore, S. J. Gregg and W. B. Jepson, J. Nucl. Mat. **2** (1960) 169
6) J. E. Antill, private communication
7) N. Zwiebel, J. Turkevich and W. W. Miller, J. Amer. Chem. Soc. **71** (1949) 376
8) W. W. Scott and N. H. Furman, Standard Methods of Chemical Analysis, Vol. I (Technical Press Ltd, 1939) p. 141
9) J. Williams and J. W. S. Jones, quoted in ref.[1])

JOURNAL OF NUCLEAR MATERIALS 2, No. 3 (1960) 234–247, NORTH-HOLLAND PUBLISHING CO., AMSTERDAM

THE PLASTIC DEFORMATION OF ALPHA-URANIUM

A. G. YOUNG, K. M. GARDINER and W. B. ROTSEY

Atomic Power Department, English Electric Co. Ltd., Whetstone, Leicestershire, UK

Received 31 March 1960

Experiments on the plastic behaviour of magnesium reduced alpha-uranium at temperatures above 300° C are reported. The first part of the work describes the results of uniaxial creep tests under isothermal conditions and presents a relation between secondary creep rate, stress and temperature which applies between 450° C and 650° C. The second part of the work describes the effects of thermal cycles on the plastic deformation under load. Experimental results are given and a theory developed to relate the plastic deformation to the applied stress and the amplitude of the cycle.

Le comportement plastique de l'uranium préparé par la méthode de réduction au magnésium a été étudié aux températures supérieures à 300° C. La première partie du travail décrit les résultats d'essai de fluage uniaxial en condition isotherme et donne une relation entre la vitesse de fluage secondaire, la tension et la température. Cette relation s'applique entre 450° et 650° C. La seconde partie du travail décrit les effets de cyclage thermique sur la déformation plastique sous charge. Des résultats expérimentaux sont donnés et une théorie est développée pour relier la déformation plastique à la tension appliquée et à l'amplitude du cycle.

Es wird über Versuche zum Verformungsverhalten von α-Uran bei Temperaturen über 300° C berichtet. Das verwendete Uran war mit Magnesium reduziert worden. Im ersten Teil der Arbeit sind die Ergebnisse von uniaxialen Kriechversuchen bei konstanter Temperatur zwischen 450 und 650° C beschrieben. Hierbei ergibt sich ein Zusammenhang zwischen der Geschwindigkeit des sekundären Kriechens, der aufgebrachten Spannung und der Temperatur. Im zweiten Teil ist die Auswirkung einer zyklischen Temperaturführung auf die plastische Verformung unter Last besprochen. Neben den experimentellen Befunden wird eine Theorie aufgeführt, die einen Zusammenhang zwischen der plastischen Deformation und der angelegten Spannung bzw. der Amplitude der Temperaturzyklen herstellt.

1. Introduction

The plastic behaviour of magnesium reduced beta-quenched alpha-uranium has recently been investigated in support of the fuel element design for gas-cooled reactors as part of the programme of the UK Nuclear Power Collaboration Committee.

To establish the isothermal creep properties, tensile tests in the temperature range 450–650° C were carried out on standard creep machines. The test results and derivation of a secondary creep law are described in Section 2.

Cottrell [1]) predicted that thermal cycling or irradiation would reduce the strength of alpha-uranium due to the generation of internal stresses. This was confirmed in the case of irradiation by the experimental work of Cottrell and Roberts [2]). Further work presented in Section 3 examines the effect of thermal cycles when imposed during a conventional creep test on uranium. Experimental results are given of the extra strain produced by single and multiple cycles applied to uranium creeping in the temperature range 300–500° C, together with a theoretical analysis of the problem using standard elasticity and plasticity relationships.

2. Isothermal Creep

2.1. Experimental method

The tests were carried out using standard tensile creep equipment employing purified argon atmospheres to minimise oxidation. The gauge length of the specimens was 7.5 cm and the cross sectional area 1.6 cm^2. Because the

effects of thermal cycling were appreciated, particular attention was paid to thermal fluctuations occurring during the tests.

It was not possible to make continuous accurate records of the temperatures during all the tests reported. However, checks were made on individual machines for periods up to 15 hours.

There are two types of variation, a variation of short (10 min) duration being called a "ripple" and a variation of long duration (12 h) being called a "drift". Both these variations must be evaluated because of the effect thermal cycling has on the creep rate of uranium. The temperature history of some of the tests has been monitored and has shown that the ripple is less than $\pm$ 0.1° C and the overall drift less than $\pm$ 0.4° C.

All bars were radiographed to establish their soundness before the creep specimens were prepared.

During test, strain and time records were taken. After the period of primary creep was complete, the strain-time relationship became linear and secondary creep rates could be measured.

2.2. Results

Table 1 shows the results obtained from the creep tests. The grain size of all specimens were comparable [0.020 cm (0.008″)] and no significant change occurred during test. Cast to cast variations were small.

Table 1

Results of isothermal creep tests

Temp. (°C)	Stress (psi)	Secondary creep rate (h^{-1})	Temp. (°C)	Stress (psi)	Secondary creep rate (h^{-1})
450	600	6.5×10^{-8}	550	560	3.5×10^{-6}
450	1120	1.8×10^{-7}	550	784	6.7×10^{-6}
450	1680	1.3×10^{-6}	550	1120	2.5×10^{-5}
450	2240	1.5×10^{-6}	550	1680	5.1×10^{-5}
450	3360	4.7×10^{-6}	550	2240	1.1×10^{-4}
450	4480	9.6×10^{-6}	550	2240	8.4×10^{-5}
500	560	6.0×10^{-7}	600	224	4.5×10^{-6}
500	672	7.2×10^{-7}	600	224	4.5×10^{-6}
500	784	2.0×10^{-6}	600	448	5.9×10^{-6}
500	1120	3.8×10^{-6}	600	448	1.0×10^{-5}
500	1120	7.5×10^{-7}	600	448	8.6×10^{-6}
500	1120	1.9×10^{-6}	600	560	1.4×10^{-5}
500	1120	1.4×10^{-6}	600	560	9.4×10^{-6}
500	1120	2.8×10^{-6}	600	672	3.3×10^{-5}
500	1680	8.1×10^{-6}	600	1120	2.5×10^{-4}
500	1680	5.0×10^{-6}	600	1120	5.7×10^{-5}
500	2240	8.5×10^{-6}	600	1120	5.9×10^{-5}
500	2240	1.4×10^{-5}	600	1680	2.7×10^{-4}
500	3360	2.4×10^{-5}	600	2240	5.4×10^{-4}
500	4480	6.4×10^{-5}	650	224	1.0×10^{-5}
500	6720	2.2×10^{-4}	650	560	9.4×10^{-5}
500	6720	2.1×10^{-4}	650	784	1.4×10^{-4}
500	8960	4.9×10^{-4}	650	1120	1.0×10^{-3}

2.3. Analysis of results

2.3.1. *Creep rate as a function of stress in the temperature range* 450–650° C

For many materials it has been shown [3]) that the relation between stress and secondary creep rate may be expressed as

$$\dot{\varepsilon} = B\sigma^n$$

where

$\dot{\varepsilon}$ is the secondary creep rate,

σ is the applied stress,

and B and n are constant at any given temperature.

If this law holds for uranium then at constant temperature a plot of log $\dot{\varepsilon}$ against log σ should yield a straight line of slope n.

This has been done for each temperature and the data yields the following results.

Temperature °C	Correlation coefficient	n
450	0.987	2.56
500	0.979	2.44
550	0.992	2.42
600	0.947	2.21
650	0.974	2.67

A correlation coefficient of 1 denotes perfect linearity between log $\dot{\varepsilon}$ and log σ whilst a value of 0 means that no linear relation exists.

The correlation coefficients leave no doubt that the above law is obeyed. However, n appears subject to some variation with temperature. To test whether this is true the 95 %

confidence interval for each value of n was evaluated. The result is clearly seen in fig. 1. Since all the confidence intervals are mutually overlapping there is no justification for supposing n to vary with temperature.

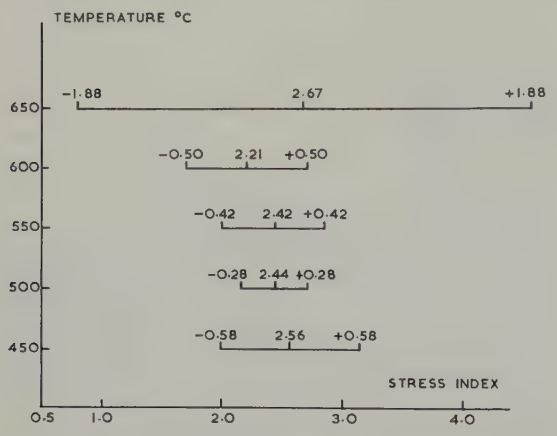

Fig. 1. Values of the stress index in the creep equation with 95 % confidence limits vs temperature.

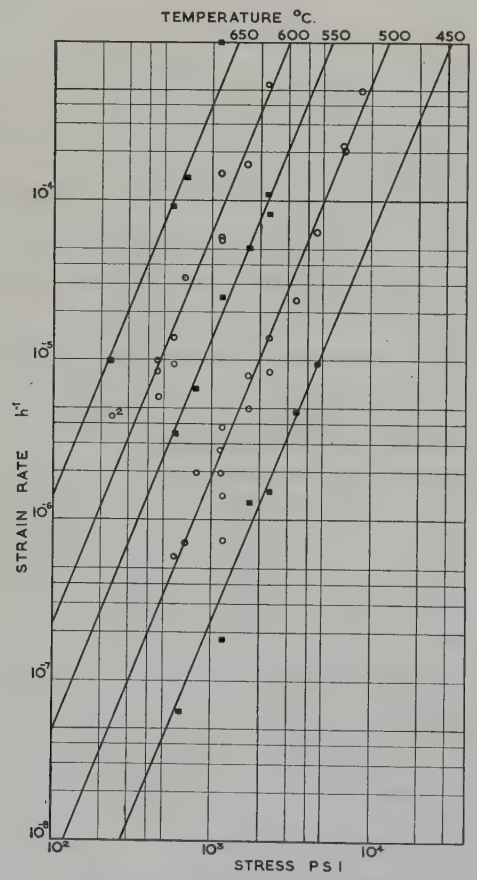

Fig. 2. Secondary creep rate vs stress in the temperature range 450–650° C.

The data are presented graphically in fig. 2 where the lines are drawn through the centre of gravity of each set of points with a slope corresponding to the weighted mean value of n.

2.3.2. *Creep rate as a function of temperature in the range* 450–650° C

The dependence of creep rate upon temperature at constant stress may be assumed to be given by

$$\dot{\varepsilon} = C \exp(-Q/RT)$$

where

$\dot{\varepsilon}$ is the secondary creep rate,
Q is the activation energy,
R is the gas constant,
T is the absolute temperature,
and C is a constant.

If this law is obeyed then for constant stress $\log \dot{\varepsilon}$ should vary linearly with $1/T$ and the slope will be $-Q/R$.

Using a mean value of n derived from section 2.3.1. and taking a constant stress of 1000 psi values of $\dot{\varepsilon}$ are obtained for each temperature. These values are presented graphically in fig. 3 which shows that a linear relation exists between $\log \dot{\varepsilon}$ and $1/T$, the correlation coefficient being 0.999.

2.3.3. *The complete equation and the determination of the best set of values of k, Q/R and n*

Sections 2.3.1. and 2.3.2. have demonstrated that the creep law can be written as

$$\dot{\varepsilon} = \sigma^n \exp(k - Q/RT)$$

where $\dot{\varepsilon}$, σ, R, T and n are as defined above and k is a constant.

It now remains to determine the best set of values of the three constants, n, Q/R and k in accordance with the above equation by the simultaneous minimisation of the sum of the squares of the deviations, $\sum s^2$ with respect to n, Q/R and k where $\ln \dot{\varepsilon} = k' + n \ln \sigma - Q/RT + S$

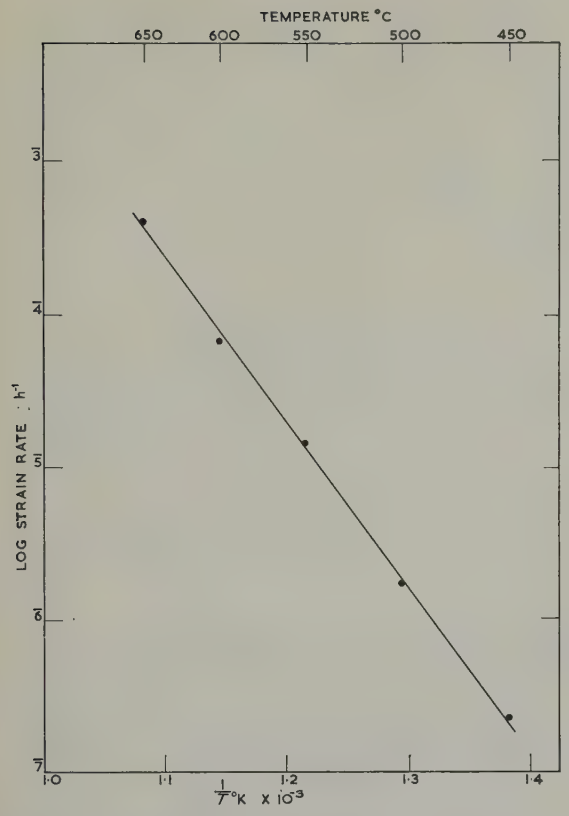

Fig. 3. Logarithm of secondary creep rate vs reciprocal of absolute temperature for a constant stress of 1000 psi.

which on solution yield the following results

$$n = 2.41$$
$$Q/R = 2.48 \times 10^4$$
$$k = +2.39 \ .$$

Thus the above data is expressed as

$$\dot{\varepsilon} = \sigma^{2.41} \exp\,(2.39 - 2.48 \times 10^4/T)$$

where $\dot{\varepsilon}$ is in h^{-1}, σ in psi and T in ° K. The activation energy is 49.6 ± 3.4 kcal/mole.

3. Effects of Thermal Cycling

3.1. Experimental work

3.1.1. *Method*

Creep tests which had attained a steady secondary creep rate were subjected to thermal transients of both heating and cooling. The maximum rate of change of temperature was 3° C/min and as an example a 30° C cooling cycle was completed in 60 minutes. Strain readings during the cycle were unreliable because of the differential thermal expansion of the specimen and the extensometers; however, the strain was measured immediately isothermal conditions had been restored and subsequently as in a normal creep test. The normal creep strain which would have occurred in the time taken for a cycle was less than 0.001 %.

3.1.2. *Results*

The effect of a typical set of cooling cycles imposed on a creep test is shown in fig. 4. Each cycle has produced an increment of strain which is additional to the creep strain under normal isothermal conditions. The first part of the strain increment, termed the "immediate" strain, is produced during the temperature cycle and the remainder termed the "recovery" strain, over a period of time after the cycle has been completed. In the case of single cycles, the specimens were allowed time to recover fully, i.e. to achieve a steady creep-rate, before another cycle was imposed. Results for specimens at 300, 350, 400 and 450° C are given in table 2. Results at 500° C and 1120 psi are given in figs. 5*a* and 5*b* in which the total strain due to the cycle and the "recovery" portion of this strain are plotted against amplitude of cycle for heating and cooling cycles respectively.

Fig. 5 shows that, for amplitudes less than about 50° C, the strain produced varies linearly with amplitude of cycle for both heating and cooling cycles and that in this range the strains produced by heating or cooling are of the same order. At higher amplitudes the total strain due to a heating cycle is considerably more than that due to a cooling cycle. The "recovery" strains, on the other hand, are similar for heating and cooling cycles. At the lower amplitudes, fig. 5 shows that uranium at 500° C can accommodate cycles up to 9° C amplitude without plastic strain. Table 2 shows that this amplitude increases as the normal temperature decreases.

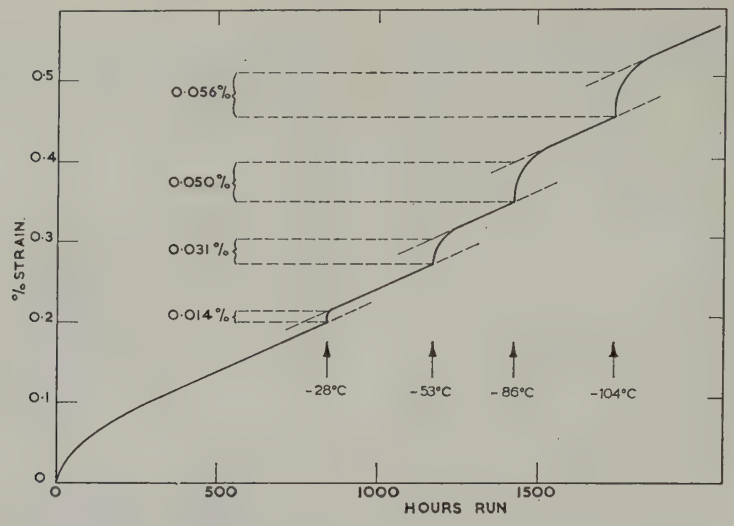

Fig. 4. Strain/time curve for 500° C, 1120 psi, showing effects of single cooling cycles.

TABLE 2

Results of plastic strain due to single temperature cycles in the range 300–450° C

Test No.	Specimen No.	Normal Temp.	Stress (psi $\times 10^{-3}$)	Cycle Amplitude (°C)	Plastic strain increment (%)		
					Immediate	Recovery	Total
1	S. 1301	300	22.4	— 30	0.000	0.000	0.000
2	S. 1301	300	22.4	— 60	0.001	0.003	0.004
3	S. 1390	300	33.6	— 60	0.057	0.038	0.095
4	S. 1197	300	13.4	— 98	0.006	0.000	0.006
5	S. 1425	300	17.9	— 98	0.010	0.000	0.010
6	S. 1301	300	22.4	— 98	0.019	0.002	0.021
7	S. 1505	300	26.9	— 98	0.038	0.015	0.053
8	S. 1390	300	33.6	— 98	0.150	0.102	0.252
9	S. 1323	350	13.4	— 30	0.000	0.000	0.000
10	S. 1323	350	13.4	— 41	0.000	0.000	0.000
11	S. 1323	350	13.4	— 46	0.000	0.000	0.000
12	S. 1323	350	13.4	— 60	0.001	0.004	0.005
13	S. 1323	350	13.4	— 101	0.026	0.023	0.049
14	S. 1305	400	6.7	— 31	0.002	0.002	0.004
15	S. 1305	400	6.7	— 59	0.005	0.002	0.007
16	S. 1305	400	6.7	— 100	0.008	0.001	0.009
17	S. 1379	400	13.4	— 100	0.050	0.047	0.097
18	S. 1306	450	4.5	— 32	0.001	0.005	0.006
19	S. 1306	450	4.5	— 60	0.009	0.010	0.019
20	S. 1306	450	4.5	— 99	0.017	0.015	0.032

The effect of imposing successive thermal cycles of the same amplitude and sign, without allowing the uranium time to recover, is shown in table 3.

This gives the total plastic strain due to successive cycles of $-20°$ C amplitude at 500° C and shows that the plastic strain is only slightly increased by increasing the number of

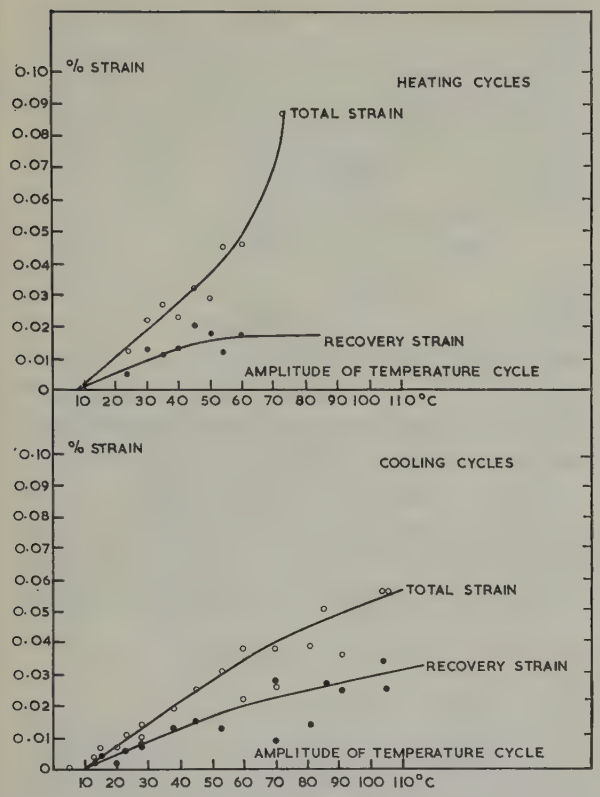

Fig. 5. Plastic strain produced by temperature cycles at 500° C and 1120 psi.
Fig. 5a. Heating cycles. Fig. 5b. Cooling cycles.

TABLE 3

Plastic strain due to successive cycles of − 20° C at 500° C and 1120 psi

Test No.	Specimen No.	No. of cycles	Plastic strain (%)
21	S 1072	1	0.007
22	S 1066	2	0.010
23	S 1066	3	0.010
24	S 1156	12	0.014

cycles. For example, twelve successive cycles are needed to double the strain produced by a single cycle.

The effect of the applied stress on the strain increment is shown by the results of Tests 4–8 at 300° C where the stress is varied but the amplitude of cycle is constant at − 98° C. These results are plotted in fig. 6.

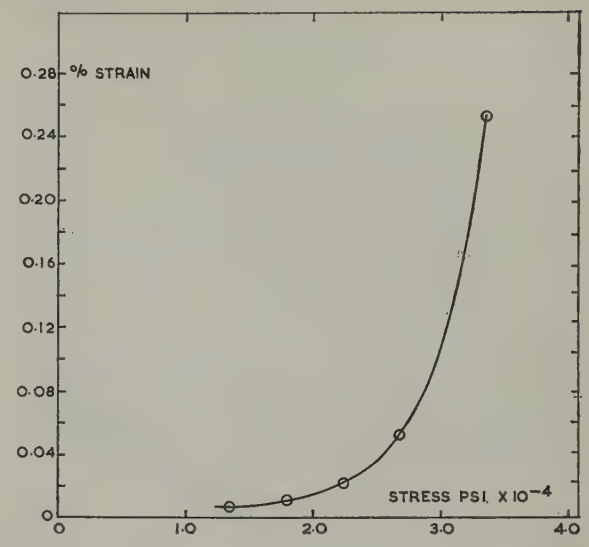

Fig. 6. Strain increment due to cooling cycles of — 98° C on creep tests at 300° C showing effects of varying applied stress.

3.2. THEORY

3.2.1. *Internal Stresses*

From the experimental results it is evident that, above a certain amplitude, thermal cycles produce plastic strain. This is attributed to the anisotropic thermal expansion characteristics of α-uranium; a change in temperature causes neighbouring crystals to interact and so generates internal stresses which may produce yielding. An estimate of the internal stresses produced in an aggregate by thermal cycling can be made if it is assumed that each grain undergoes the same deformation as the aggregate.

The aggregate will be taken to be macroscopically isotropic; that is, it contains a large number of anisotropic grains of random orientation. Let the coefficients of thermal expansion of the grain in the a, b, and c lattice directions be α_a, α_b, α_c respectively. Assuming negligible hydrostatic pressure in the aggregate, the linear coefficient of thermal expansion of the aggregate is the mean of these three values and so the macroscopic thermal expansion for a rise in temperature ΔT is $\frac{1}{3}\Delta T\ (\alpha_a+\alpha_b+\alpha_c)$. With each grain undergoing the same deformation

as the aggregate, internal stresses are generated corresponding to strains of

$$\varepsilon_a = \tfrac{1}{3}\Delta T(\alpha_b + \alpha_c - 2\alpha_a)$$
$$\varepsilon_b = \tfrac{1}{3}\Delta T(\alpha_c + \alpha_a - 2\alpha_b)$$
$$\varepsilon_c = \tfrac{1}{3}\Delta T(\alpha_a + \alpha_b - 2\alpha_c).$$

Taking $\alpha_a = \alpha_c$ [4]), these strains become

$$\varepsilon_a = \varepsilon_c = -\tfrac{1}{2}\varepsilon_b \qquad (1)$$

where

$$\varepsilon_b = \tfrac{2}{3}\Delta T(\alpha_a - \alpha_b) = \tfrac{2}{3}\Delta T\,\Delta\alpha.$$

In the elastic range, the internal stresses are derived from (1) using Hooke's Law, and are

$$\sigma_a = \sigma_c = -\tfrac{1}{2}\sigma_b \qquad (2)$$

where

$$\sigma_b = \frac{\varepsilon_b E}{(1+\nu)} = \frac{2}{3}\frac{\Delta T \Delta\alpha E}{(1+\nu)}.$$

E and ν are Young's Modulus and Poisson's Ratio respectively and are taken to be independent of crystallographic direction. The above stress system can be regarded as the sum of a tensile stress $\frac{3}{2}\sigma_b$ in the b lattice direction and a hydrostatic stress of $-\frac{1}{2}\sigma_b$. The yielding of a material is generally presumed to be unaffected by hydrostatic pressure [5]). Assuming this to be true for α-uranium, yielding will take place, in the absence of external load, when

$$\tfrac{3}{2}\sigma_b = Y \qquad (3)$$

where Y is the yield stress in tension, assumed to be independent of crystallographic direction.

3.2.2. *Macroscopic Strain during a Temperature Cycle*

Assume that the stress/strain curve for uranium at constant temperature is represented by the diagram shown in fig. 7. Between O and P Hooke's Law is obeyed; at P yield occurs and plastic strain takes place at constant stress. On removal of the stress at Q say, elastic recovery takes place along QR parallel to OP.

Consider a polycrystalline aggregate of α-uranium at constant temperature under a uniaxial stress S_1 which is small relative to Y. Let the temperature change. Internal strains given by (1) are generated which produce internal stresses given by (2). As the temperature continues to change, the stresses increase along OP until P is reached. From (1), (2), and (3) this occurs when the temperature increment is

$$\Delta T_p = \frac{Y(1+\nu)}{E\Delta\alpha}. \qquad (4)$$

The above expression is approximate as the effect of S_1 on the temperature increment required to cause yield has been neglected. Calculations made by Anderson and Bishop [6]) show that little error is introduced by this assumption when S_1 is small relative to Y.

It follows that no plastic flow is produced by a cycle of amplitude less than ΔT_p.

If, on the other hand, the amplitude of the cycle is greater than ΔT_p, plastic flow occurs

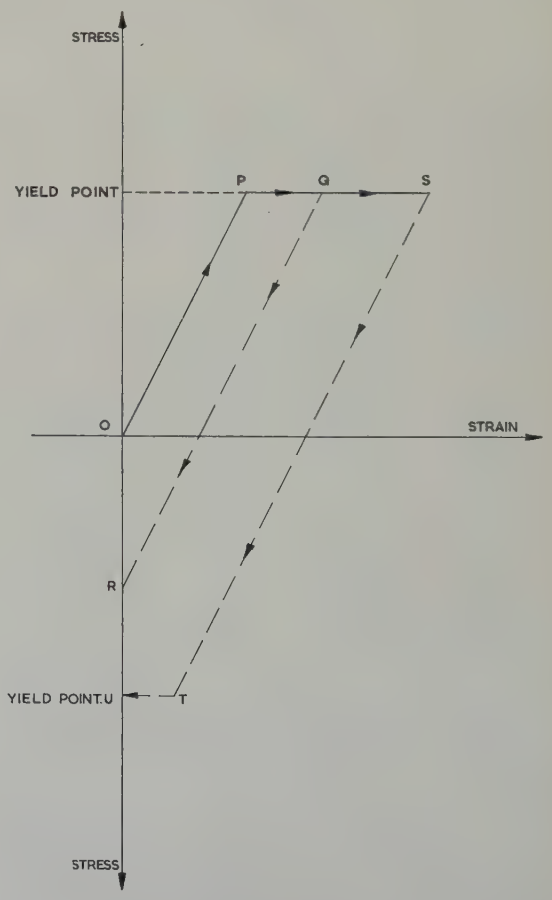

Fig. 7. Idealised stress/strain curve for uranium at constant temperature.

corresponding to PQS on the diagram. The plastic deformation produced by such a cycle is obtained by using the Levy–Mises equations [7]) which relate stress to plastic strain increment. These equations assume identity of principal axes of stress and of strain, constancy of volume, and proportionality of shear stress and strain, and may be written in the form

$$d\varepsilon_{ij} = \sigma_{ij}' d\lambda \qquad (5)$$

where $d\varepsilon_{ij}$ are the plastic components of the strain-increment, σ_{ij}' are the reduced stress components (i.e. the ordinary stress components minus the hydrostatic stress), and $d\lambda$ is a scalar factor of proportionality.

The scalar factor of proportionality for the aggregate is identical to that for the individual grain, and it follows from (5) that

$$\frac{d\varepsilon_1}{\frac{2}{3}S_1} = \frac{d\varepsilon_a}{\sigma_a'} = \frac{d\varepsilon_b}{\sigma_b'} = \frac{d\varepsilon_c}{\sigma_c'} \qquad (6)$$

where $d\varepsilon_1$ is the macroscopic plastic strain increment in the direction of the applied load, $d\varepsilon_a$, $d\varepsilon_b$, $d\varepsilon_c$ are the plastic strain increments in the a, b, c lattice directions of the grain respectively, $\frac{2}{3}S_1$ is the reduced stress component in the direction of the applied uniaxial stress, and σ_a', σ_b', σ_c' are reduced stress components in the a, b, c lattice directions respectively.

Since S_1 is taken to be small relative to Y, the values of reduced stress components in the grain during plastic flow are approximately those given by (2) and (3) and therefore

$$\sigma_b' \approx \sigma_b \approx \tfrac{2}{3}Y. \qquad (7)$$

The total plastic strain ${}_p\varepsilon_b$ in the b direction of the grain due to a temperature cycle of amplitude ΔT_Q, where $\Delta T_p < \Delta T_Q < 2\Delta T_p$ (the yield point is assumed the same in tension and compression) is from (1)

$${}_p\varepsilon_b = \tfrac{2}{3}\Delta\alpha(\Delta T_Q - \Delta T_p). \qquad (8)$$

Substituting from (6) and integrating, the following expression for the macroscopic plastic strain in the direction of the applied load is obtained.

$$\varepsilon_1 = \frac{2}{3}\frac{S_1}{Y}\Delta\alpha(\Delta T_Q - \Delta T_p) \qquad (9)$$

where

$$\Delta T_p < \Delta T_Q < 2\Delta T_p.$$

When the temperature is restored to its original value, elastic recovery takes place along QR and internal stresses corresponding to OR are left in the aggregate. The relaxation of these residual stresses by creep processes results in additional plastic deformation; this aspect of the problem is considered in Section 3.2.3.

The plastic deformation produced by a cycle of amplitude ΔT_s where $\Delta T_s > 2\Delta T_p$ is similarly obtained. The macroscopic plastic strain produced during the first half of the cycle is

$$\frac{2}{3}\frac{S_1}{Y}\Delta\alpha(\Delta T_s - \Delta T_p)$$

and that during the second half (as plastic flow then takes place corresponding to TU in fig. 7) is

$$\frac{2}{3}\frac{S_1}{Y}\Delta\alpha(\Delta T_s - 2\Delta T_p).$$

The total macroscopic strain during the cycle is therefore given by

$$\varepsilon_1 = \frac{4}{3}\frac{S_1}{Y}\Delta\alpha(\Delta T_s - 3/2\,\Delta T_p) \qquad (10)$$

where $\Delta T_s > 2\Delta T_p$.

On completion of the cycle, internal stresses corresponding to OU are left in the aggregate.

3.2.3. *Accelerated Creep produced by Internal Stresses*

The expression for the stress-dependence of steady creep of α-uranium at constant temperature and under uniaxial stress conditions has been shown in Section 2 to be of the form

$$\dot{\varepsilon}_1 = B S_1^n \qquad (11)$$

where B and n are constants.

Under multi-axial stress conditions, such as exist when internal stresses are present, it has been suggested that the following creep law applies [8])

$$\dot{\varepsilon}_{ij} = \sigma_{ij}' \cdot \tfrac{3}{2} B(3J_2')^{\frac{1}{2}(n-1)} \qquad (12)$$

where $\dot{\varepsilon}_{ij}$ are the components of the creep rate, σ_{ij}' are the reduced stress components as before

and J_2' is the second invariant of the reduced stress tensor defined as $\frac{1}{2}(\sigma_{ij}'\sigma_{ji}')$: written in terms of principal components of stress σ_{ii}, σ_{jj}, σ_{kk}, this tensor becomes $\frac{1}{2}[(\sigma_{ii}')^2+(\sigma_{jj}')^2+(\sigma_{kk}')^2]$. Equating the behaviour of the aggregate and the individual grain, as in the derivation of (6), it follows from (12) that, under a uniaxial stress S_1,

$$\frac{\dot{\varepsilon}_1}{\frac{2}{3}S_1}=\frac{\dot{\varepsilon}_a}{\sigma_a'}=\frac{\dot{\varepsilon}_b}{\sigma_b'}=\frac{\dot{\varepsilon}_c}{\sigma_c'}=\frac{3}{2}B(3J_2')^{\frac{1}{2}(n-1)} \quad (13)$$

where $\dot{\varepsilon}_1$ is the macroscopic strain-rate in the direction of the applied load and $\dot{\varepsilon}_a$, $\dot{\varepsilon}_b$, $\dot{\varepsilon}_c$ are the strain-rates in the a, b, c lattice directions of the grain respectively.

With no internal stresses present,

$$\sigma_{ii}'=\tfrac{2}{3}S_1$$
$$\sigma_{jj}'=\sigma_{kk}'=-\tfrac{1}{3}S_1$$

and (13) reduces to (11), the expression for the isothermal creep-rate.

With internal stresses present which are large compared with S_1, (2) may be used to give

$$\sigma_{ii}'=\sigma_b$$
$$\sigma_{jj}'=\sigma_{kk}'=-\tfrac{1}{2}\sigma_b.$$

Substituting these values in (13),

$$\dot{\varepsilon}_1=\dot{\varepsilon}_b\frac{S_1}{\frac{3}{2}\sigma_b}=BS_1(\tfrac{3}{2}\sigma_b)^{n-1}$$

or

$$\dot{\varepsilon}_1=BS_1{}^n\left(\frac{\frac{3}{2}\sigma_b}{S_1}\right)^{n-1} \quad (14)$$

where $\sigma_b>S_1$.

The term within brackets can be regarded as the factor by which the isothermal creep-rate is magnified by the presence of internal stresses. If the internal stresses are continually regenerated by temperature cycling in such a way that σ_b remains substantially constant then, from (1) and (2), the magnification factor R remains constant at a value

$$R=\left[\frac{E\Delta\alpha\Delta T}{S_1(1+\nu)}\right]^{n-1} \quad (15)$$

where ΔT is the effective cycling amplitude. A somewhat similar expression has been derived by Anderson [9]) using a different approach.

In the case of a single temperature cycle where residual stresses are left in the aggregate on completion of the cycle, the isothermal creep rate will be accelerated until relaxation to the normal stress level of the aggregate is accomplished. The macroscopic plastic strain in the direction of the applied load during this process, i.e. the "recovery" strain, is obtained by integrating (6) to give

$$\varepsilon_1=\frac{2}{3}\frac{S_1(1+\nu)}{E}\ln(\sigma_m/\sigma_n) \quad (16)$$

where σ_m is the residual stress in the grain immediately after the cycle and σ_n the stress in the grain under the restored steady-state condition.

3.3. Comparison of theory and experiment

Tensile tests have shown that the stress/strain curve of α-uranium at temperatures between 300° C and 500° C corresponds fairly closely to the model curve in fig. 7. From these tests, values of Y and E have been estimated. The limit of proportionality has been chosen to define Y. With these and the values of $\Delta\alpha$ given by Foote [4]), the cycle amplitudes theoretically required to cause plastic flow at temperatures of 300, 350, 400, 450 and 500° C have been calculated using eq. (4) and are as listed in table 4. ν is taken to be 0.25.

Table 4

Cycle amplitude theoretically required to produce plastic flow

Normal Temp. (°C)	Y (psi $\times 10^{-3}$)	E (psi $\times 10^{-6}$)	$\Delta\alpha$ (°C $\times 10^{6}$)	ΔT_p (°C)
300	51	21.0	37	82
350	46	19.5	42	70
400	41	18.0	49	58
450	36	16.0	55	51
500	31	13.5	60	48

The values of Y, E and $\Delta\alpha$ vary with temperature and for large cycles these variations must be taken into account. This effect is discussed later in Section 4. In table 4, the values listed correspond to the steady state temperatures.

Cycles of amplitude less than those given in table 4 should be accommodated elastically and hence cause no plastic strain. Reference to table 2 shows that this is largely true in the range 300–450° C, the extra strain in all cases but one being less than 0.006 %. The discrepancies are attributed to deviations in the behaviour of the uranium from the ideal behaviour assumed in the model. However, the maximum value of 0.006 % is so small that it may be assumed that the model is adequate. The exception is Test 3 where the measured strain is 0.095 %; this is due to the high applied stress, in this case equal to $0.66Y$. Evidently the theory breaks down at stresses of this magnitude.

Reference to fig. 5 shows that at 500° C the amplitude predicted in table 4 is incorrect as considerable plastic strain is produced by cycles of less than 48° C. In fact the minimum amplitude which will cause plastic flow is about 9° C. This discrepancy is attributed to the considerable effect that strain-rate has on the value of Y at this temperature. The tensile tests referred to earlier indicated that below 500° C the effect of strain-rate on the value taken for Y was not significant over the range of rates produced by thermal cycles. At 500° C and above, the effect of strain-rate was marked: the slower the rate, the lower the value of Y. To check the effect of strain-rate at 500° C, experiments were carried out to find the stresses generated by the application of strain at a rate corresponding to that imposed internally in an aggregate during a typical temperature cycle. It was not possible to test a single crystal under the theoretical three-dimensional strain system and so the tests were done on an isotropic aggregate (considered to have mechanical properties representative of those of a grain) under uniaxial strain.

The equivalent uniaxial strain is obtained as follows. Because a cycle of amplitude ΔT_p produces yield, a change of 1° C produces a uniaxial strain of $Y/E\Delta T_p$. Knowing the temperature/time plot for a given thermal cycle it is possible by means of the above expression to convert it into a strain/time plot. This is done

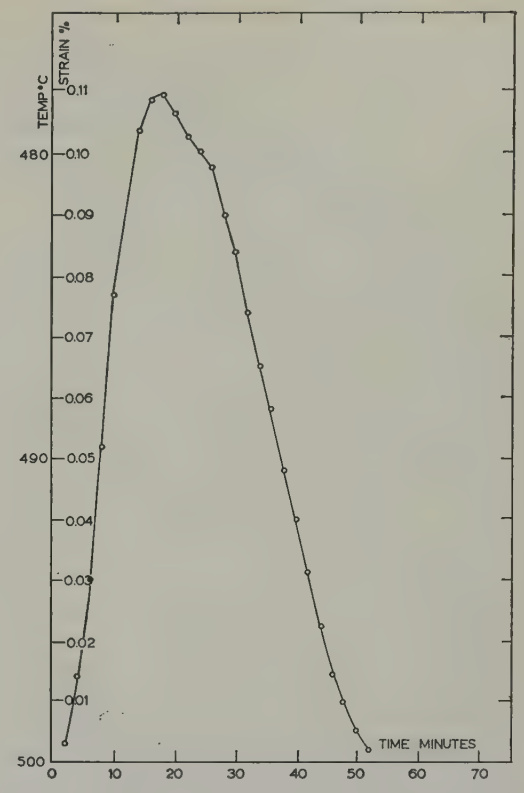

Fig. 8. Equivalent uniaxial strain/time curve to simulate temperature cycle of — 23° C from 500° C.

in fig. 8 which represents the test cycle of −23° C from 500° C (see fig. 5*b*).

Strain was applied to a uranium specimen at 500° C at the rate shown in fig. 8. The resulting stress/strain graph is shown in fig. 9. Curve OPQR describes the first loading cycle and STUV the second. RR′ is the projection of the first curve representing the compression part of the cycle which it was not possible to simulate experimentally. RS and VS are the result of anelastic recovery. It is immediately obvious from OPQR that plastic flow occurs well below the value of Y, given in Table 4, of 31000 psi. Indeed the maximum stress recorded is only 7800 psi. The discrepancy is due entirely to the difference in strain-rates in the two cases. In the standard tensile test from which Y in table 4 was estimated, the strain-rate was 2.5 % per minute. In the present test, the maximum strain-rate is only 0.01 % per minute.

The value of Y to be used in the theory

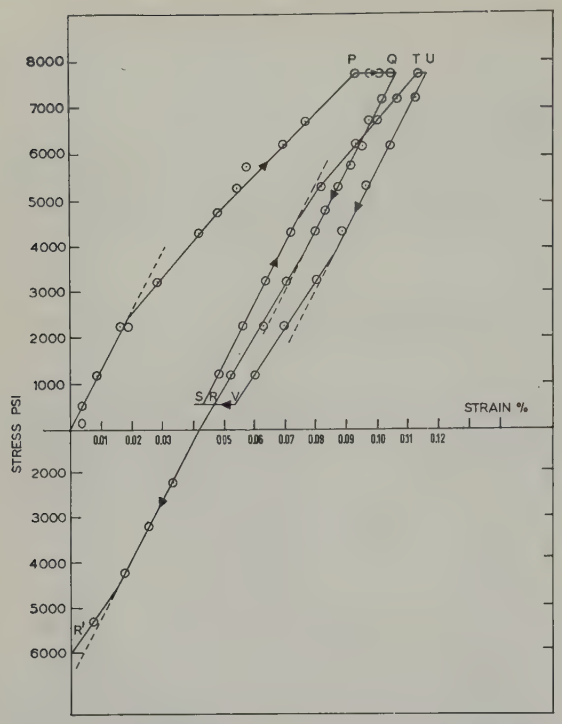

Fig. 9. Stress/strain curve resulting from application of strain at rate shown in fig. 8.

therefore depends upon the amplitude of cycle and the rate of change of temperature at temperatures of 500° C and above. This variation of Y with strain-rate accounts for the discrepancy between the predicted and the experimentally determined value of ΔT_p. Nevertheless the shape of the stress/strain curve obtained at these higher temperatures is still comparable with the model stress/strain curve of fig. 7 and so the model may still be valid.

The plastic strain resulting from a temperature cycle greater than ΔT_p can be split into "immediate" and "recovery" strains. Equations (9) and (10) predict the "immediate" strain and a comparison of theoretical and experimental values for this strain in the range 300–450° C is contained in table 5.

The agreement is to within $\pm$ 0.005 % strain except in tests 7, 8 and 16. In tests 7 and 8, the ratio of applied stress to yield stress is 0.50 and 0.66 respectively and the theory breaks down. This breakdown is illustrated in fig. 6, which shows a rapid departure from linearity at stress

Table 5

Comparison of immediate plastic strain increments

Normal temp. (°C)	Test No.	Plastic strain increment (%)	
		Theory	Experiment
300	4	0.010	0.006
300	5	0.014	0.010
300	6	0.018	0.019
300	7	0.021	0.038
300	8	0.026	0.150
350	13	0.025	0.026
400	15	0.001	0.005
400	16	0.022	0.008
400	17	0.045	0.050
450	19	0.004	0.009
450	20	0.022	0.017

greater than 0.5 Y. In test 16, the measured strain is 0.014 % less than predicted; the reason for this discrepancy is unknown.

At 500° C, the value of Y used in (9) and (10) depends upon the type of temperature cycle. For the 23° C cycle studied, the majority of plastic strain has been shown to occur at a stress of 7800 psi. Substituting this value for Y in (9), the calculated "immediate" strain is 0.006 % compared with the experimental value of 0.005 %. In the simulation of a 45° C cycle, the majority of plastic strain occurred at a stress of 11 600 psi. Substituting this value for Y in (9) gives a calculated "immediate" strain of 0.010 % compared with the experimental value of 0.010 %. Thus, there is good agreement when the value of Y used in the theory is determined from a test which simulates the cycle.

Equation (16) gives the "recovery" strain produced by the relaxation of residual stresses. It predicts that the strain will increase with cycle amplitude up to a maximum value when the residual stresses reach the yield point. To evaluate equation (16) the ratio of the stress in the grain immediately after the cycle to that under steady-state conditions must be known. With residual stresses equal to the yield point, this ratio will be of the order Y/S_1. Taking $Y = 11\,600$ psi at 500° C (the value appropriate to a 45° C cycle), substitution into

equation (16) leads to a maximum value of "recovery" strain at a stress of 1120 psi of 0.016 %. The results given in figs. 5*a* and 5*b* show that this is the value of "recovery" strain at cycles of around $\pm$ 45° C.

Higher amplitudes produce larger "recovery" strains, probably due to the sensitivity of Y to the rate of loading, but there is a tendency, particularly in fig. 5*a*, for the curve of "recovery" strain to level off above amplitudes of 45° C.

The total strain due to several successive cycles of -20° C at 500° C (see table 3) was not much greater than that due to a single cycle. The stress/strain graph in fig. 9 offers an explanation; the immediate reloading of the specimen along STU resulted in little plastic strain due to the combined effect of the presence of residual stresses and strain-hardening of the uranium. An identical curve to the first cycle is obtained if 48 hours are allowed to elapse before repeating the cycle.

4. Discussion

The theoretical model has been shown to represent adequately the effect of a thermal cycle on the deformation of α-uranium. Above 450° C, the effects of creep during the cycle became important but the theory can be modified to cater for these by using an equivalent value of Y which depends upon the rate of change of temperature during the cycle. The important part played by creep during cycling above 450° C is shown by the remarkable drop in the amplitude of cycle which the uranium can sustain elastically, from $\pm$ 51° C at 450° C to $\pm$ 9° C at 500° C.

With this modification the theory predicts reasonably accurate values of "immediate" and "recovery" strain due to a temperature cycle for values of applied stress less than half the yield stress. In practice, this limitation on the magnitude of applied stress is not restrictive as the loads carried by the fuel in current reactor designs are quite small.

For cycles of small amplitude there is no significant difference between the amounts of strain produced by either heating or cooling cycles. As the magnitude of the cycle increases, however, heating cycles produce more strain than cooling cycles. This is a result of the changes in the values of $\Delta\alpha$, E and Y with temperature. Over a small range in temperature these values remain sensibly constant but with large cycles allowance has to be made for their variation during the cycle. Pending a fuller analysis, this can most simply be done by using the average values during the cycle in the calculation of "immediate" strain. The "recovery" strain depends on the values of $\Delta\alpha$, E and Y at the steady state temperature and should therefore be unaffected by the sign of the cycle.

Only the maximum value of the "recovery" strain has been evaluated. The "recovery" strain becomes a maximum when the residual stresses after the cycle reach the yield point. This theoretically occurs when the amplitude of the cycle is $2\Delta T_p$; below this amplitude, theory predicts that the recovery strain depends upon the logarithm of the residual stress.

The type of cycle studied in this report is typical of those encountered in reactor service during trips, shut-downs and control rod trimming. An operation such as refuelling a channel entails a grabhead going into a channel a number of times in quick succession, causing thermal cycles in the neighbouring channels. Since it has been shown that closely-spaced successive cycles are scarcely more effective than a single cycle in producing strain, the refuelling operation may only have the effect of a single cycle on the adjacent channels.

It has also been shown that the effect of continuous cycles of small amplitude which arise from such causes as "dead band" in the control system, is to accelerate the isothermal creep rate. This effect can be quite large; for example, eq. (15) predicts that the isothermal creep rate of a fuel element running at 500° C and 1120 psi stress will be accelerated by a factor of 4.5 when subjected to a continuous cycle of $\pm$ 5° C, at a frequency which maintains the internal stress constant. This creep acceleration is due to the constant regeneration of

internal stresses of low magnitude in the aggregate and should not be confused with the main phenomenon discussed in this report which is the yielding of the aggregate due to large single cycles (or a limited number of such cycles). The strain produced by a large single cycle should not be affected by a background of small continuous cycles providing the amplitude of continuous cycling is small compared with ΔT_p.

Radiation effects must also be considered. It is known [10]) that irradiation by neutrons alters the mechanical properties of a metal by a process akin to dispersion hardening. The effects of this can be assessed by altering the stress/strain characteristics of the model to suit.

Irradiation above 450° C also leads [11]) to significant increases in volume due to the production of fission gases. Greenwood *et al.*[12]) have shown that the volume increase will only be a few per cent if bubbles of fission gas are nucleated on a sufficiently fine scale, the fission gases being contained at high pressure by surface energy forces. Thermal cycling can enhance the rate of swelling in two ways:

a) It may damage the structure of the uranium, giving rise to intercrystalline cracks in which the fission gases accumulate or it may alter the scale of bubble formation. In either case, surface tension forces have smaller significance and the cracks or bubbles grow by creep of the surrounding matrix.

b) It reduces the strength of the surrounding matrix in the manner shown by this paper.

5. Conclusions

1. The isothermal creep properties over the range 450–650° C can be summarised in the expression

$$\dot{\varepsilon} = \sigma^{2.41} \exp\,(2.39 - 2.48 \times 10^4/T)$$

where $\dot{\varepsilon}$ is the creep rate in h^{-1}, σ the applied stress in psi, and T the temperature in ° K.

The activation energy is about 49.6 ± 3.4 kcal/mole.

2. Thermal cycles generate internal stresses which cause yielding if the amplitude of the cycle is sufficiently large. The amplitude required to cause yielding decreases with increasing temperature, particularly above 450° C where creep effects during the cycle are important. It is independent of applied stress for stresses less than half the yield stress at the given temperature.

3. The plastic strain produced by a thermal cycle can be estimated using the theory given in this paper. The theory is valid for values of applied stress less than half the yield stress. At temperatures greater than 450° C, the rate of cycle is important; the faster the cycle, the smaller is the plastic strain produced. When the amplitude of cycle is large (e.g. greater than $\pm 50°$ C at 500° C), allowance must be made for variations in the mechanical and physical properties with temperature.

4. The strain produced by several large cycles depends upon the frequency of the cycles. The higher the frequency, the smaller is the total strain produced.

Acknowledgements

The authors wish to thank Professor A. H. Cottrell for several useful discussions, and Mr. J. Chamberlain and the many members of the Whetstone Creep Laboratory who have assisted in the experimental work.

This paper is published by permission of the English Electric Company Limited, and the United Kingdom Nuclear Power Collaboration Committee.

References

1) A. H. Cottrell, Harwell (UK) Report, AERE M/M 102 (1955)
2) A. C. Roberts and A. H. Cottrell, Phil. Mag. 1 (1956) 711
3) J. E. Dorn, National Physical Laboratory Symposium on Creep and Fracture of Metals at High Temperature, (H.M. Stationery Office, 1956).
4) F. G. Foote, Physical Metallurgy of Uranium (London and New York, Pergamon Press, 1956)
5) P. W. Bridgman, Large Plastic Flow and Fracture (New York, McGraw-Hill, 1950)
6) R. G. Anderson and J. F. W. Bishop, UKAEA Industrial Group (Culcheth) Report, IGR–TN/C 681 (1957).

[7]) R. Hill, The Mathematical Theory of Plasticity (Oxford University Press, 1950)
[8]) A. E. Johnson, Proceedings of the Institution of Mechanical Engineers **164** (1951) 432
[9]) R. G. Anderson, UKAEA Industrial Group (Culcheth) Report, IGR–TN/C 854 (1958)
[10]) A. H. Cottrell, Proceedings of the Institution of Mechanical Engineers, Forty-sixth Thomas Hawksley Lecture, 1959
[11]) G. W. Greenwood, J. Inst. of Metals **88** (1959) 31
[12]) G. W. Greenwood, A. J. E. Foreman and D. E. Rimmer, J. Nucl. Mat. **1** (1959) 305

JOURNAL OF NUCLEAR MATERIALS 2, No. 3 (1960) 248–260, NORTH-HOLLAND PUBLISHING CO., AMSTERDAM

THE EFFECT OF NEUTRON IRRADIATION ON THE TENSILE PROPERTIES OF ZIRCALOY-2

L. M. HOWE and W. R. THOMAS

Research Metallurgy Branch, Atomic Energy of Canada Ltd., Chalk River, Ontario, Canada

Received 20 October 1959

Tensile specimens of annealed, 13.1 per cent cold-worked, and tempered 25.5 per cent cold-worked Zircaloy-2 were irradiated at 220° C and 280° C with integrated fast-neutron fluxes of 3.6×10^{19} n/cm^2 and 2.7×10^{20} n/cm^2 respectively.

Post-irradiation tensile tests performed at room temperature and 280° C showed that considerable irradiation hardening occurred in all the irradiated material. This change was characterized by an increase in the proportional limit, yield stress, and ultimate tensile strength, and a decrease in the total and uniform per cent elongations. The per cent changes in mechanical properties as a result of the irradiation were greater in the annealed material than in the cold-worked material. The tensile properties of irradiated 13.1 per cent cold-worked material were almost identical to those for the irradiated tempered 25.5 per cent cold-worked material for both levels of irradiation.

A yield point was developed in irradiated annealed material tested at 280° C whereas no yield point was present in the same material tested at room temperature.

Results are also given for post-irradiation annealing studies performed on the annealed and cold-worked material irradiated at 280° C.

Des éprouvettes de traction de Zircaloy-2 recuits, écrouis de 13,1 % et de Zircaloy-2, écrouis de 25 % et revenus, ont été irradiés à 220 et 280° C avec un flux intégré de neutrons rapides de $3{,}6 \times 10^{19}$ n/cm^2 et $2{,}7 \times 10^{20}$ n/cm^2 respectivement.

Les essais de traction après irradiation effectués à température ordinaire et à 280° C ont montré qu'un durcissement considérable par irradiation était apparu dans tous les matériaux irradiés. Ce fait était caractérisé par un accroissement de la limite de proportionnalité, de la limite élastique et de la charge de rupture par traction et par un abaissement de l'allongement total et réparti %. La variation en pour cent des propriétés mécaniques résultant de l'irradiation était plus grande pour le matériau recuit que pour le matériau écroui. Les propriétés mécaniques à la traction de l'alliage écroui à 13,1 % était presque identique à celles des alliages écrouis à 25,5 % et revenus après l'une ou l'autre des irradiations.

A 280° C, une limite élastique avec palier apparaissait dans les échantillons recuits et irradiés tandis qu'aucun palier ne se formait pour le même matériau tractionné à température ambiante. Des résultats sont aussi donnés concernant les études de recuit après irradiation d'échantillons recuits ou écrouis irradiés à 280° C.

Zerreissstäbe von geglühtem, von 13,1 % kaltverformtem und von angelassenem, 25,5 % kaltverformtem Zirkaloy-2 wurden bei 220° C und bei 280° C mit schnellen Neutronen bestrahlt, wobei das Zeitintegral des Flusses $3{,}6 \times 10^{19}$ n/cm^2 und $2{,}7 \times 10^{20}$ n/cm^2 betrug.

Anschliessend bei Raumtemperatur und bei 280° C vorgenommene Zugversuche liessen bei allen bestrahlten Proben eine beträchtliche, durch die Bestrahlung bewirkte Verfestigung erkennen. Dies wurde angezeigt durch einen Anstieg der Proportionalitätsgrenze, der Streckgrenze und der Zugfestigkeit, sowie durch eine Abnahme der Dehnung. Die prozentuale Änderung der mechanischen Eigenschaften war bei geglühtem Material grösser als bei kaltverformten Material. So hatte nach der Bestrahlung das 13,1 % kaltverformte Material fast gleiche Eigenschaften wie das 25,5 % kaltverformte und angelassene Material.

Nach der Bestrahlung wies das geglühte Material eine Streckgrenze auf, wenn bei 280° C geprüft wurde, während dies bei Raumtemperaturprüfungen nicht der Fall war.

Weitere Ergebnisse beziehen sich auf Glühversuche die mit geglühten und kaltverformten Proben nach der bei 280° C vorgenommenen Bestrahlung durchgeführt wurden.

1. Introduction

Zircaloy-2 is so far the best structural material for use in water-cooled power reactors because of its corrosion resistance, strength, and low neutron capture cross section. The Canadian approach to the design of this type of reactor is to use pressure tubes which are allowed to run at the same temperature as the pressurized coolant flowing within them. The pressure-tube material therefore must have sufficient strength to contain the coolant and maintain this strength under the conditions of high temperature and neutron irradiation over long periods of time (20 years). The material chosen for the Canadian demonstration power reactor, NPD-2, is Zircaloy-2 and in this reactor the coolant will be at a temperature of 280° C and at a pressure of 1200 psi.

To increase the mechanical properties and therefore the design stress, it was suggested that the pressure tubes should be used in the cold-worked condition. Objections were raised to this suggestion on the grounds that the mechanical properties of metastable materials may recover more quickly under neutron irradiation than without.

Kemper and Zimmerman [1]) studied the effects of neutron irradiation (1.4×10^{21} n/cm^2 thermal at 40–60° C) on the room-temperature tensile properties of annealed and cold-worked Zircaloy-2. Annealed material exhibited a 60 per cent increase in yield strength, and a 35 per cent decrease in total elongation and 50 % cold-worked material showed a 30 per cent increase in yield strength and a 51 per cent decrease in total elongation. Kelly and Burgess[2]) exposed 30 % and 50 % cold-worked Zircaloy-2 to integrated thermal neutron fluxes of 6.2×10^{19} and 5.5×10^{19} n/cm^2 at 94° C and 194° C respectively. The 30 % and 50 % cold-worked material irradiated at 94° C showed a 5 to 15 per cent increase in the room-temperature tensile and yield strengths, whereas the same properties for material irradiated at 194° C exhibited about a 2 per cent increase. Pravdyuk *et al.*[3]) report results on annealed zirconium irradiated at 80° C with an integrated neutron flux of 4×10^{19} n/cm^2 and at 300° C with 1×10^{20} n/cm^2. The changes in mechanical properties increased appreciably with increasing integrated flux, thus pointing out the large effect of increased neutron exposure as compared with any annealing of radiation damage which might be expected at 300° C. Makin and Minter [4]) investigated the effect of neutron irradiation on the tensile properties of heavily cold-worked zirconium. Specimens were irradiated at 100° C with 5.1×10^{19} neutrons/cm^2 and were tested at temperatures between 20° C and 200° C. From their examination, it was concluded that the effect of irradiation on the cold-worked material was to anneal out a part of the cold-work damage, replacing it by irradiation damage.

The main purpose of the present investigation was to determine the effect of neutron irradiation on the mechanical properties of Zircaloy-2 in three different states of stability; namely: (1) fully annealed; (2) cold-worked 13.1 per cent; and (3) cold-worked 25.5 per cent and tempered at a temperature below the recrystallization temperature to give mechanical properties similar to material which had been cold-worked 13.1 per cent. An additional purpose of the present study was to examine further some of the items discussed in the above investigations. Tensile specimens, in the three different conditions were irradiated at 220° C and 280° C with 3.6×10^{19} n/cm^2 and 2.7×10^{20} n/cm^2 repsectively. This paper contains a description of the effect of irradiation on the tensile properties of specimens tested at room temperature and 280° C as well as the effect of post-irradiation annealing.

2. Material

All the Zircaloy-2 material used in this study was from a trial production-run pressure tube for a pressurized-water loop (E-20) in the NRU reactor. The analysis of the ingot FZ-644 used in the fabrication of this tube is given in table 1.

The tube was originally hot-extruded over size and then bored out to final size. The various steps undertaken to obtain mechanical-

TABLE 1
Analysis for Zircaloy-2 from Ingot FZ 644

Element	Composition	Element	Composition
Sn	1.36 %	Cu	<25
Fe	0.13 %	Ti	<25
Cr	0.10 %	V	<25
Ni	0.05 %	Mn	35
N	35 ppm	Mg	<10
C	90	Pb	<20
O	<1200	Mo	<20
H	45	Co	<10
Si	77	W	<21
Al	38	B	<0.3
Hf	<100	Cd	<0.2

test specimens, in various metallurgical conditions, from sections of the pressure tube were as follows:

(1) Rods 0.66 inches (1.67 cm) diameter and approximately 2 feet long were machined from the pressure tube section.

(2) Rods were hot swaged (500° C) from 0.66 inches (1.67 cm) to 0.40 inches (1.02 cm) diameter, followed by a cold swage to straighten.

(3) All the rods were then annealed for 1 hour at 750° C in a Houghton 980 salt bath. $\frac{1}{3}$ of the rods were left in this annealed condition.

(4) $\frac{1}{3}$ of the rods from (3) were cold-drawn from 0.400 inches (1.02 cm) to 0.373 inches (0.95 cm) diameter, i.e.: 13.1 % cold-work.

(5) The remaining $\frac{1}{3}$ of the rods from (3) were cold-drawn from 0.400 inches (1.02 cm) to 0.344 inches (0.87 cm) diameter, i.e.: 25.5 % cold-work.

(6) Tensile specimens were machined from the annealed, 13.1 % cold-worked, and 25.5 % cold-worked material.

(7) The 25.5 % cold-worked samples were sealed in vacuo in vitreosil tubing and tempered for 15 minutes at 425° C.

The tensile sample used in this investigation had a 1 inch (2.54 cm) gauge length and was 0.160 inches (0.406 cm) in diameter along the gauge length.

3. Irradiation History

One group of tensile samples was irradiated in a pressurized water loop (CR-V [5]) in the NRX reactor together with some fuel elements. The samples were attached to the outside of a Zircaloy-2 flow director, which contained the fuel elements, and were in direct contact with the loop cooling water which was maintained at 280° C during the test. Total irradiation received by the specimens was 2.7×10^{20} fast neutrons/cm^2.

The integrated flux values quoted in this paper are for neutrons with energies greater than 500 eV and are based on the estimates of the Theoretical Physics Branch at AECL. These estimates should be reliable to within 30 per cent.

Another group of tensile samples were irradiated to an integrated flux of 3.6×10^{19} fast neutrons/cm^2 at 220° C in a high-temperature fast-neutron transformer rod [6]) in the NRX reactor.

4. Experimental Details

Tensile tests were performed using an Instron Tensile Machine which had been modified for use with active specimens. A loading frame was inserted in the hot cell along with modified specimen grips, load cell, and furnace for pulling samples at elevated temperatures. Operation of the loading frame was carried out using controls situated outside the cell.

Using this equipment, approximately 25 room temperature tests or 10 elevated temperature tests could be performed in 12 hours. In addition, mechanical tests were performed on irradiated samples which had been given 1-hour anneals at temperatures up to 700° C.

5. Results

5.1. Discussion of stress-strain curves obtained

Without an extensometer attached to the specimen, the autographic record from the tensile machine gives only a crude indication of the elastic portion of the stress-strain curve. It was possible to determine a "spring constant" for the machine which consists of the elastic deflection of the grips, connectors and load cell. The curves presented in this paper have all been

TABLE 2

Room temperature tensile properties of unirradiated and irradiated Zircaloy-2

Irradiation history	Metallurgical condition	Proportional Limit (psi × 10^{-3})	0.2 % Offset Yield Stress (psi × 10^{-3})	U.T.S. (psi × 10^{-3})	Total % Elong.	% Uniform Elong.	P.L./U.T.S.	Rockwell-B Hardness
unirradiated	annealed	44.8	51.2	78.5	23.5	14	0.59	87.7
out-of-pile (280° C) †	annealed	44.3	49.4	76.0	19.6	12	0.61	—
3.6×10^{19} n/cm² (220° C)	annealed	60.9	65.6	85.1	19.5	7	0.72	89.5
2.7×10^{20} n/cm² (280° C)	annealed	75.7	79.3	91.4	12.7	4	0.83	91.9
unirradiated	13.1 % C.W.	84.1	88.1	92.9	14.0	3	0.91	90.1
out-of-pile (280° C) †	13.1 % C.W.	70.5	74.5	84.3	12.3	4	0.84	—
3.6×10^{19} n/cm² (220° C)	13.1 % C.W.	85.8	90.5	96.7	10.2	2	0.89	93.2
2.7×10^{20} n/cm² (280° C)	13.1 % C.W.	98.1	102.0	104.1	9.3	1	0.94	95.4
unirradiated	tempered, 25.5 % C.W.	72.6	77.1	92.5	15.5	6	0.79	91.2
out-of-pile (280° C) †	tempered, 25.5 % C.W.	70.0	76.0	90.0	13.0	6	0.78	—
3.6×10^{19} n/cm² (220° C)	tempered, 25.5 % C.W.	83.7	88.1	99.0	11.6	3	0.85	94.2
2.7×10^{20} n/cm² (280° C)	tempered, 25.5 % C.W.	95.1	99.4	105.8	9.4	3	0.90	95.3

† Samples maintained at 280° C for 128 days.
Results listed represent the average of 6 samples tested in each of the above conditions.

corrected using the "spring constant" and give results for the elastic modulus at room temperature in the region of 14×10^6 psi, which compares favourably with values quoted in the literature [2,7,8]).

It is important to note that the values of proportional limit, 0.2 % yield stress, and ultimate tensile strength are not affected by the fact that the tensile machine can only give a crude indication of the elastic region. The only values significantly affected are those for the per cent uniform elongation.

5.2. Effect of irradiation on the room-temperature tensile properties of annealed and cold-worked Zircaloy-2

Results of the room-temperature tensile and hardness † tests are summarized in tables 2 and 4. The corresponding corrected stress-strain diagrams are given in figs 1, 2, 3. The values of per cent uniform elongation were obtained from the corrected curves.

A comparison of the values obtained for the annealed material with and without the 128-day heat treatment at 280° C illustrates the amount of scatter which may be expected in the tests since samples in these two groups should have identical properties. The results for irradiated annealed material reveal that considerable irradiation hardening has occurred, which is dependent upon integrated fast-neutron flux. It should be noted that there was a 60° C temperature difference between the two irradiation facilities used. The samples irradiated at the higher temperature (280° C) received the higher flux and exhibited the greatest change in tensile properties. Since any effect of annealing during irradiation would be greater the higher the temperature, it appears that the degree of irradiation hardening increases with increasing fast flux. The samples irradiated in the water-cooled loop at 280° C were distributed over a 58-inch length such that the minimum flux was

† Hardness measurements were made on the shoulders of tensile specimens before tensile tests were performed.

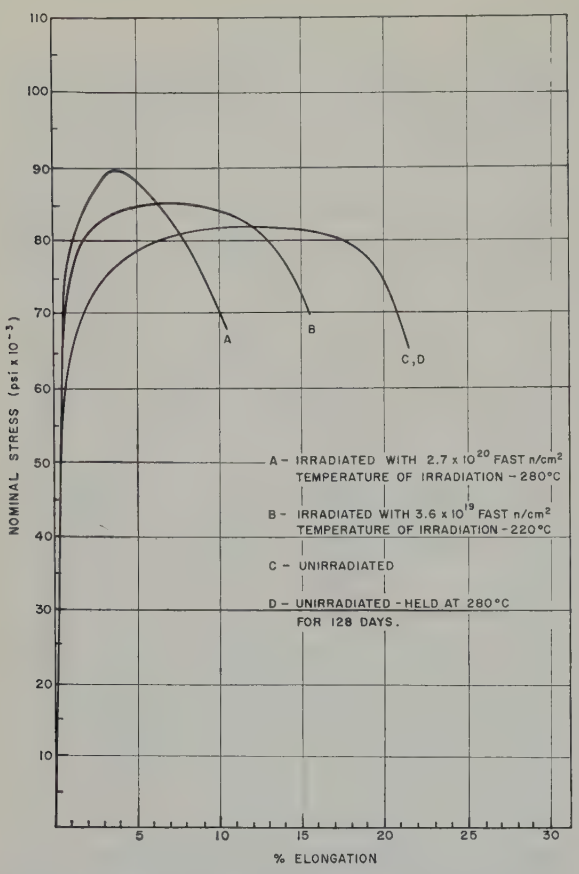

Fig. 1. Effect of neutron irradiation on the room temperature tensile properties of annealed Zircaloy-2.

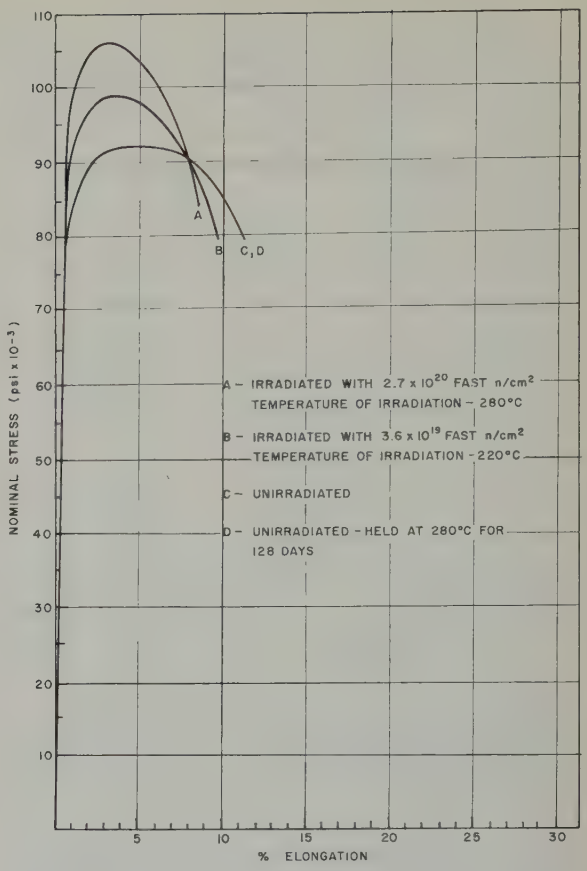

Fig. 2. Effect of neutron irradiation on the room temperature tensile properties of tempered 25.5 % cold worked Zircaloy-2.

about 75 per cent of the maximum flux. Samples tested in each of the metallurgical conditions gave consistent results over all flux positions from 0.75 to the maximum. It is possible therefore that the change in mechanical properties saturates at an integrated fast flux between 3.6×10^{19} n/cm^2 and 2×10^{20} n/cm^2. On the other hand, the difference between the tensile properties of material irradiated to the maximum integrated flux and those irradiated to 75 per cent of the maximum may be the same as the experimental scatter in the results.

Irradiation of the tempered 25.5 % cold-worked material produced appreciable increases in proportional limit, yield stress, and ultimate tensile strength with an attendant decrease in per cent elongation. The dependence upon fast flux was also similar to that for the annealed material. However, the per cent changes in mechanical properties as a result of the neutron irradiation were not as large in the cold-worked material as they were in the annealed material (see table 4).

Consider next the data for 13.1 % cold-worked material. The unirradiated tempered 25.5 % cold-worked material had lower tensile properties than the as-received 13.1 % cold-worked material. However, as shown in table 2, unirradiated 13.1 % cold-worked material which had been held at 280° C for 128 days exhibited almost identical tensile properties to those of the tempered 25.5 % cold-worked material. In addition, the tensile properties of irradiated 13.1 % cold-worked material are almost identical to those for the irradiated tempered 25.5 % cold-worked material for both levels or irradi-

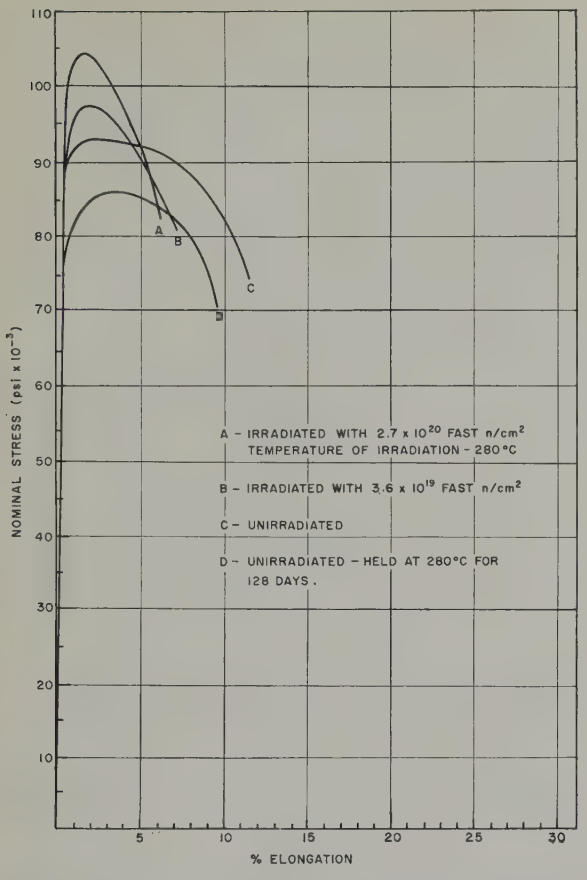

Fig. 3. Effect of neutron irradiation on the room temperature tensile properties of 13.1 % cold worked Zircaloy-2.

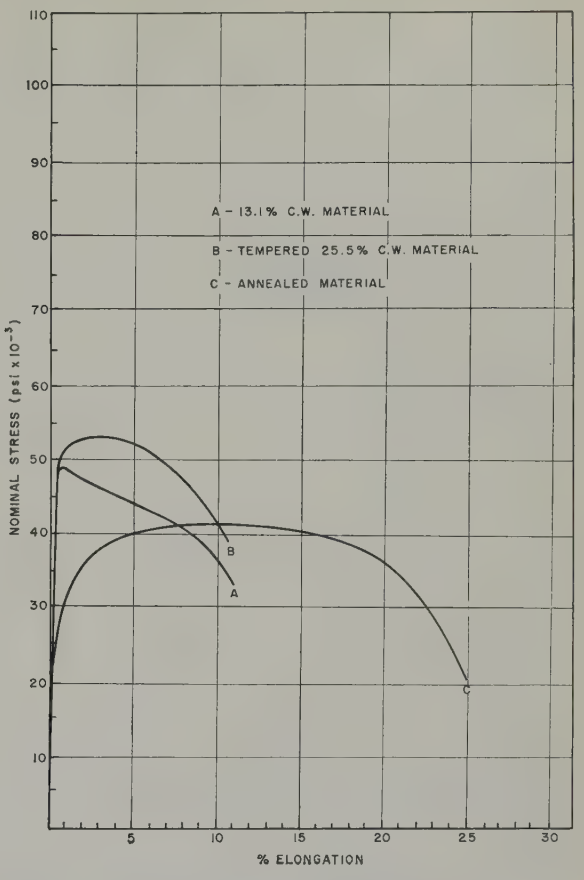

Fig. 4. Tensile properties of unirradiated Zircaloy-2 specimens pulled at 280° C.

TABLE 3

Tensile properties of unirradiated and irradiated Zircaloy-2 at 280° C

Irradiation history	Metallurgical condition	Proportional Limit (psi × 10^{-3})	0.2 % Offset Yield Stress (psi × 10^{-3})	U.T.S. (psi × 10^{-3})	Total % Elong.	% Uniform Elong.	P.L./U.T.S.
unirradiated	annealed	18.4	21.9	40.3	29.0	14	0.46
out-of-pile (280° C)	annealed	21.4	24.3	38.5	21.0	11	0.56
2.7 × 10^{20} n/cm² (280° C)	annealed	43.3 Y.P.	43.3	46.1	14.4	2	0.94
unirradiated	13.1 % C.W.	41.0	47.8	48.8	13.0	1	0.84
out-of-pile (280° C)	13.1 % C.W.	43.1	45.0	46.8	13.3	1	0.92
2.7 × 10^{20} n/cm² (280° C)	13.1 % C.W.	57.7	61.0	62.1	9	0.5	0.93
unirradiated	tempered, 25.5 % C.W.	43.9	47.9	53.1	12.5	3	0.83
out-of-pile (280° C)	tempered, 25.5 % C.W.	45.1	48.1	52.2	12.7	4	0.86
2.7 × 10^{20} n/cm² (280° C)	tempered, 25.5 % C.W.	58.6	61.7	62.1	9	1	0.94

Results listed represent the average of 6 samples tested in each of the above conditions.
Y.P. = Yield point observed in these samples.

ation. If one assumes that thermal recovery is occurring in the 13.1 % cold-worked material during irradiation at 220° C or 280° C, such that the material in this partially recovered state is not too different mechanically and structurally from tempered 25.5 % cold-worked material, than it is not surprising that the two materials have similar post-irradiation properties.

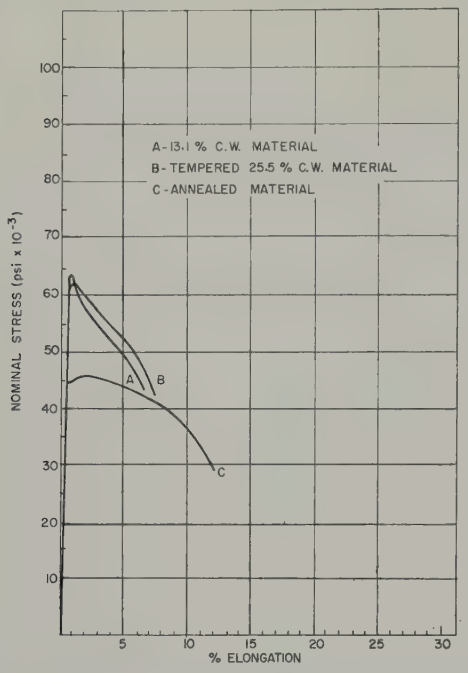

Fig. 5. Effect of neutron irradiation on the tensile properties of Zircaloy-2 samples pulled at 280° C.

5.3. Effect of irradiation on the tensile properties of annealed and cold-worked zircaloy-2 at 280° C

The results of tensile tests at 280° C are given in tables 3 and 4 and the corresponding stress-strain curves are shown in figs. 4 and 5. These tests were performed on the samples irradiated at 280° C in the CR-V loop. A rough idea of the type of scatter to be expected in these tests at 280° C can be seen by comparing the result on unirradiated annealed material before and after the out-pile heat treatment at 280° C; the tempered material shows a similar effect.

Irradiation of annealed material with 2.7×10^{20} n/cm² at 280° C produced large changes in the tensile properties at 280° C as shown by the substantial increase in propor-

Table 4
Changes in the tensile properties of Zircaloy-2 with neutron irradiation

Irradiation history	Metallurgical condition	Testing Temp.	% Increase, Proportional Limit	% Increase, Yield Stress	% Increase, U.T.S.	% Decrease, Total Elong.	% Decrease, Uniform Elong.
3.6×10^{19} n/cm² (220° C)	annealed †	R.T.	37	30	10	10	46
2.7×10^{20} n/cm² (280° C)	annealed	R.T.	70	58	18	41	69
2.7×10^{20} n/cm² (280° C)	annealed	280° C	122	87	17	42	84
3.6×10^{19} n/cm² (220° C)	temp. 25.5 % C.W.†	R.T.	15	14	7	25	50
2.7×10^{20} n/cm² (280° C)	temp. 25.5 % C.W.	R.T.	31	29	14	39	50
2.7×10^{20} n/cm² (280° C)	temp. 25.5 % C.W.	280° C	24	29	18	29	71
3.6×10^{19} n/cm² (220° C)	13.1 % C.W.†	R.T.	22	22	15	17	50
2.7×10^{20} n/cm² (280° C)	13.1 % C.W.	R.T.	39	37	24	24	75
2.7×10^{20} n/cm² (280° C)	13.1 % C.W.	280° C	34	35	33	32	50
3.6×10^{19} n/cm² (220° C)	13.1 % C.W.††	R.T.	2	3	4	27	33
2.7×10^{20} n/cm² (280° C)	13.1 % C.W.	R.T.	17	16	12	34	66
2.7×10^{20} n/cm² (280° C)	13.1 % C.W.	280° C	41	28	27	31	50

† per cent changes listed are with respect to unirradiated material held out pile at 280° C.
†† per cent changes listed are with respect to unirradiated material as received.

tional limit and yield stress, and decrease in elongation. In addition, a yield point was developed characterized by an increase in elongation at practically constant load whereas no yield point was found in the room-temperature test. The per cent changes for the irradiated tempered material tested at 280° C were not as large as those for the annealed material, and no yield point was present. It is also interesting to note that the per cent uniform elongation was quite low (at 280° C) for both unirradiated and irradiated tempered material.

Unirradiated 13.1 % cold-worked material, tested at 280° C, had essentially the same properties before the 280° C out-of-pile heat treatment as afterwards. This is not unreasonable since the specimens were held at 280° C for approximately one hour before testing. During this period, approximately 25 per cent of the recovery (of room temperature mechanical properties) which would take place during a 128-day anneal occurs. Irradiated 13.1 % cold-worked material tested at 280° C had similar properties to the irradiated tempered 25.5 % cold-worked material also tested at 280° C; this is consistent with the room temperature tensile tests.

5.4. Recovery of irradiation damage

An investigation was made to compare the annealing behaviour of unirradiated samples with material irradiated in the CR-V loop. Irradiated specimens were given 1-hour anneals in a vacuum furnace and unirradiated samples were annealed in vacuo in vitreosil capsules. The vacuum in both cases was approximately one micron. All specimens were then tested at room temperature.

From the recovery curves for irradiated annealed Zircaloy-2 (fig. 6) the following can be noted:

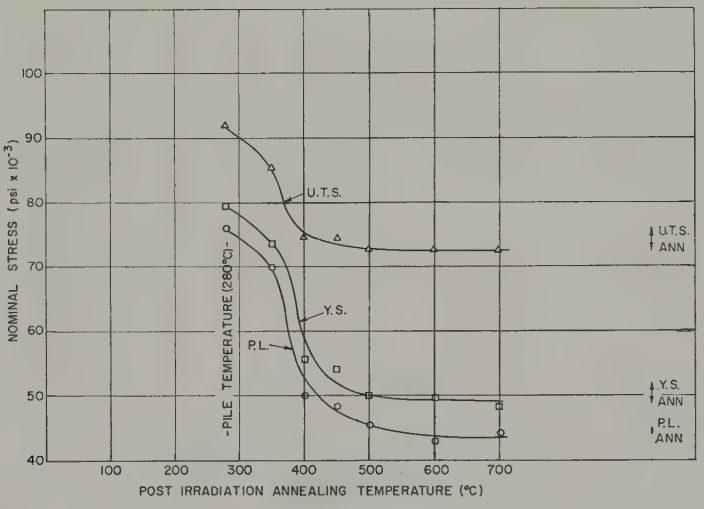

Fig. 6. Recovery curves for irradiated annealed Zircaloy-2.

(1) the irradiation-induced hardening is completely annealed out at temperatures above 500° C;

(2) most of the recovery occurs in the temperature range 300° C to 400° C;

(3) the sharp drop in the initial portion of the recovery curve suggests that some recovery of irradiation damage is probably occurring during the irradiation at 280° C;

(4) the ultimate tensile strength recovers faster than the proportional limit or yield stress; and

(5) the work-hardening range following the yield is increased with annealing.

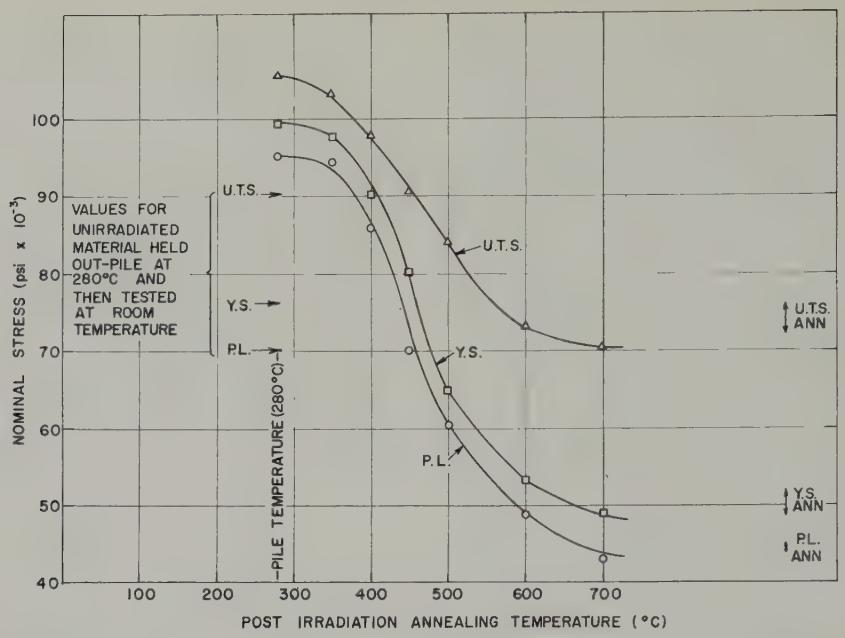

Fig. 7. Recovery curves for irradiated tempered 25.5 % C.W. Zircaloy-2.

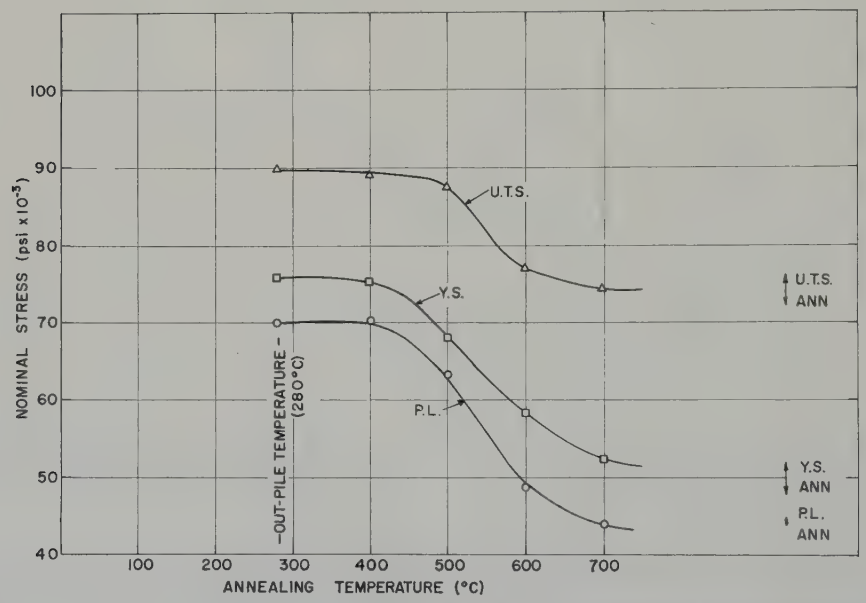

Fig. 8. Recovery curves for unirradiated tempered 25.5 % C.W. Zircaloy-2 (material held out-of-pile at 280° C for 128 days).

Similarly, examining the recovery data for tempered 25.5 % cold-worked material, in both the unirradiated and irradiated conditions, (figs. 7, 8) one can conclude that:

(1) the recovery occurring in the temperature range 280° C to 450° C is the annealing out of irradiation damage rather than cold-work;

(2) the irradiation damage is completely annealed out at approximately 450° C and some recovery of irradiation damage is probably occurring at 280° C;

(3) the recovery curve from 450° C to 700° C for irradiated material is fairly similar to that for unirradiated material; there is an indication

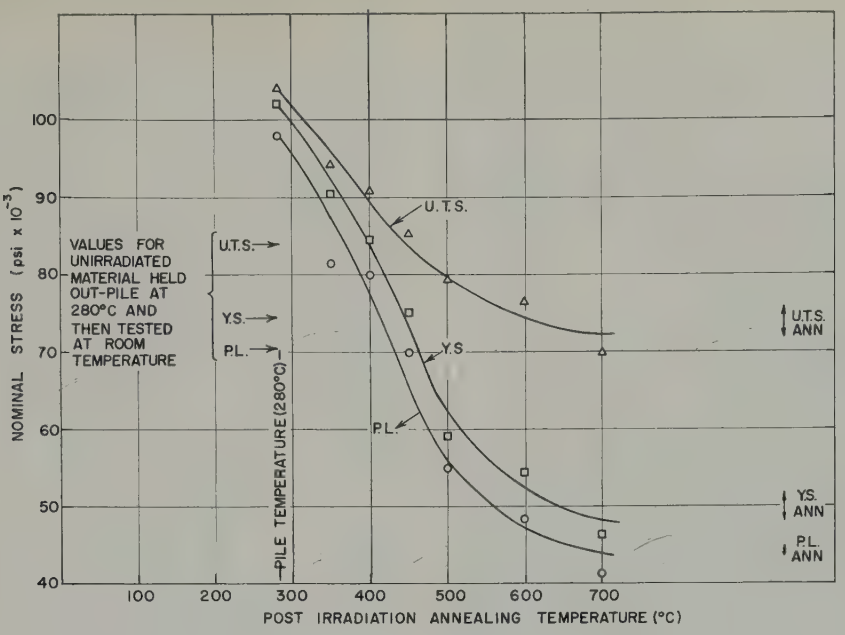

Fig. 9. Recovery curves for irradiated 13.1 % C.W. Zircaloy-2.

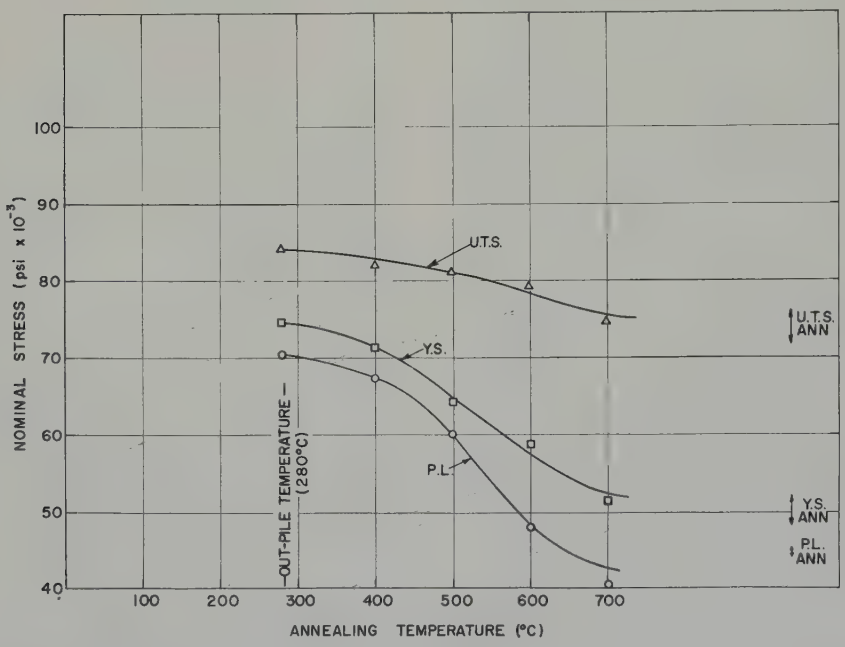

Fig. 10. Recovery curves for unirradiated 13.1 % C.W. Zircaloy-2 (material held out-of-pile at 280° C for 128 days).

that the irradiated material does recover slightly faster;

(4) the ultimate tensile strength recovers before the proportional limit and yield stress in both the irradiated and unirradiated material; and

(5) the work-hardening range following the yield is increased with annealing.

The results for the recovery of irradiated and unirradiated 13.1 % cold-worked material are given in figs. 9 and 10. In general the recovery characteristics are identical to those for temper-

ed 25.5 % cold-worked material except that in the case of 13.1 % cold-worked material some recovery of cold-work does occur between 280° C and 450° C. However most of the recovery occurring in this temperature range appears to be the annealing out of irradiation damage rather than cold-work.

6. Discussion of Results

It is evident from the results obtained in this study that a considerable increase in proportional limit, yield stress and ultimate tensile strength has occurred in annealed and cold-worked Zircaloy-2 irradiated at 220° C and 280° C, and that the magnitude of this irradiation-induced hardening increases in the range 3.6×10^{19} to 2.7×10^{20} n/cm^2. In addition, in the irradiated material, the flow curve after yielding exhibits a region of lower work hardening than in the unirradiated material, as indicated by the reduction in uniform elongation and the increase in the ratio of proportional limit to ultimate tensile strength. The fact that the uniform elongation is quite low in the irradiated material does not necessarily mean that the material is brittle, but is a consequence of the very low rate of work hardening. Once deformation starts at a particular point, it continues in this region until fracture occurs, because it is impossible for the material to work-harden.

The specimens irradiated in the pressurized-water loop were in contact with the loop water at 280° C and therefore susceptible to hydrogen absorption. The hydrogen analysis of irradiated and unirradiated samples, Table 5, indicate a maximum possible pick-up of 19 ppm. The work of Wheeler and Kelly [9]) and Yeniscavitch *et al.*[10]) suggests that the hydrogen pick-up of Zircaloy-2 irradiated in pressurized hot water is quite low. There is evidence [10,11]) that the tensile properties of Zircaloy-2 are unaffected by hydrogen until concentrations of more than 500 ppm are reached. Forscher [12]), however, has shown that less than 100 ppm of hydrogen can affect the ductility of zirconium, as measured by the percent reduction in area. Reductions in area were not measured in this investigation.

Table 5

Hydrogen analysis of unirradiated and irradiated Zircaloy-2 samples

Irradiation history	Metallurgical condition	Sample †	Hydrogen content (ppm)
unirradiated	annealed	1	51
unirradiated	annealed	2	51
irradiated	annealed	A	70
irradiated	annealed	B	58
unirradiated	13.1 % C.W.	3	58
unirradiated	13.1 % C.W.	4	59
irradiated	13.1 % C.W.	C	71
irradiated	13.1 % C.W.	D	53
unirradiated	25.5 % C.W.	5	66
unirradiated	25.5 % C.W.	6	86
irradiated	25.5 % C.W.	E	78
irradiated	25.5 % C.W.	F	46

† Note that the unirradiated and irradiated results pertain to different samples.

Thus it appears that the amount of hydrogen absorbed by the specimens in the loop water is too small to affect the measured tensile properties and therefore, the difference in properties between the specimens irradiated in loop water and those irradiated dry in a transformer rod must be due to differences in integrated flux.

Kemper and Zimmerman [1]) found that annealed Zircaloy-2 irradiated at 40 to 60° C with 1.4×10^{21} thermal neutrons/cm^2, and tested at room temperature, exhibited a yield point. In this study no yield point was observed in irradiated annealed material tested at room temperature, although a yield point was found in material tested at 280° C. The room temperature yield point reported by Kemper and Zimmerman was completely removed by annealing out of pile at 300° C. It is possible therefore, that the defects responsible for the yield point in their study may have been annealed out or redistributed during irradiation at 220° C–280° C. In addition, the integrated fast neutron fluxes in this study were probably $\frac{1}{3}$ or $\frac{1}{4}$ of theirs.

The yield point which appears in the irradiated annealed specimens at testing temperatures

of 280° C and not at room temperature is rather difficult to explain. Generally, a yield point will not be observed unless the stress required to initiate dislocation movement is larger than the stress required to move the dislocations through the lattice. The increase in yield stress is normally attributed to atmosphere formation and locking of dislocations, e.g.: carbon and nitrogen atmospheres in iron. In the present case, it is unlikely that the yield point arises due to atmosphere formation since the yield point only appears at the higher temperature whereas the yield point disappears in iron above a temperature of 700° K (427° C) since the atmospheres are no longer condensed at this temperature. The dislocations could be effectively locked, however, by jogs caused by the trapping of vacancies and interstitials produced during irradiation. If the yield stress does not decrease as rapidly with increasing temperature as the stress required to move the dislocation through the lattice, then:

(1) a yield point is not observed at room temperature because the stress to initiate movement is about the same or less than the stress required for movement, and;

(2) a yield point is observed at high temperatures because the initiation stress is not affected as much by temperature as the movement stress.

Makin and Minter [4]) report the presence of a yield point in annealed titanium irradiated at 100° C with 5.1×10^{19} thermal neutrons/cm^2 and tested at 200° C. Unirradiated and irradiated material tested at lower temperatures (20° C and −78° C) exhibited no yield point. They argue that the existence of this yield point at 200° C indicates that defects, probably vacancies, produced by irradiation become mobile between 20° C and 200° C and migrate to the dislocations and anchor them. Furthermore, the development of a yield point on annealing cold-worked copper at a temperature where the vacancies produced by the deformation are mobile, has been observed by Pry and Hennig [13]) and by Blewitt [14]). It should be noted however, that in our study the yield point occurred during testing at the irradiation temperature whereas the yield point found by Makin and Minter, in titanium, occurred during testing at a temperature 100° C higher than the irradiation temperature.

The tensile properties of 13.1 % cold-worked material and tempered 25.5 % cold-worked material were almost identical after irradiation even though the two materials were structurally and mechanically different before irradiation. This may be attributed to the fact that a portion of the cold-work in the 13.1 % cold-worked material recovered during the irradiation at 280° C and in this recovered state the material was not too different structurally or mechanically from tempered 25.5 % cold-worked material. Consequently the effect of irradiation on the two materials would be expected to be very similar.

The results of the recovery study on irradiated and unirradiated Zircaloy-2 may be summarized as follows:

(1) Irradiation damage could be annealed out during a 1-hour anneal in the region of 450° C for material in all three different metallurgical conditions.

(2) It appears that there is a slight recovery of irradiation damage occurring in all the material during the irradiation at 280° C (no recovery data are available for the 220° C irradiation).

(3) Recovery curves for unirradiated and irradiated cold-worked material were very similar in the range 450° C to 700° C which implies that recovery of cold-work alone is occurring in this temperature region. The irradiated material did recover slightly more than the unirradiated at any given temperature in this range.

It should be borne in mind that the effect of out-of-pile annealing of irradiated material has been studied here and these results are not applicable to in-pile annealing studies. A direct comparison cannot therefore be made with the work of Kelly and Burgess [2]) who found that the recovery of irradiation-produced damage was more rapid during an elevated-temperature

irradiation than during a post-irradiation anneal at the same temperature.

It should be noted, however, that the recovery curves in the region 450° C to 700° C were fairly similar for irradiated and unirradiated cold-worked material. It thus appears that: (1) virtually no recovery of cold-work has occurred during the irradiation of tempered 25.5 % cold-worked material at 280° C; and (2) the amount of cold-work recovery occurring in 13.1 % cold-worked material during an irradiation at 280° C was not too different from that occurring during a 280° C out-of-pile annealing treatment. Hence the cold-work recovery in Zircaloy-2 is not significantly altered by an irradiation at 280° C. It may, however, be affected by higher irradiation temperatures.

Acknowledgements

The authors are very grateful to the members of the Bettis Atomic Power Laboratories, Westinghouse Electric Corporation who made the irradiation of the Zircaloy-2 specimens in the CR-V loop possible. We would also like to acknowledge the assistance given by the Mines Branch and AECL workshops in preparing the specimens and the metallurgy cave personnel in testing the active specimens. In addition, we would like to thank Mr. H. Boychuk and Mr. K. J. Roestad for their valuable assistance through this study.

References

1) R. S. Kemper and D. L. Zimmerman, Hanford (USA) Report, HW-52323 (1957)
2) W. S. Kelly and A. B. Burgess, Hanford (USA) Report, HW-52004 (1957)
3) N. F. Pravdyuk *et al.*, Second Geneva Conference 15/P/2052 (1958)
4) M. J. Makin and F. J. Minter, J. Inst. Metals **85** (1957) 397
5) NRX Reactor Staff, Atomic Energy of Canada Report, AECL-101-49 (1955)
6) J. G. Melvin and D. T. Nishimura, Atomic Energy of Canada Report, AECL-NEI-117 (1959)
7) A. R. Kephart, Knolls Atomic Power Laboratory (USA) Report, KAPL-M-ARK-1 (1957)
8) "Materials Handbook", Westinghouse Atomic Power Division (UAS) Document, WAPD-AIW(M)-642. (Section on "Properties of Zircaloy-2 and Zircaloy-3")
9) R. G. Wheeler and W. S. Kelly, Hanford (USA) Report, HW-39805 (1955)
10) W. Yeniscavich, R. A. Wolfe and R. M. Liebermann, J. Nucl. Mat. **1** (1959) 271
11) G. T. Muehlenkamp and A. D. Schwope, Battelle (USA) Report, BMI-845 (1953)
12) F. Forscher, Trans. Amer. Inst. Min. Metall. Engrs. **206** (1956) 536
13) R. H. Pry and R. W. Hennig, Acta Met. **2** (1954) 318
14) T. H. Blewitt, Phys. Rev. **91** (1953) 115

JOURNAL OF NUCLEAR MATERIALS 2, No. 3 (1960) 261-268, NORTH-HOLLAND PUBLISHING CO., AMSTERDAM

NOMENCLATURE PROPOSEE POUR LES PHASES DES ALLIAGES D'URANIUM

Mme J. LEHMANN

Centre d'Etudes Nucléaires de Saclay, France

et

R. F. HILLS

Atomic Energy Research Establishment, Harwell, England

1. Introduction

Depuis que Ahmann, Snow et Wilson [1]) ont étudié le diagramme uranium-molybdène, l'importance de ces alliages, comme matériaux combustibles nucléaires a conduit à l'accumulation d'une nombreuse bibliographie, mais malheureusement, celle-ci se trouve compliquée par la trop grande diversité dans la notation des phases.

Lors d'un colloque qui a eu lieu à Saclay, les représentants de différents laboratoires de métallurgie de France et d'Angleterre ont proposé les bases d'une nouvelle nomenclature. Bien que cette nomenclature se rapporte particulièrement aux alliages uranium-molybdène, elle est suffisamment générale pour permettre la désignation des phases à l'équilibre et des phases métastables dans tous les diagrammes présentant une zone de solubilité solide dans la phase γ cubique centrée.

Cette nomenclature est publiée dans l'espoir qu'elle soit appliquée et systématiquement étendue par tous ceux qui étudient les alliages d'uranium présentant des phases métastables.

2. Mise en evidence des phases metastables

A Harwell [2]), un certain nombre de phases métastables ont été observées dans les alliages d'uranium dont les teneurs vont jusqu'à environ 15 % at de molybdène, ces phases ont été mises en évidence, dans des échantillons ayant subi des trempes à partir de la phase γ cubique centrée. Les alliages contenant de 5 à 10 % at de molybdène trempés à partir de 900° C, se transforment par un mécanisme de cisaillement, les phases obtenues présentent différents aspects micrographiques, correspondant, dans la plupart des cas à des microstructures en bandes.

A Saclay, une étude détaillée a été faite sur les structures en bandes dans les alliages uranium-molybdène de teneurs allant jusqu'à 10 % at de

PROPOSED NOMENCLATURE FOR PHASES IN URANIUM ALLOYS

Mme J. LEHMANN

Centre d'Etudes Nucléaires de Saclay, France

and

R. F. HILLS

Atomic Energy Research Establishment, Harwell, England

1. Introduction

Since the uranium-molybdenum system was first investigated by Ahmann, Snow and Wilson [1]), the importance of these alloys as potential nuclear fuels has led to the accumulation of an extensive fund of information, unfortunately confused by a diversity of terminology. At a meeting held at Saclay between representatives of metallurgy laboratories associated with uranium alloy studies in France and England, an agreed basis of nomenclature was proposed. Although the nomenclature has special reference to uranium-molybdenum alloys, it is believed to be sufficiently general to cover equilibrium and metastable phases existing in all uranium systems showing solubility in the body centered cubic gamma phase.

This account is published in the hope that the nomenclature set out below will be applied and systematically extended as necessary by all those studying uranium alloys wherein metastable phases are encountered.

2. The occurrence of metastable phases

At Harwell [2]), in uranium alloys containing up to approximately 15 at % molybdenum, a number of these metastable phases have been observed after quenching from the high temperature cubic γ phase field. Alloys containing 5 or 10 at % molybdenum, when quenched into water from 900° C, transformed by means of a shear mechanism, to structures which, although of somewhat different metallographic appearance, were in both cases banded. At Saclay, a detailed study was made on the formation of the banded structures in uranium-molybdenum alloys containing up to 10 at % molybdenum [3]). The results obtained by the British and French workers are in reasonable agreement, although nomenclature has hitherto been somewhat different. These different

Tableau 1

Publications AERE	Publications Saclay	Nouvelle Nomenclature
α	$\left\{ \begin{matrix} \alpha'' \\ \alpha''' \end{matrix} \right.$	α_a'
α_s'	α_b'	α_b'
α_s''	α_b'	α_b''
α_n'	α sursaturé	α_n'
γ	γ	γ
γ° ou γ_1	γ_0	γ°
γ_0 avec des déformations	γ_0 avec des déformations	$\gamma_d{}^\circ$
γ'	γ'	γ'

Table 1

AERE Publications	Saclay Publications	Agreed Nomenclature
α	$\left\{ \begin{matrix} \alpha'' \\ \alpha''' \end{matrix} \right.$	α_a'
α_s'	α_b'	α_b'
α_s''	α_b'	α_b''
α_n'	supersaturated α	α_n'
γ	γ	γ
γ° or γ_1	γ_0	γ°
if showing deformation markings	if showing deformation markings	γ_d'
γ'	γ'	γ'

molybdène [3]). Les résultats obtenus par les chercheurs anglais et français sont en bon accord bien que, jusqu'ici, la nomenclature ait été quelquefois différente. Ces différentes notations sont présentées dans le tableau 1 qui montre également les nouvelles désignations correspondantes.

Des structures en bandes similaires ont été observées dans d'autres diagrammes binaires: uranium-titane [4,5,6]), uranium-niobium [7,8,9]), uranium-vanadium [10]), uranium-rhénium [11]), uranium-aluminium et uranium-étain [12]).

Toutes ces structures en bandes qui sont des modifications de la structure α orthorhombique ont été nommées par de nombreux chercheurs: α distordu.

En plus des variantes de la phase α, une phase métastable basée sur la structure γ a été observée par des chercheurs américains [13]), anglais [2]) et français [14]). Cette phase est obtenue par trempe à partir de la phase γ, dans le cas d'alliages uranium-molybdène ou uranium-niobium de teneur en élément d'addition un peu supérieure à 10 % at.

3. Nomenclature

La terminologie et les notations proposées sont montrées dans le tableau 2 et illustrées par les planches de micrographies, la nomenclature est basée sur les principes ci-dessous:

a) Les structures qui sont des modifications de la structure α orthorhombique seront désignées: α.

Les indices placés en position supérieure indiqueront le remplacement de la structure orthorhombique d'équilibre par une variante mise en évidence par la diffraction des rayons X. Deux variantes ont ainsi été identifiées:

(i) une contraction relative du paramètre b sera indiquée par une seule apostrophe, par exemple: α'.

(ii) une contraction relative du paramètre b et un

notations are related in table 1 which also shows the corresponding agreed nomenclatures.

Similar banded structures have also been observed in other binary uranium alloy systems: uranium-titanium [4,5,6]), uranium-niobium [7,8,9]), uranium-vanadium [10]), uranium-rhenium [11]), uranium-aluminium and uranium-tin [12]). All of these banded structures appear to be modifications of the α uranium structure and have been widely designated "distorted alpha".

In addition to the variations of the α uranium phase, a metastable phase based on the cubic γ phase has been observed by American [13]), British [2]) and French [14]) investigators. This phase is formed when alloys of uranium containing above approximately 10 at % of molybdenum or niobium are quenched from the γ phase field.

3. Nomenclature

The proposed terminology and notations, set out in table 2 and illustrated by the chart of micrographs, is based on the principles set out below:

(a) All structures which are modifications of the orthorhombic α uranium phase to be designated α.

Any superscript attached will indicate a departure from the equilibrium orthorhombic structure, as determined by X-ray diffraction analyses. Two such variations have so far been identified, namely:

(i) A relative contraction of the b parameter only, which will be indicated by a single dash, e.g., α'.

(ii) A relative contraction of the b parameter, together with a change from an orthorhombic to a monoclinic structure, as found by one of us [14]), to be indicated by two dashes, e.g., α''.

Subscripts, if used, will indicate metallographic identification. Acicular, banded and nucleation and growth structures have already been observed. These are designated by the subscripts "a", "b" and "n" respectively; these subscripts are chosen to have

TABLEAU 2
Nomenclature et microstructures

α	Phase α à l'équilibre, grain de forme irrégulière (fig. 1).
α_a'	Aspect aciculaire, contraction relative du paramètre b (fig. 2).
α_b'	Bandes bien définies, contraction relative du paramètre b (fig. 3).
α_b''	Aspects variant des bandes régulières s'interpénétrant (fig. 4) aux bandes très irrégulières (fig. 5). Les forts grossissements montrent des bandes plus fines à l'intérieur des bandes régulières (fig. 6) contraction relative du paramètre b et passage à la structure monoclinique.
α_n'	Structure produite par germination et croissance, contraction relative du paramètre b (fig. 7).
γ	Grains équiaxes isotropes (fig. 8).
γ°	Grains légèrement anisotropes, structure tétragonale avec rapport c/a de 0,98 environ (fig. 9).
γ_d°	Identique à γ°, grains présentant des bandes en quantités variables (fig. 10 et 11).
γ'	Aspect quadrillé à larges bandes, phase ordonnée U_2Mo du diagramme uranium-molybdène (fig. 12).
γ_1, γ_2	Phases cubiques centrées de différents paramètres, formées dans la zone de nonmiscibilité du diagramme uranium-niobium (fig. 13).

Les schémas correspondant aux diagrammes de rayons X sont présentés fig. 14.

TABLE 2
Nomenclature and microstructures

α	Equilibrium α phase, irregular grain shape (fig. 1).
α_a'	Acicular appearance, relative contraction in the b parameter (fig. 2).
α_b'	Well defined bands, relative contraction in the b parameter (fig. 3).
α_b''	Appearance ranges from regular interpenetrating bands (fig. 4) to very irregular bands (fig. 5). High magnification shows structure within the regular bands of both α_b' and α_b'' (fig. 6). Relative contraction in the b parameter, change to monoclinic structure.
α_n'	Nucleation and growth structure, relative contraction in the b parameter (fig. 7).
γ	Equi-axed grains, isotropic (fig. 8).
γ°	Weakly anisotropic grains, slight tetragonality, c/a ratio approximately 0.98 (fig. 9).
γ_d°	As for γ°, with varying amount of bands in the grains (figs. 10 and 11).
γ'	Cross banded appearance, broad bands, ordered form in the uranium-molybdenum system (U_2Mo) (fig. 12).
γ_1, γ_2	These are both body centred cubic phases, with differing parameters, occuring within the immiscibility loop in the uranium-niobium system (fig. 13).

Drawings corresponding to X-ray diagrams are assembled in fig. 14.

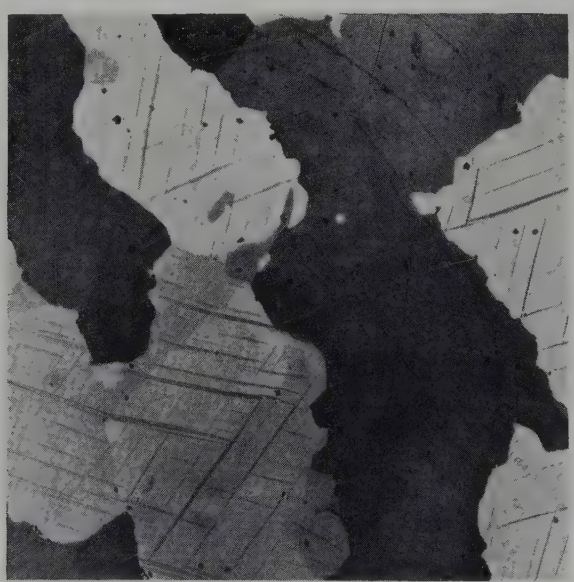

Fig. 1. Uranium naturel. Polissage attaque en solution chromique-acétique, lumière polarisée. × 30
Natural uranium. Attack polished in chromic acid/acetic acid solution. Polarised light. × 30

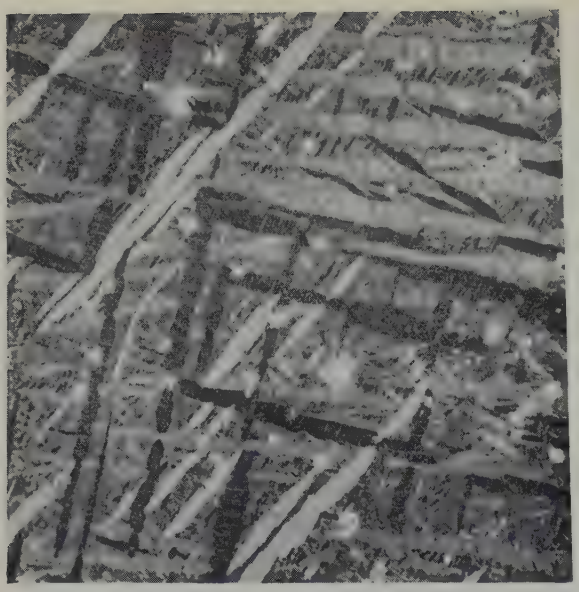

Fig. 2

α_a' – alliage U–Mo à 2 % at Mo. Trempé à l'huile à partir de 950° C. Polissage électrolytique en solution phosphorique-sulfurique. Lumière polarisée. × 450

α_a'. 2 at % molybdenum-uranium alloy. Oil quenched from 950° C. Electro-polished in phosphoric acid/sulfuric acid solution; Polarised light. × 450

Fig. 4

α_b'' – alliage U–Mo à 7,2 % at Mo. Trempé à l'huile à partir de 950° C. Polissage électrolytique en solution phosphorique-sulfurique. Oxydation sous pression partielle d'oxygène (10^{-2} mm) et 1 000 volts. Lumière normale. × 450

α_b''. 7.2 at % molybdenum-uranium alloy. Oil quenched from 950° C. Electro-polished in phosphoric acid/sulfuric acid solution, oxidized under partial pressure of oxygen (10^{-2} mm) and 1 000 volts. Normal light. × 450

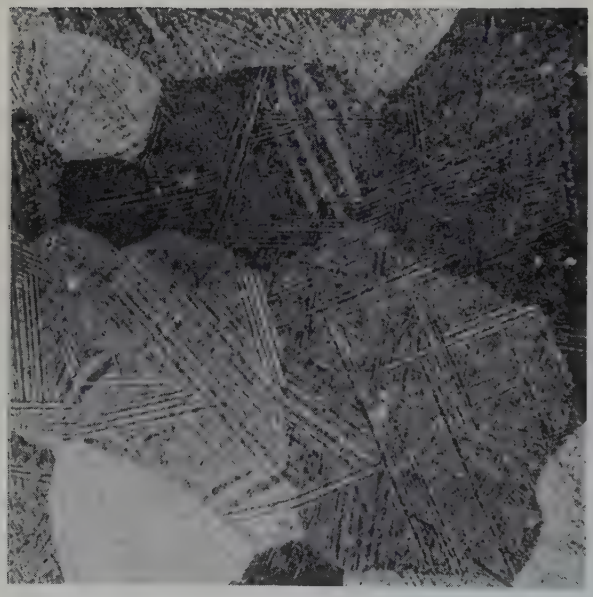

Fig. 3

α_b' – alliage U–Mo à 5 % at Mo. Trempé en bain de mercure à partir de 1 000° C. Polissage attaque en solution chromique-acétique. Lumière polarisée. ×500

α_b'. 5 at % molybdenum-uranium alloy. Mercury quenched from 1 000° C. Attack polished in chromic acid/acetic acid solution. Polarised light. × 500

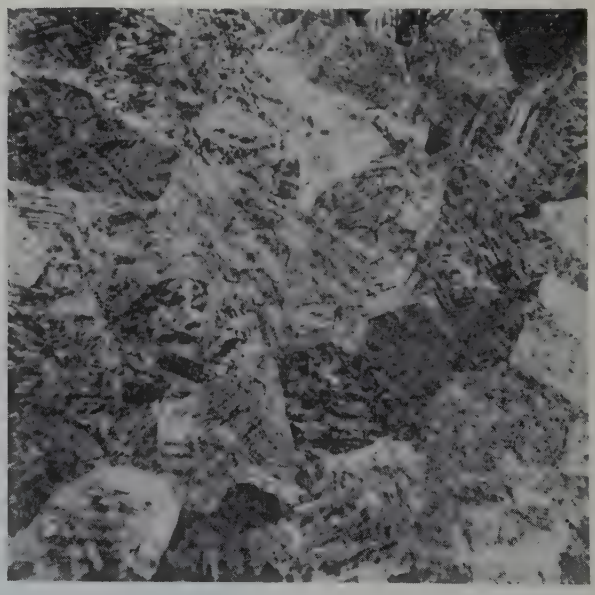

Fig. 5

α_b'' – alliage U–Mo à 10 % at Mo. Trempé en bain de mercure à partir de 1 000° C. Polissage attaque en solution chromique-acétique. Lumière polarisée. ×500

α_b''. 10 at % molybdenum-uranium alloy. Mercury quenched from 1000° C. Attack polished in chromic acid/acetic acid solution. Polarised light. × 500

Fig. 6

α_b'' – alliage U–Mo à 7,2 % at Mo. Trempé à l'huile à partir de 950° C. Polissage électrolytique en solution phosphorique-sulfurique. Oxydation sous pression partielle d'oxygène (10^{-2} mm) et 1 000 volts. Lumière normale. × 450

α_b''. 7.2 at % molybdenum-uranium alloy. Oil quenched from 950° C. Electro-polished in phosphoric acid/sulfuric acid solution, oxidized under partial pressure of oxygen (10^{-2} mm) and 1 000 volts. Normal light. × 450

Fig. 8

γ – alliage U–Mo à 22 % at Mo. Trempé à l'huile. Polissage électrolytique en solution phosphorique-sulfurique. Attaque en solution nitrique-acétique. Lumière normale. × 150

γ. 22 at % molybdenum-uranium alloy. Oil quenched. Electro-polished in phosphoric acid/sulfuric acid solution, etched in nitric acid/acetic acid solution. Normal light. × 150

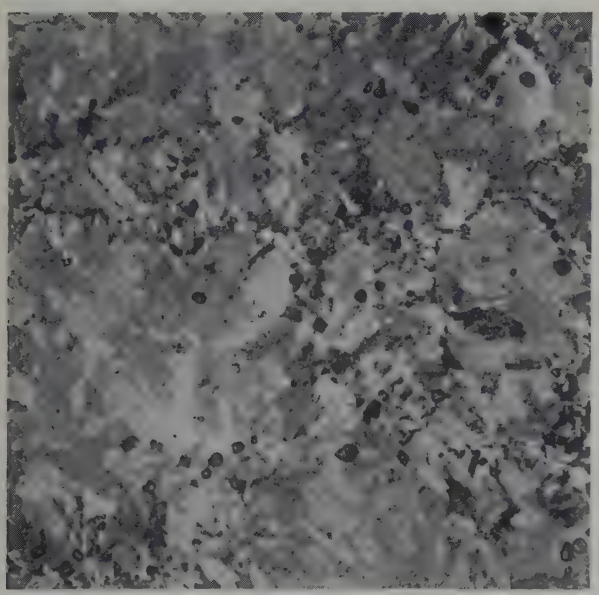

Fig. 7

α_n' – alliage U–Mo à 7,2 % at Mo. Trempe étagée de 950° C à 560° C pendant 5 min. Polissage électrolytique en solution phosphorique-sulfurique. Lumière polarisée × 150

α_n'. 7.2 at % molybdenum-uranium alloy. Step quenched from 950° C to 560° C for 5 min. Electro-polished in phosphoric acid/sulfuric acid solution. Polarised light. × 150

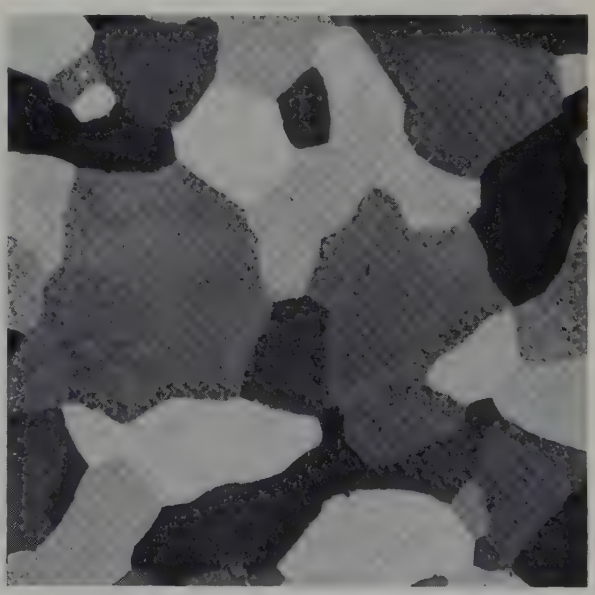

Fig. 9

γ° – alliage U–Mo à 15 % at Mo. Trempé en bain de mercure à partir de 1 000° C. Polissage attaque en solution chromique-acétique. Lumière polarisée. ×500

γ°. 15 at % molybdenum-uranium alloy. Mercury quenched from 1000° C. Attack polished in chromic acid/acetic acid solution. Polarished light. × 500

Fig. 10

γ_d° – alliage U–Mo à 10 % at Mo. Trempé à l'huile à partir de 950° C. Polissage électrolytique en solution phosphorique-sulfurique. Oxydation sous pression partielle d'oxygène (10^{-2}mm) et 1000 volts. Lumière normale. × 150

γ_d°. 10 at % molybdenum-uranium alloy. Oil quenched from 950° C. Electro-polished in phosphoric acid/sulfuric acid solution. Oxidized under partial pressure of oxygen (10^{-2} mm) and 1000 volts. Normal light. × 150

Fig. 12

γ' – alliage U–Mo à 30 % at Mo. Traité à 500° C pendant 28 jours. Polissage attaque en solution chromique-acétique. Lumière polarisée. × 500

γ'. 30 at % molybdenum-uranium alloy. Transformed 28 days at 500° C. Attack polished in chromic acid/acetic acid solution. Polarised light. × 500

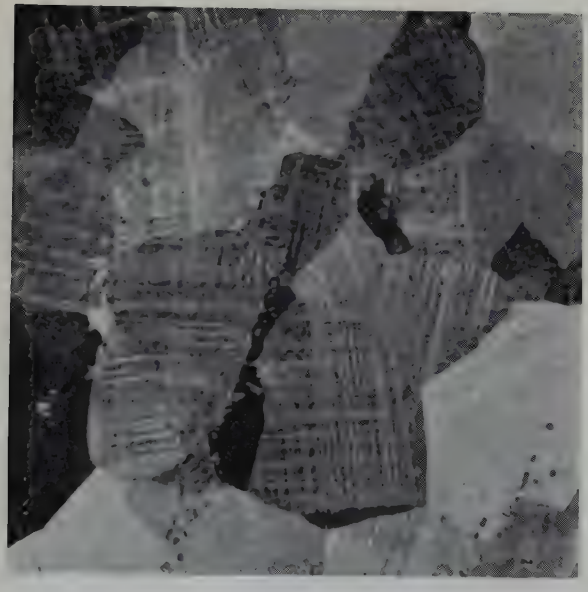

Fig. 11

γ_d° – alliage U–Mo à 11,5 % at Mo. Trempé en bain de mercure à partir de 1 000° C. Polissage attaque en solution chromique-acétique. Lumière polarisée. ×500

γ_d°. 11.5 at % molybdenum-uranium alloy. Mercury quenched from 1 000 °C. Attack polished in chromic acid/acetic acid solution. Polarised light. × 500

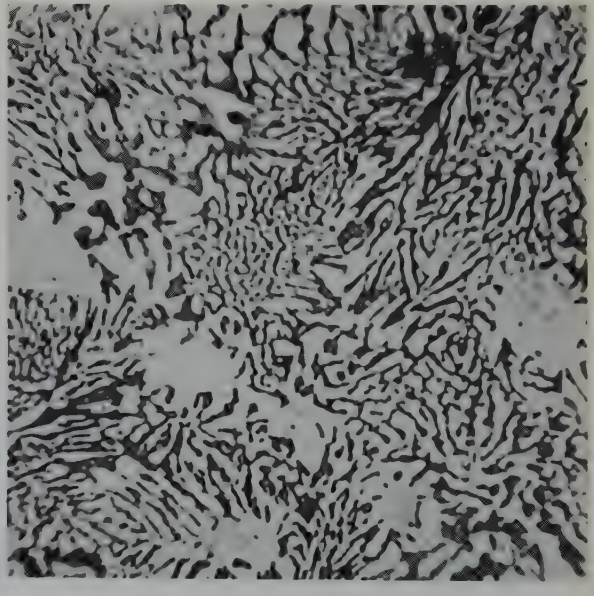

Fig. 13

γ_1, γ_2 – alliage U–Nb à 56 % at Nb. Traité à 850° C pendant 28 jours. Polissage attaque en solution chromique-acétique. Attaque en solution chlorure ferrique-acide fluorhydrique. Lumière normale. ×500

γ_1, γ_2. 56 at % niobium-uranium alloy. Transformed 28 days at 850° C. Attack polished in chromic acid/acetic acid solution. Etched in ferric chloride/hydrofluoric acid solution. Normal light. × 500

changement de structure cristalline correspondant au passage au système monoclinique, comme cela a été mis en évidence par l'un de nous [14]), seront représentés par une double apostrophe, par exemple: α''.

Les indices placés en position inférieure indiqueront une différenciation métallographique.

Des structures aciculaires, en bandes ou formées par germination et croissance ont été observées, elles sont désignées par les indices a, b et n, respectivement. Ces indices correspondent aux mots français et anglais:

— a: acicular, aiguilles
— b: banded, en bandes
— n: nucleation and growth, germination et croissance.

Ainsi un alliage présentant une microstructure en bandes et pour lequel l'analyse aux rayons X montre

significance in both French and English, namely: a = aiguilles, acicular; b = en bandes, banded; n = nucléation (germination) et croissance, nucleation and growth. Thus, an alloy exhibiting a banded structure and which was found by X-ray analysis to have undergone a contraction in the b parameter of the normal orthorhombic structure would be designated as α_b'.

(b) All structures based on the cubic γ phase to be designated γ.

As in the case of α phase variants, superscripts will indicate some crystallographic deviation from the cubic state, and subscripts some metallographic identification.

Only one variation has so far been identified, namely, a structure that has been variously identified as body centred tetragonal [15]) or base centred orthorhombic [13]). This has been designated $\gamma°$. Metallo-

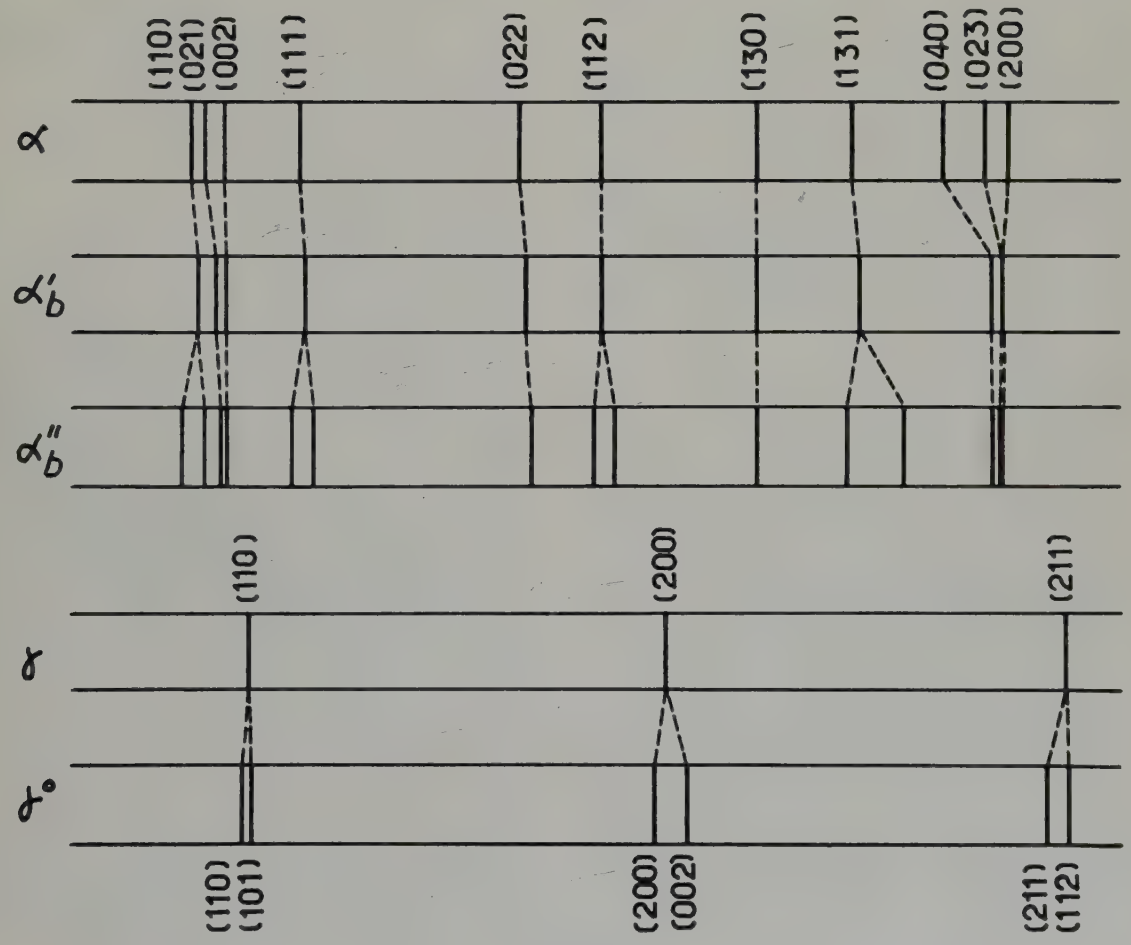

Fig. 14
Représentation schématique des diagrammes de diffraction des rayons X des différentes phases.
Diagrammatic representation of the X-ray diffraction pattern of the phases.

une contraction du paramètre b par rapport à la structure orthorhombique normale, sera désigné: α_b'.

b) Les structures basées sur celle de la phase cubique γ, seront désignées γ.

Comme dans le cas des variantes de la phase α, les indices supérieurs indiqueront une variation cristallographique par rapport à la structure cubique et les indices inférieurs indiqueront une différenciation métallographique.

Une seule phase de ce type a été identifiée et désignée γ°. D'après certains chercheurs sa structure est tétragonale centrée [15]) et d'après d'autres, orthorhombique à base centrée [13]).

Au point de vue métallographique, γ° se distingue facilement de γ, à cause de son action sur la lumière polarisée.

De plus, une forme de γ° dont les grains présentent des bandes, a été mise en évidence; ces bandes semblent provenir de contraintes, soit thermiques, soit mécaniques; les diagrammes de diffraction des rayons X, effectués sur la phase γ°, présentant ou non des bandes, sont identiques. Ainsi les bandes sont considérées comme un phénomène purement métallographique et sont mentionnées par un indice inférieur: d, signifiant: deformed ou déformé.

La phase ordonnée U_2Mo dans le diagramme uranium-molybdène, a souvent été désignée γ'. Les notations proposées sont en accord avec cette désignation.

Il en est de même pour la décomposition de la solution solide γ en deux solutions de compositions différentes, désignées: γ_1 et γ_2.

graphically, γ° can be identified because it responds slightly to polarised light examination. In addition, it is possible to obtain a γ° which exhibits banding within the grains. These bands seem to be the result of stress, either thermal or mechanical. Since the X-ray diffraction patterns of a γ°, with or without bands, are identical, the bands are considered to be a purely metallographic phenomenon and thus are denoted by a subscript "d", meaning "déformé" or "deformed".

The ordered phase (U_2Mo) in the uranium-molybdenum system has often been referred to as γ' which is consistent with the proposed means of notation. Also, breakdown of a γ solid solution into two solutions differing in composition can still be denoted as $\gamma_1 + \gamma_2$.

Bibliographie — References

1) D. Ahmann, A. I. Snow et A. S. Wilson, USAEC, Report CT-2946 (1945)
2) R. F. Hills, D. R. Harries, D. J. Hodkin et M. B. Waldron, AERE (Harwell) Report M/R 2840 (1959)
3) Mme J. Lehmann, thèse, Université de Paris, série A. n° 872, N° 896 (1959)
4) R. W. Buzzard, R. B. Liss et D. P. Fickle, USAEC, Report AECD 2418 (1952)
5) A. G. Knapton, J. Inst. of Metals 83 (1954) 497
6) A. G. Harding, M. B. Waldron et C. Knight, AERE (Harwell) Report, M/R 2673 A (1958)
7) P. C. L. Pfeil, J. D. Browne et G. K. Williamson, AERE (Harwell) Report, M/R 2498 (1958)
8) R. K. McGeary, USAEC, Report WAPD 127, part. I (1951)
9) D. E. Thomas et B. Lustman, USAEC, Report WAPD–MM 413 (1954)
10) Ibid
11) B. A. Hatt et G. B. Brook, Fulmer Research Institute — private communication
12) Mme J. Lehmann et H. Aubert, communication au Symposium sur la Recristallisation, Saclay, 1957
13) E. F. Losco et Z. M. Shapiro, USAEC Report WAPD–PWR–PMM–282 (1955)
14) Mme J. Lehmann, Comptes Rendus des Séances de l'Académie des Sciences **248** (1959) 2098
15) G. I. Williams, Fulmer Research Institute, — private communication.

JOURNAL OF NUCLEAR MATERIALS 2, No. 3 (1960) 269–273, NORTH-HOLLAND PUBLISHING CO., AMSTERDAM

LETTER TO THE EDITORS — LETTRE AUX REDACTEURS

ELECTRON MICROSCOPE STUDIES OF DAMAGE IN IRRADIATED URANIUM DIOXIDE †

H. W. NEWKIRK, Jr.,†† J. L. DANIEL and B. MASTEL
Hanford Laboratories, General Electric Co., Richland, Washington, USA

Received 18 January 1960; revised version received 20 April 1960

This note describes the effects of a short term reactor irradiation on uranium dioxide specimens of moderate density (87 to 94 % of theoretical, 10.97 g/cc). The specimens were examined by fractography, conventional electron microscopy, and pre-characterized surface electron microscopy techniques [1]). The results suggest that reactor irradiation can (1) change the mode of fracture from transcrystalline to intercrystalline, (2) create holes or cracks at grain boundaries, and (3) activate transport mechanisms which distort free surfaces.

Uranium dioxide powder prepared from ammonium diuranate was extruded, hydrostatically pressed, then sintered in hydrogen for four to eight hours at 1700° C. (The rod specimens, 3.00 inches long, were finished to a diameter of 0.248 inch in a centerless grinder. Specimens were inserted in aluminum capsules, which were evacuated, backfilled with helium, and sealed by inert gas welding. They were then irradiated in a water cooled, graphite moderated reactor to 0.005 at %, 0.016 at % and 0.033 at% burnup, at a temperature at the capsule surface of less than 100° C.)

Fractography specimens were prepared before encapsulation by notching the rods midway along their length. After irradiation these specimens were fractured at room temperature (20° C) and the resultant fractured surfaces replicated [1]). In order that the fractographic analysis could be directly related to conventional electron microscopy results, the fractured surfaces were ground down approximately 2 mm, etched, and again replicated. Control specimens were chosen from each density range and treated in a similar manner but were not irradiated. Specimens with pre-characterized surfaces were prepared by cutting the rods in half. The cut face of one of the sections was ground, polished, etched, and replicated. The cut face of the other section was counter-bored to a depth of 0.031 inch to prevent scratching and marring of the polished and etched surface when in contact. After irradiation the pre-characterized surfaces were again replicated.

Fig. 1 shows representative micrographs of replicas of the fractured surface of unirradiated and irradiated specimens. The structure of the fracture surface of the unirradiated specimen illustrates that uranium dioxide fractures in a brittle fashion, predominantly by transcrystalline cleavage. Cleavage step "river patterns" found within the individual grains arise when screw dislocations cut the cleavage plane. The large holes at grain boundaries are associated with the original open and closed porosity of the specimen. The structure of the fracture surface of the irradiated specimens indicates that after irradiation fracture occurs predominantly by

† This work was performed under Contract No. AT(45-1)-1350 between the U.S. Atomic Energy Commission and the General Electric Company, Richland, Washington.

†† Now at University of California, Radiation Laboratory, Livermore, California.

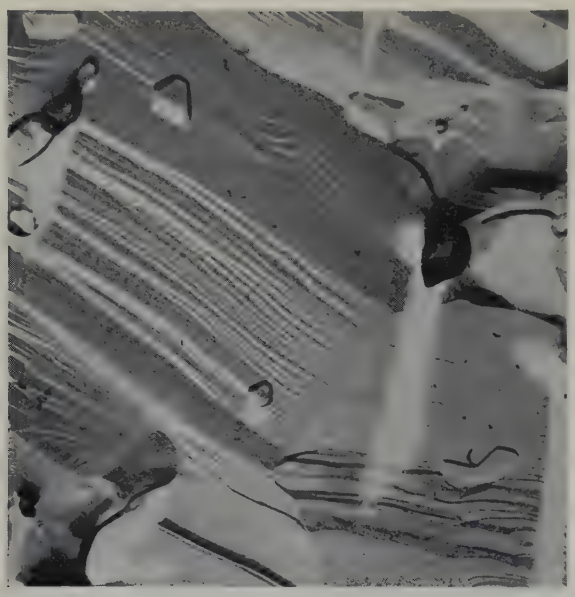

(a) 88.1 % Theoretical density.

intercrystalline cleavage; consequently, cleavage step "river patterns" are absent. Small holes (100–1000 Å in diameter) or cracks at the grain boundaries, apparently not related to the original open and closed porosity, occur frequently in specimens having burnups of 0.005 at %. Such microporosity, however, was uncommon or absent in the specimens having burnups greater than 0.005 at %.

Fig. 2 shows the microstructure of the same specimens as illustrated in fig. 1 after conventional metallographic grinding, polishing, and etching of the fractured surfaces. The micrographs confirm the presence of small holes or cracks at grain boundaries in specimens irradiated to 0.005 at % burnup. The absence of similar holes or cracks in the unirradiated control specimens is additional evidence that irradiation to very low burnup can cause marked

(b) 88.6 % Theoretical density.

(c) 89.2 % Theoretical density.

Fig. 1. Surfaces created by the impact fracture of uranium dioxide specimens; (a) Unirradiated; (b) Irradiated to a burnup of 0.005 at %; (c) Irradiated to a burnup of 0.016 at %. Note the change in the mode of fracture from transcrystalline to intercrystalline, the microporosity along grain boundaries, and the absence of cleavage step "river patterns" in the irradiated specimens. Carbon backed, uranium dioxide pre-shadowed negative replicas; 10 000 ×.

changes in the properties of uranium dioxide.

Fig. 3 shows representative micrographs of replicas of the precharacterized surfaces, before and after irradiation. The free surfaces of the individual grains have become distorted as a consequence of the irradiation. However, point to point comparisons of the microstructure for the pre-irradiation and post-irradiation states by optical microscopy show no indication of microstructural changes. Since electron microscopy revealed no changes in unirradiated precharacterized specimens of uranium dioxide heated in air at 200° C for 8 days, the observed distortion cannot be attributed to a low temperature oxidation reaction. Apparently transport mechanisms are activated in uranium dioxide during irradiation which are capable of distorting free surfaces.

A number of processes have been considered

(a) 88.1 % Theoretical density.

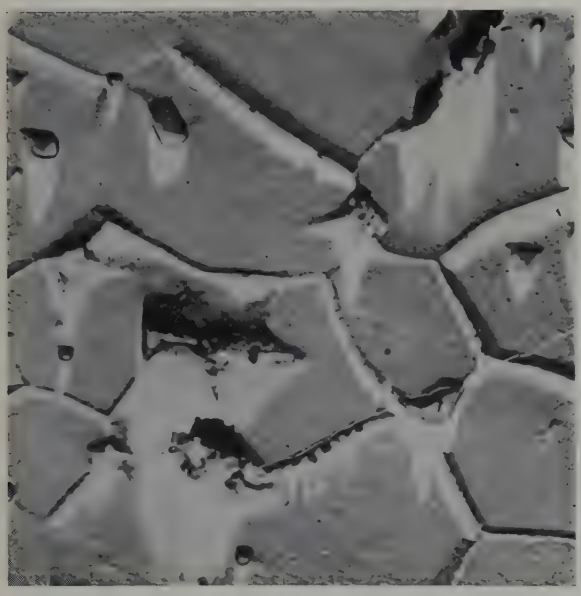

(b) 88.6 % Theoretical density.

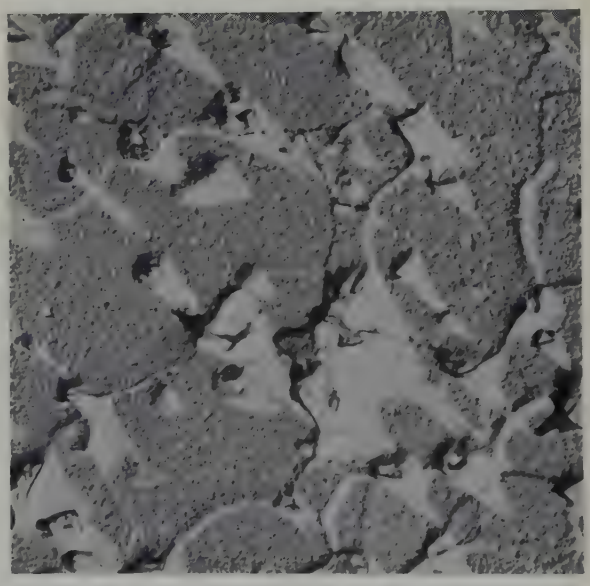

(c) 89.2 % Theoretical density.

Fig. 2. Microstructure of the specimens shown in fig. 1 after grinding, polishing and etching of the fractured surface: (a) Unirradiated; (b) Irradiated to a burnup of 0.005 at %; (c) Irradiated to a burnup of 0.016 at %. Note the microporosity along grain boundaries similar to that observed by fractography. Carbon backed, uranium dioxide pre-shadowed negative replicas; 8000 ×.

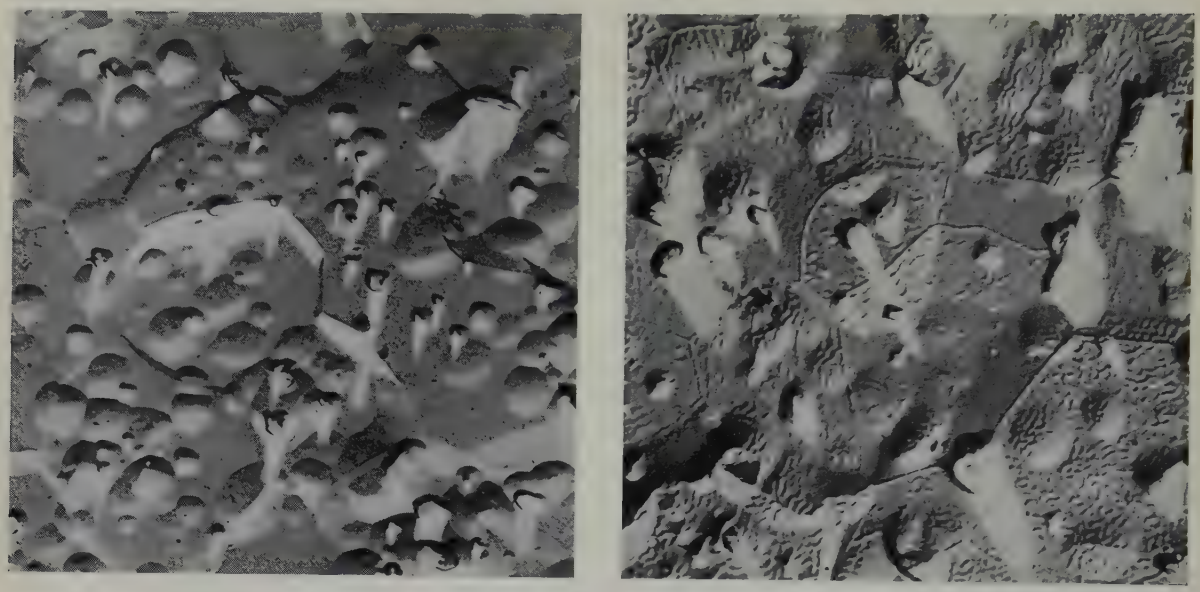

93.4 % Theoretical density. 4000 ×.

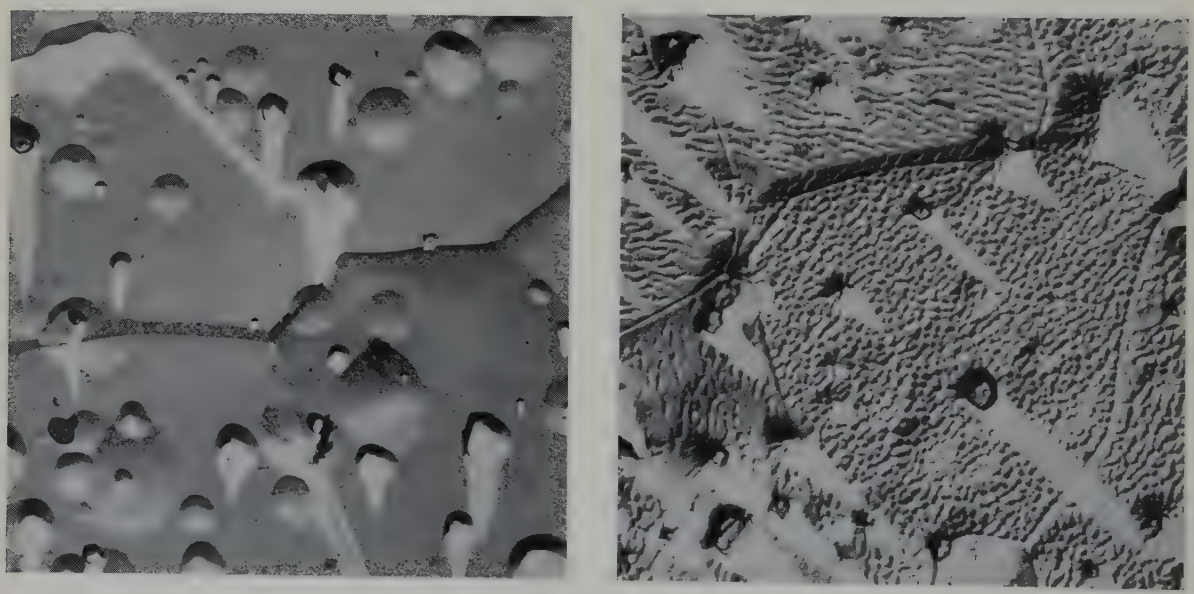

93.6 % Theoretical density. 7000 ×.

Fig. 3. Microstructure of uranium dioxide specimens. Left column: Pre-irradiated state; Right column: Post-irradiation state; Top: 0.005 at % burnup (4000 ×); Bottom: 0.033 at % burnup (7000 ×). Note the distortion of the free surface of the individual grains of irradiated specimens. Carbon backed, uranium dioxide pre-shadowed negative replicas.

in attempting to interpret these observations. Unfortunately, the limited number of specimens studied and the microscopic nature of the data do not permit statistically reliable conclusions. However, a satisfactory quantitative model and theory for radiation damage in uranium dioxide may eventually evolve from qualitative considerations. For example, if residual gases and rare gas atoms (xenon and krypton, generated during fission within the volume of the individual grains) diffuse interstitially to grain boundaries, they may collect vacancies, agglomerate and grow as bubbles. Grain boundaries would thereby be weakened. The ambient temperature along the axis of the rod specimens is unlikely to have exceeded 250° C; at such low temperatures it is generally assumed that gas mobility is controlled by processes other than diffusion. However, it is conceivable that thermal fission spikes generate momentary temperatures of 1000° C or more within small volumes of individual grains, and diffusion could then be a significant factor. Excessive pressures of accumulated gases trapped within the specimen might therefore lead to plastic deformation of the matrix, microporosity and eventual fracture. Similarly, the thermal energy associated with the fission of uranium atoms situated close to a free surface may result in surface distortion by a vaporization or surface migration process. Lack of microporosity in the higher burnup specimens is not explained.

Another possibility is an intergranular fracture process. During irradiation, thermal and fission spikes create stresses in the individual grains. These stresses are relieved initially by plastic deformation within the grains. Hardening occurs as a consequence of the interaction of dislocations with each other and with foreign and interstitial atoms. As hardening develops the localized stresses become high enough to initiate intergranular fracture. A decrease in microporosity or continuous healing of cracks during irradiation might be expected if densification occurs by microsintering resulting from thermal and fission spikes.

Further experiments are needed to permit a reliable interpretation of the observations described above. Relative importance should be established for such parameters as density and stoichiometry of the UO_2, concentration of residual gases, temperatures, and extent of burnup. Results should be correlated with fission gas release and thermal conductivity. We feel that the high resolution microscopy techniques used here may provide a direct means of studying radiation damage, self-healing, and sintering of UO_2 on a micro scale, and lead to development of feasible mechanisms for these phenomena.

Reference

1) T. K. Bierlein and B. Mastel, Second Geneva Conference, Paper P/1855 (1958)

JOURNAL OF NUCLEAR MATERIALS 2, No. 3 (1960) 274-276, NORTH-HOLLAND PUBLISHING CO., AMSTERDAM

BOOK REVIEWS

CHAUNCEY STARR and R. W. DICKINSON, *Sodium Graphite Reactors* (Addison-Wesley Publishing Company, Inc., Reading, Mass., USA, 1958) xii + 288 pages, 49s, $ 6.50.

The authors have given a matter-of-fact progress report on the program of developing nuclear reactors cooled with sodium, moderated with graphite to be used for producing economic electrical power. Work aimed specifically at developing this type of reactor has been underway since about 1952, and has been part of the program of the U.S. Atomic Energy Commission to develop reactors for commercial power. The book was prepared under contract with the USAEC, and became a part of the information offered by the United States to the world at the time of the Second Geneva Conference on Atoms for Peace.

During the early days of reactor development, a number of workers pointed out that liquid sodium provided two features which seemed to be essential to nuclear power reactors: (1) outstanding heat transfer capabilities, thus making it possible to remove the large amounts of heat available from a nuclear reactor; and (2) a boiling point high enough to promise the generation of steam power at temperatures currently used in the steam power industry without a high pressure in the reactor itself. These two features should permit maximum power generation with a given capital investment. As pointed out in the book, these features seemed of unusual value in the Commission's program at a time when careful consideration was being given to reactors which would produce both electrical power and plutonium. For producing power only, the features have seemed equally attractive to many individuals. The real prospect remains that for a plant of a given size, sodium cooling would permit the generation of the maximum amount of useful power.

Starr and Dickinson show very clearly the results of some six years work, first to develop and study a pilot plant-sized reactor—the Sodium Reactor Experiment (SRE)—and the Sodium Graphite Reactor (SGR)—a full-scale plant for the Consumers' Public Power District of Nebraska and based on the results of the development program.

The first chapter indicates how some of the major features of the design of the reactor experiment arose. Chapters 2 through 7 take up in detail the SRE and give its design, the materials problems which it gives rise to, the development of fuel elements for the reactor and for studies connected with it, the many components and systems which have to be associated with the reactor, and finally the operation of the reactor as an experiment. These chapters show very nicely how all the different aspects of the reactor were tackled and disposed of. This portion of the book should provide an excellent case study for anyone coming into the field and wishing to learn in detail the steps attending the development of a nuclear reactor power plant. In addition, people who have developed other type reactors will be interested in comparing notes, as it were.

Chapter 2 gives all the major components of the reactor system and shows how the power plant is put together, cooled, shielded, enclosed, and connected to the steam power system. Chapter 3 gives the essential results of the use of two-group diffusion theory in calculations of the SRE, and compares the calculations with many of the experimentally-interesting quantities of the neutronics of the assembly. Perhaps the question of temperature coefficient, taken together with the transient and safety characteristics of the reactor, are the interesting new results showing that the assembly is very stable. Chapter 4 shows that the essential feature of the coolant and structural materials technology were ways and means to avoid contaminating zirconium by oxygen which may be transferred out of sodium unless it is controlled, or out of the graphite unless it is suitably purified. Fuel element development is discussed in Chapter 5. From this chapter one learns that a major function of the SRE is to test fuel materials and fuel elements for sodium cooling. One does not learn about the extensive problem of finding, measuring, and controlling the independent variables which control the response of fuel elements. The fairly standard, but rather elaborate engineering, for handling sodium, transferring heat from the sodium to water for cooling and protecting various parts of the system, and for handling fuel elements, together with equipment for instrumentation and control are described in Chapter 6. Power generation and detailed features of reactor operation, including the blow-by-blow account of testing and

initiation of operation, are all described in Chapter 7. Chapter 8 attempts to tell how the sodium reactor concept may be scaled from the SRE to an operating plant, particularly the Hallam nuclear power facility for the CPPD.

The story on the development of the SRE is very interesting, convincing, and useful. It seems, however, to this reviewer that all writers on nuclear reactors are in the following dilemma: One wishes to acknowledge and take advantage of the novelty of nuclear reactors and emphasize their great potential advantages if certain things work out, but at the same time he wishes to yield to the rather conservative profession of standard engineering and create the impression that there are no technological risks. Thus, this book does not come to grips with the things that will eventually permit the sodium-cooled systems to live up to their great potential. These items are: (1) a fuel element which can put out heat at the large rate which sodium can accept and thus truly take advantage of the sodium's heat transfer characteristics in realizing the large amounts of power from a given assembly; (2) simple inexpensive and effective coolant handling and steam generation equipment which contains sodium adroitly. These items are mentioned but the reader gets no feeling as to how conventional engineering will be broken away from to achieve these objectives. But these things will be accomplished.

JOHN P. HOWE

F. BENESOVSKY (editor): *Plansee Proceedings 1958*. (Pergamon Press and Metallwerk Plansee A.G., 1959. xii + 465 pages. 83s. 6d.)

The proceedings of the Plansee Seminars in Powder Metallurgy have since their inception in 1952 become required reading for specialists in the field. As Dr. Schwarzkopf recounts in his opening address, here reprinted, the first Seminar embraced the whole field of powder metallurgy, experimental and theoretical; the second Seminar in 1955 concentrated more on refractory sintered materials, and this restriction was made more specific in the 1958 Seminar, which was concerned with the powder metallurgy of refractory metals.

A distinguished international group of participants presented 33 papers, dealing both with general problems of technique and with the behaviour of individual metals, alloys and cermets. 18 papers are in English, 12 in German and 3 in French. Many papers are followed by a record of the (polyglot) discussion.

Five papers are of specific interest to nuclear metallurgy specialists: Sedlatschek and Kieffer describe (in German) the production of alloys of wolfram, molybdenum, tantalum and columbium with uranium, by impregnating sintered bodies of the refractory metals with molten uranium. Details of the procedure and of the resulting structures are presented. The wolfram-uranium alloys, with densities up to 19 g/cm^3, are proposed as valuable for γ-ray shielding. Lloyd reports (in English) on the compatibility of molybdenum, tantalum and niobium with liquid bismuth- and bismuth-uranium solution. The first two metals have good static compatibility, but columbium did not show up well in static tests. Molybdenum also behaved well in dynamic compatibility tests with bismuth.

Brauer and Müller report (in German) on the oxidation behaviour of columbium and tantalum powders. Several new unstable suboxides were found; a new hydride of columbium was also discovered. Brauer, Kieffer and Sedlatschek give a full account of the powder metallurgical preparation of the complete range of tantalum-wolfram solid solutions, and include results of exhaustive tests of density, lattice parameter, hardness, elastic modulus, resistivity, hydridability, oxidation resistance, corrosion resistance and deformability. Tantalum-rich alloys up to 30 at % wolfram are cold-workable, wolfram-rich alloys up to 20 at % tantalum can be hot-worked, other alloys are very difficult to work even at high temperatures. This paper is a most full and valuable contribution.

Williams and Heal (in English) give a detailed account of the consolidation and fabrication of columbium for reactor use and of its physical and mechanical properties up to 600° C ((and in some cases higher). The compatibility of the metal with sodium is also discussed. These results are the fruit of a research programme carried out by the Industrial Group of the UKAEA.

A number of other papers in this collection should also be of interest to readers of this Journal, for instance the paper by Hausner describing the slip casting technique; Robins and Jenkins' account of their methods of preparing samples of very pure refractory metals; Gebhardt and Seghezzi's investigation of the tantalum-nitrogen system; and Harwood and Promisel's excellent survey of requirements for high temperature materials, the presently available metals and alloys, and prospects for the future. This last paper should also be useful reading for students.

The standard of printing, illustrations and proof-reading is high; the only error discovered occurs on page 129, where the indices in an equation have been misleadingly positioned. As prices go nowadays for reports of specialist conferences, this book is good value for money.

R. W. CAHN

Nuclear Metallurgy, Volumes I–VI, 1955–1959. (Published by, and available from, the American Institute of Mining, Metallurgical and Petroleum Engineers (AIME), 29 West 39th Street, New York 18, N.Y., U.S.A.)

Vol. I. Material Problems in Reactors; Physical Metallurgy of Plutonium, Thorium, Uranium. (1955) $ 3.75.

Vol. II. Behavior of Materials in Reactor Environment. (1956) $ 3.75.

Vol. III. The Effects of Radiation on Metals. (1956) $ 3.75.

Vol. IV. Uranium and Uranium Dioxide. (1957) $ 7.00.

Vol. V. Ceramic Base Elements; Metal Base Fuels and Jacket Components. (1958) $ 6.00.

Vol. VI. Effects of Irradiation on Fuel and Fuel Elements. (1959) $ 7.00.

These symposia have been published for some years past by the Nuclear Energy Committee of the Institute of Metals Division of the AIME, so as to coincide with the Institute's meetings at which they were discussed. The booklets, ranging from 50 to 140 pages in length, each contain several papers giving either the results of original work, or summarising unclassified knowledge in a field of nuclear metallurgy.

The appearance of the first volume coincided with the First Geneva Conference and consists largely of Geneva papers. Vol. II is mainly concerned with corrosion problems. Vol. III deals in an elementary way with the theory of irradiation damage and in more detail with experimental facts, especially about physical metallurgical processes. Vol. IV contains 16 papers devoted to the casting and fabrication of uranium and uranium dioxide. Vol. V contains a number of useful technological accounts of the development of specific kinds of fuel and fuel elements.

The latest volume returns in more detail to the irradiation theme; it includes an excellent theoretical survey of the nature of fission damage by Brinkman, two up-to-date reviews of the swelling problem by Churchman and Barnes, two reports on the irradiation behaviour of uranium dioxide, and several accounts of the behaviour of other less conventional mixed fuels.

Together, these six volumes can be recommended as a useful, authoritative addition to any reference library in the nuclear energy industry. Being lithoprinted from typescripts, the volumes are not particularly elegant examples of the printer's art; nevertheless the reproduction is very clear and easy to read.

R. W. CAHN